

A STUDY OF THE CHLORINATION BEHAVIOUR OF VARIOUS TITANIA FEEDSTOCKS

Samantha Moodley

A research report submitted to the Faculty of Engineering and the Built Environment, University of the Witwatersrand, Johannesburg, in partial fulfilment of the requirements for the degree of Master of Science in Engineering.

Johannesburg, 2011

DECLARATION

I declare that this research report is my own unaided work. It is being submitted to the Degree of Master of Science to the University of the Witwatersrand, Johannesburg. It has not been submitted before for any degree or examination to any other University.

.....
(Signature of Candidate)

..... **day of****year**.....

Abstract

Due to the cost and availability of rutile (*i.e.* the preferred feedstock for the chloride process) a number of chloride producers are now forced to feed a blend of feedstock's to the chlorinator. Although the TiO_2 content of the feedstock's may be the same, the feedstock's (*i.e.* slag, rutile, synthetic rutile and ilmenite) vary in TiO_2 content, impurity content and physical properties (*i.e.* size distribution, density and shape factor). These factors can have a significant effect on chlorinator performance such as process stability, throughput, elutriation figures (*i.e.* blowover from the chlorinator), waste generation and thus influence the design of the chlorination circuit. In this research report, individual feedstock's (*i.e.* Slag A, Slag B and rutile) and a blend of Slag A and rutile were chlorinated. The study aims to highlight the difference in chlorination mechanism between rutile and slags, compare the chlorination of different TiO_2 containing slags and behaviour of a blend compared to the individual components.

The major findings of this investigation included the following:

- Due to its shape, density and particle size distribution rutile was found to be the ideal fluidising material in the hydrodynamic study. Addition of rutile to Slag A (*i.e.* 50 wt% Slag A and 50wt% Rutile) lowered the overall elutriation of slag.
- At 1000°C, the blend (*i.e.* 50 wt% Slag A and 50wt% Rutile) had the highest chlorination conversion rate, followed by Slag B, Slag A and rutile. The blowover mass and degree of conversion of the blend of rutile and Slag A was better than the individual components. Blend samples (*i.e.* 50 wt% Rutile and 50wt% Slag A) of varying particle size was chlorinated and the mix with the widest particle size distribution exhibited the highest conversion rates.
- The mechanism for slag and rutile chlorination differs; slag becomes porous after the chlorination of FeO and MnO whilst rutile remains solid throughout the reaction. Porous material has a greater tendency to be elutriated from the bed
- The chlorination of Fe and Mn oxides is not significantly affected by the temperature whilst the chlorination of TiO_2 and Al_2O_3 is highly dependent on the temperature.

The most interesting findings of the experiments were that the blend of rutile and Slag A performed better than the individual components. This is most likely due to the particle size distribution of the mixture which yields better hydrodynamic characteristics. The performance of blends is of significant industrial importance, it is therefore recommended that the effect of particle size distribution is further investigated and that 3 or more component blends are also studied.

Acknowledgements

I would like to make the following acknowledgements:

My supervisors, Prof Eric and Prof Kucukkaragoz for inputs and guidance.

Aditya Kale and Mintek for providing the resources to do the testwork and for knowledge sharing

Deon Bessinger for providing motivation, encouragement and guidance throughout the project duration

Annabe Walliser for SEM and QEMSCAN work

Jill Richards for XRD results

Jackson Mathaba for assistance in the literature research

Thomas Mnisi for sample preparation and logistics

Hennie Burger and Gerhard Grobler from Exxaro for financial assistance for the research

To my family and friends for always supporting me

To Nischal for love and support throughout this work

Table of Contents

Declaration.....	2
Abstract	3
Acknowledgements	4
List of Figures	8
List of Tables	10
List of Symbols	12
List of Abbreviations.....	14
1. INTRODUCTION	15
1.1 INDUSTRY BACKGROUND.....	16
1.1.1 Uses and properties of titanium compounds.....	16
1.1.2 Pigment Processing Technology	17
1.2 JUSTIFICATION	20
1.3 PROBLEM STATEMENT	20
1.4 HYPOTHESIS	21
1.5 OBJECTIVES OF THE RESEARCH.....	21
1.6 LAYOUT OF THESIS	21
2. LITERATURE REVIEW	23
2.1 TITANIA FEEDSTOCKS FOR THE PIGMENT INDUSTRY.....	24
2.1.1 Rutile	24
2.1.2 Processed Ilmenite as Feedstock.....	24
2.1.3 Feedstock requirements for the chloride process.....	29
2.2 CHLORINATION.....	31
2.2.1 Effect of Carbon and CO.....	31
2.2.2 Chlorination Mechanism.....	31
2.2.3 Chlorination of Ti^{3+}	33
2.2.4 CHLORINATION REACTIONS	35
2.2.5 Kinetic Models.....	36
2.3 FLUIDISATION BACKGROUND	42
2.3.1 Fluidisation principles.....	42
2.3.2 Fluidisation Stages.....	44
2.3.3 Geldart Classification	45
2.3.4 Elutriation	46

2.3.5	<i>Bubbling Fluidised beds</i>	48
3.	EXPERIMENTAL	53
3.1	SAMPLES	53
3.2	FLUIDISATION TESTWORK	56
3.2.1	<i>Experimental Sample</i>	57
3.2.2	<i>Experimental Apparatus</i>	57
3.2.3	<i>Experimental Procedure</i>	58
3.2.4	<i>Experimental Technique</i>	59
3.3	CHLORINATION TESTWORK	59
3.3.1	<i>Experimental sample</i>	59
3.3.2	<i>Experimental Apparatus</i>	59
3.3.3	<i>Experimental Procedure</i>	62
3.3.4	<i>Experimental Technique</i>	64
3.4	SAFETY, HEALTH AND ENVIRONMENTAL	66
3.4.1	<i>Chlorine</i>	66
3.4.2	<i>Carbon monoxide</i>	66
3.4.3	<i>Chlorine leaks</i>	66
3.4.4	<i>Fumes</i>	67
4.	RESULTS AND DISCUSSION	68
4.1	FLUIDISATION.....	68
4.1.1	<i>Geldart Classification</i>	68
4.1.2	<i>Minimum Fluidising Velocity and Terminal Velocity</i>	68
4.1.3	<i>Elutriation Constants</i>	69
4.2	CHLORINATION.....	74
4.2.1	<i>Mineralogical Characterisation of Feed Material</i>	74
4.2.2	<i>Mineralogical characterisation of Bed Samples</i>	79
4.2.3	<i>Mass Balance</i>	87
4.2.4	<i>Chlorination as a function of temperature</i>	88
4.2.5	<i>Chlorination as a function of time</i>	92
4.2.6	<i>Coke reaction</i>	100
4.2.7	<i>Blowover</i>	105
4.2.8	<i>Comparison with Theoretical Models</i>	112
4.2.9	<i>Activation Energy</i>	114
5.	CONCLUSION AND RECOMMENDATIONS	116
6.	REFERENCES	119

Appendix 1: Particle size distribution and density results for feed material	125
Appendix 2: Geldart Classification graphs.....	126
Appendix 3: SEM results	128
Appendix 4: Mass balance	132
Appendix 5: SEM results for chlorinated bed samples	142
Appendix 6: XRD Results	147

LIST OF FIGURES

Figure 1: Chloride Process Flowsheet (Burger and Rabe, 2007)	18
Figure 2: Process Routes in the Ti/TiO ₂ industry (Murty et al., 2007)	24
Figure 3: Technologies for upgrading of ilmenite (Murty et al., 2007)	25
Figure 4: Ilmenite Smelting (Zietsman, 2004)	26
Figure 5: Changes in FeO and Ti ₂ O ₃ content of ilmenite smelter (Zietsman and Pistorius, 2004)	28
Figure 6: Micrograph of slag indicating the M ₃ O ₅ , glassy and metallic iron phases (van Dyk and Pistorius, 1999).....	29
Figure 7: Boiling Points of Metal Chlorides	30
Figure 8: Fe and Mn removal during first few minutes of chlorination (Pistorius and Le Roux, 2002).....	32
Figure 9: Rates of chlorination (Den Hoed and Nell, 2003)	33
Figure 10: Bed temperature during first few minutes of chlorination (den Hoed and Nell, 2002)	34
Figure 11: Chlorination of Rutile (C-Cl ₂ system vs CO-Cl ₂ system)	39
Figure 12: Chlorination of Rutile (CO-Cl ₂ system)	40
Figure 13: Chlorination of rutile vs slag (CO-Cl ₂ system)	40
Figure 14: Chlorination of Slag (C-CO-Cl ₂ system vs CO-Cl ₂ system)	41
Figure 15: Fluidisation stages (Kunii and Levenspiel, 1969).....	44
Figure 16: Geldart Group Classification	46
Figure 17: Bubble behaviour in a fluidised bed (Kunii and Levenspiel, 1991)	46
Figure 18: Kunii and Levenspiel Model (1991).....	48
Figure 19: The effect of bubble size on the conversion of reactants in a fluidised bed, based on Kunii and Levenspiel model (Beetstra et al., 2009).....	49
Figure 20: CFD predictions of ozone conversion as a function of dimensionless rate constant for the three different size distributions (Sharma and Pugsley, 2007)	50
Figure 21: Particle size distribution of Feedstock's	55
Figure 22: Coke particle size distribution	56
Figure 23: Rotary Splitter used for 2 nd and 3 rd stage sample splitting	57
Figure 24: Photograph of the Fluidisation set-up	58
Figure 25: Schematic of experimental set up for chlorination experiments (Kale and Bisaka, 2010)	60
Figure 26: Furnace used for chlorination experiments	61
Figure 27: Photograph of heated furnace with silica reactor	61
Figure 28: Control Panel.....	62
Figure 29: Blowover from elutriation experiment as a percentage of the initial mass of feed.....	71
Figure 30: BSE Image of Slag A	74
Figure 31: BSE Image of Slag B	75
Figure 32: BSE Image of Rutile Feed.....	75
Figure 33: BSE image of Slag A particle	76
Figure 34: BSE image of Slag A after 1 minute of chlorination	79
Figure 35: BSE image of bed samples after 30 minutes of chlorination at 1000 ^o C, (a) Slag A, (b)Slag B, (c)Rutile, (d) Blend (a mixture of 50wt % rutile and 50wt% Slag A)	80
Figure 36: BSE image of bed samples after 180minutes of chlorination at 1000 ^o C, (a) Slag A, (b)Slag B, (c) Rutile, (d) Blend (a mixture of 50wt % rutile and 50wt% Slag A)	81
Figure 37: BSE image of Slag A after 1 minute of chlorination at 1000 ^o C – Sample 1	82
Figure 38: BSE image of Slag A after 30 minutes of chlorination at 1000 ^o C – Sample 2.....	83
Figure 39 : BSE image of Slag A after 30 minutes of chlorination at 1000 ^o C – Sample 3.....	83
Figure 40: BSE image of Slag B after 30 minutes of chlorination at 1000 ^o C – Sample 4.....	84
Figure 41: BSE image of Slag B after 180 minutes of chlorination at 1000 ^o C – Sample 5.....	85
Figure 42: BSE image of rutile particle after 30 minutes of chlorination at 1000 ^o C– Sample 6.....	85
Figure 43: Chlorination as a function of temperature for 180 minutes	88
Figure 44: TiO ₂ chlorination as a function of temperature for 180 minutes	89
Figure 45: Al ₂ O ₃ chlorination of as a function temperature for 180 minutes.....	89
Figure 46: MgO Chlorination as a function of temperature for 180 minutes	90
Figure 47: FeO chlorination as a function of temperature for 180 minutes.....	90
Figure 48: MnO chlorination as a function of temperature for 180 minutes	91

Figure 49: Mass chlorinated at 1000 ^o C	92
Figure 50: Bed residue after chlorination at 1000 ^o C	93
Figure 51: TiO ₂ chlorination as a function of chlorination time	94
Figure 52: Change in Gibbs free energy for FeO chlorination	96
Figure 53: Change in Gibbs free energy for MnO chlorination.....	96
Figure 54: FeO chlorination as a function of chlorination time at 1000 ^o C.....	98
Figure 55: MnO chlorination as a function of chlorination time at 1000 ^o C	98
Figure 56: MgO chlorination as a function of chlorination time at 1000 ^o C	99
Figure 57: Al ₂ O ₃ chlorination as a function of chlorination time at 1000 ^o C	99
Figure 58: Amount of coke reacted at 1000 ^o C	100
Figure 59: Coke/ore ratio vs time	101
Figure 60: Coke/ore ratio vs Mass chlorinated.....	101
Figure 61: Coke ratio vs Ti ₂ O ₃ content.....	102
Figure 62: QEMSCAN Image Grid of Slag and Rutile Particle, (a) rutile, (b).....	104
Figure 63: Blowover after chlorination at 1000 ^o C.....	105
Figure 64: Average particle size as a function of chlorination time at 1000 ^o C.....	106
Figure 65: Porosity changes as a function of chlorination time at 1000 ^o C.....	106
Figure 66: BSE image of Chlorinated Slag A after 30 minutes (a) and 180 minutes (b) of chlorination.....	107
Figure 67: BSE image of Chlorinated Rutile after 30 minutes (a) and 180 (b) of chlorination	107
Figure 68: Particle size distribution of the sample used in chlorination experiments.....	108
Figure 69: Mass chlorinated at 1000 ^o C.....	109
Figure 70: Effect of Particle size distribution on degree of conversion	110
Figure 71: Effect of particle size distribution on blowover	110
Figure 72: Comparison of experimental results for Slag with theoretical models	112
Figure 73: Comparison of experimental results of rutile with theoretical models.....	113
Figure 74: Activation Energy	114
Figure 75: Geldart Classification – Slag A.....	126
Figure 76: Geldart Classification – Slag B.....	126
Figure 77: Geldart Classification – Rutile	127
Figure 78: BSE image of Slag A after 30 minutes of chlorination at 1000 ^o C - Sample 8	143
Figure 79: BSE image of Slag A after 30 minutes of chlorination at 1000 ^o C – Sample 9.....	144
Figure 80: BSE image of Slag A after 30 minutes of chlorination at 1000 ^o C – Sample 10.....	145
Figure 81: BSE image of Slag B after 30 minutes of chlorination at 1000 ^o C- Sample 11	146
Figure 82: Diffractograms for feed materials	149
Figure 83: Diffractograms for Slag A	150
Figure 84: Diffractograms for Slag B.....	151
Figure 85: Diffractograms for Rutile	152
Figure 86: Diffractograms for Blend	153

LIST OF TABLES

Table 1: Refractive Indices (DuPont, 2007)	16
Table 2: Typical Slag Qualities (Murty et al., 2007)	27
Table 3: Summary of kinetic studies conducted on TiO ₂ feed stocks	38
Table 4: Feedstock Chemical Analysis	54
Table 5: Coke Analysis.....	54
Table 6: Feedstock d ₅₀	55
Table 7: Feedstock Density	56
Table 8: Sample Mass Before and After Heat Up	63
Table 9: Test Plan for Chlorination Experiments.....	64
Table 10: Minimum fluidisation velocity.....	69
Table 11: Terminal Velocity of different feedstocks	69
Table 12: Experimental data for Slag A elutriation calculation.....	70
Table 13 : Experimental data for Slag B elutriation calculation.....	70
Table 14: Experimental data for Rutile elutriation calculation	70
Table 15: Experimental data for Blend elutriation calculation	71
Table 16: Elutriation Constants	73
Table 17: Average composition of the M ₃ O ₅ phase in Slag A (Point analysis)	77
Table 18: Average composition of the Glassy phase in Slag A (Point analysis).....	77
Table 19: Average composition of rutile and iron in Slag A (Point analysis).....	77
Table 20: Average composition of the rutile phase in Slag A (Point analysis).....	77
Table 21: Average Composition of the M ₃ O ₅ phase in Slag B Feed Material (Point analysis)	78
Table 22: Average Composition of the glassy phase in Slag B Feed Material (Point analysis)	78
Table 23: Average Composition of the Fe phase in Slag B Feed Material (Point analysis)	78
Table 24: Average Composition of rutile phase	78
Table 25: Average Composition of Zircon in rutile	78
Table 26: Average composition of iron silicate phase	78
Table 27: Normalised Point analysis of Slag A – Sample 1	82
Table 28: Normalised Point analysis of Slag A –Sample 2	83
Table 29: Normalised Point analysis of Slag A – Sample 3	84
Table 30: Normalised Point analysis of Slag B – Sample 4 [‡]	84
Table 31: Normalised Point analysis of Slag B – Sample 5	85
Table 32: Normalised Point analysis of rutile particle – Sample 6	86
Table 33: Blowover after 180 minutes of chlorination at 1000 ^o C	93
Table 34: Mass Balance for 1 minute chlorination of Slag A.....	95
Table 35: Mass Balance for chlorination of MnO and FeO with Ti ₂ O ₃	97
Table 36: D ₅₀ of sample used in chlorination experiments.....	108
Table 37: Effects of varying the slag to rutile ratio in the blend.....	111
Table 38: Calculated Activation Energy	115
Table 39: Activation energy from literature.....	115
Table 40: Particle size distribution.....	125
Table 41: Density.....	125
Table 42: Normalised Point analysis of the M ₃ O ₅ phase in Slag A	128
Table 43: Normalised Point analysis of Glassy phase Slag A	128
Table 44: Normalised Point analysis of rutile phase in Slag A.....	128
Table 45: Normalised Point analysis of M ₃ O ₅ phase in Slag B	129
Table 46: Normalised Point analysis of glassy phase in Slag B	129
Table 47: Normalised Point analysis of Fe in Slag B	130
Table 48: Normalised Average Composition of the Rutile Feed Material	131
Table 49: Normalised Average Composition of Zircon in rutile feed material	131
Table 50: Normalised Average Composition of Fe silicate phase	131
Table 51: Chlorination Results for Slag A	132
Table 52: Chlorination Results for Slag B	135

Table 53: Chlorination Results for Rutile.....	138
Table 54: Chlorination Results for Blend.....	140
Table 55: Normalised Point analysis of Slag A - Sample 3.....	142
Table 56: Normalised Point analysis of Slag B - Sample 4.....	142
Table 57: Normalised Point analysis of Slag A - Sample 8.....	143
Table 58: Normalised Point analysis of Slag A - Sample 9.....	144
Table 59: Normalised Point analysis of Slag A – Sample 10.....	145
Table 60: Normalised Point analysis of Slag B - Sample 11.....	146
Table 61: XRD Results for the Feed samples.....	147
Table 62: XRD Results for Slag A chlorination.....	147
Table 63: XRD Results for Slag B chlorination.....	147
Table 64: XRD Results for Rutile chlorination.....	148
Table 65: XRD Results for the blend chlorination.....	148

LIST OF SYMBOLS

Φ_s	shape factor of the particles
ϵ_{mf}	voidage at minimum fluidisation
g	gravitational velocity, (cm/s ² , m/s ²)
L	length of fluidized bed, (cm)
ΔP	pressure drop across depth L , (Pa)
U	superficial gas velocity, (cm/s)
Re_p	Reynolds number
A_B	cross section area of bed, (cm ²)
$_{mf}$	subscript meaning “at minimum fluidizing conditions”
F_B	total entrainment rate at bed surface, (kg/m ² s)
A	cross sectional area of the column, (m ²)
D_B	bubble diameter at the bed surface, (m)
D_c	degree of conversion, (%)
$M_{chlorinated}$	mass chlorinated, (g)
$M_{initial}$	mass of initial feedstock, (g)
M_{bed}	mass of feedstock remaining in bed, (g)
$M_{blowover}$	mass of blowovers, (g)
W_{io}	initial weight of mass fraction, (g)
W_i	total weight of mass fraction, (g)
W	total weight of sample before fluidisation, (g)
t	time, (sec, minutes)
k_i^*	elutriation constant, (kg/m ² .s)
P_{Cl_2}	chlorine Partial Pressure, (kPa, atm)
P_{CO}	CO Partial Pressure, (kPa, atm)
u_{mf}	minimum fluidising velocity, (m/s)
d_p	average particle diameter, (μ m, cm, m)
μ	gas Viscosity, (kg/m.s, g/cm.s)
u_t	terminal velocity, (m/s)
ρ_g	gas density, (kg/m ³ , g/cm ³)
ρ_s	solid density, (kg/m ³ , g/cm ³)

X	fractional conversion of TiO_2
R	gas constant, (cal/mol.K, J/mol.K)
T	reaction temperature, (K)
N	molar ratio of $\text{Ti}^{3+}/\text{Ti}^{4+}$
h	elevation above distributor, (cm,m)
D'_{BO}	initial bubble diameter, (cm,m)
d_p^*	measure of particle diameter, dimensionless
u^*	measure of particle velocity, dimensionless

LIST OF ABBREVIATIONS

Ar	Argon
BET	Brunauer Emmett Teller
Cl ₂	Chlorine
CO	Carbon monoxide
HCl	Hydrochloric acid
ICP-OES	Inductively Coupled Plasma Optical Emission Spectroscopy
KZN	Kwa-Zulu Natal
N ₂	Nitrogen
PSD	Particle size distribution
RBM	Richards Bay Minerals
SA	South Africa
SEM	Scanning Electron Microscope
SR	Synthetic Rutile
Vol	Volume
Wt	Weight
UGS	Upgraded slag
QIT	Quebec Iron and Titanium
PMA	Particle Mineral Analysis
EDS	Energy Dispersive Spectroscopy
QEMSCAN	Quantitative Evaluation of Minerals by Scanning Electron Microscopy
CFD	Computational Fluid Dynamics
RI	Refractive Indices

CHAPTER 1

1. INTRODUCTION

The main use for TiO_2 dioxide is as pigment for paints, toothpaste, plastics, paper, cosmetics, inks etc. TiO_2 pigment is valued because it imparts whiteness, brightness and opacity to paints, paper, plastics and ceramics. Two processing routes exist for the production of TiO_2 pigments i.e. a sulphate based process or a chloride based process. The chloride process is a newer technology and has several advantages over the sulphate process, it generates less waste, uses less energy, is less labour intensive and permits the direct recycle of chlorine back into the production process (Tronox, 2007). Since the late 1980's, the vast majority of TiO_2 production capacity that has been built utilises the chloride process (Tronox, 2007). Feedstock quality is dependant on the process route followed, maximum limits are placed on the FeO , SiO_2 , Cr_2O_3 , MnO , CaO , MgO and V_2O_5 contents of chloride feedstock.

Fluidised bed technology is employed for the chlorination process, so feedstock physical characteristics such as density, size and shape factor is also of importance. The feedstock has to have sufficient grain size and bulk density to minimize blowover in the chlorinator.

The feed to the chlorinator includes a number of titania feedstock's namely,

- Synthetic rutile (SR),
- Natural rutile,
- Upgraded titania slag (UGS),
- High grade QIT slag and
- Titania slag produced from ilmenite smelting

Natural Rutile is the preferred feedstock for chlorination but due to dwindling reserves other titania feedstocks are substituted as feed for pigment production. Since feedstock's differ in physical properties and mineralogy, this impacts the way each feedstock reacts in the chlorinator, even though the TiO_2 content might be similar. The aim of this investigation is to compare the chlorination of slag, rutile, and a blend of material (i.e. slag and rutile) considering chlorination mechanism and elutriation.

1.1 INDUSTRY BACKGROUND

1.1.1 Uses and properties of titanium compounds

Titanium dioxide (TiO₂) is the most common compound of titanium, about 95 - 98% of extracted titanium minerals is processed into TiO₂ white pigment (Kotze et al., 2006). The remaining 5% is used as flux for electric welding rods and for the manufacture of titanium. Titanium metal is known for its low density, high strength to weight ratio and corrosion resistance. When alloyed with other elements such as vanadium and aluminium it is suitable for use in the following industries i.e. aerospace, chemical and petro-chemical industry, dental implants and dental equipment.

TiO₂ pigment is valued because it imparts whiteness, brightness and opacity to paints, paper, plastics and ceramics. This pigment has the ability to scatter light whilst absorbing ultraviolet light and has excellent covering power.

Table 1 shows the refractive indices of various pigments and the refractive indices of media in which the pigment can be dispersed. In general, the greater the difference between the refractive indexes of the pigment and the immersion media, the greater the light scattering and the more opaque, white and bright the object appears. TiO₂ pigment has the highest refractive index and therefore provides the greatest light scattering power.

Table 1: Refractive Indices (DuPont, 2007)

White Pigments	Refractive Indices (RI)	Vehicles or Media	Refractive Indices (RI)
Diatomaceous earth	1.45	Vacuum	1.00
Silica	1.45 – 1.49	Air	1.0003
Calcium Carbonate	1.63	Water	1.333
Barytes	1.64	Polyvinyl acetate resin	1.47
Clay	1.65	Soybean Oil	1.48
Magnesium silicate	1.65	Refined linseed oil	1.48
Lithopone	1.84	Vinyl resin	1.48
Zinc oxide	2.02	Acrylic resin	1.49
Antimony oxide	2.09 – 2.29	Tung oil	1.52
Zinc sulphide	2.37	Oxidising soya alkyd	1.52 – 1.53
Titanium dioxide (anatase)	2.55	Styrene butadiene resin	1.53
Titanium dioxide rutile	2.73	Alkyd/melamine (75/25)	1.55

1.1.2 Pigment Processing Technology

Two process technologies are used for the production of white TiO₂ pigment i.e. the chloride route and the sulphate route. The sulphate route is the older of the two processes and is becoming less popular as waste disposal costs increase and environmental concerns grow over waste generation. Although the sulphate process requires less capital and has low energy consumption, the sulphate process generates up to 3 times more waste than the newer chloride process (DuPont, 2007). The chloride route was commercialised in 1958 and approximately 60% of the world's production of pigment is now produced by the chloride process. Chloride pigment production is expected to reach 70% by the end of 2010 (Veldhuisen, 2000).

Titanium dioxide pigments are manufactured in two different crystal forms, i.e. anatase and rutile. Both crystal forms can be produced via the sulphate route. The chloride process produces 100% rutile pigment which has a superior colour, more effective particle size distribution and a higher gloss than sulphate pigments (South Africa Department of Minerals and Energy (DME), 2008).

1.1.2.1 Chloride Processing Route

The first commercial chlorination process was introduced in the late 1950's; leucoxene was used as feedstock and only thirty years later did producers start using rutile. The aim of the chlorination process is to separate titanium from the host mineral in the form of a chloride (TiCl₄), convert it to TiO₂ pigment in an oxidation reactor and recover the chlorine (Fisher, 1997). TiCl₄ is an intermediate for both chloride route pigment producers and titanium metal producers (Bungu, 2004). When pure, TiCl₄ is a colourless liquid with a boiling point of 136^oC (Rowe and Opie, 1955).

TiCl₄ is commercially produced by chlorinating titania feedstocks plus reductant in a bubbling fluidised bed at approximately 1000^oC. Static bed chlorinators were used in the past but today all pigment producers use fluidised bed chlorinators (Reeves and Reeves, 1997). The excellent heat transfer and absence of channelling in the fluidized reactor permit a three to fourfold production rate per unit area as compared to the fixed bed reactor (Rowe and Opie, 1955).

The main steps of the chloride pigment processing route are illustrated in Figure 1.

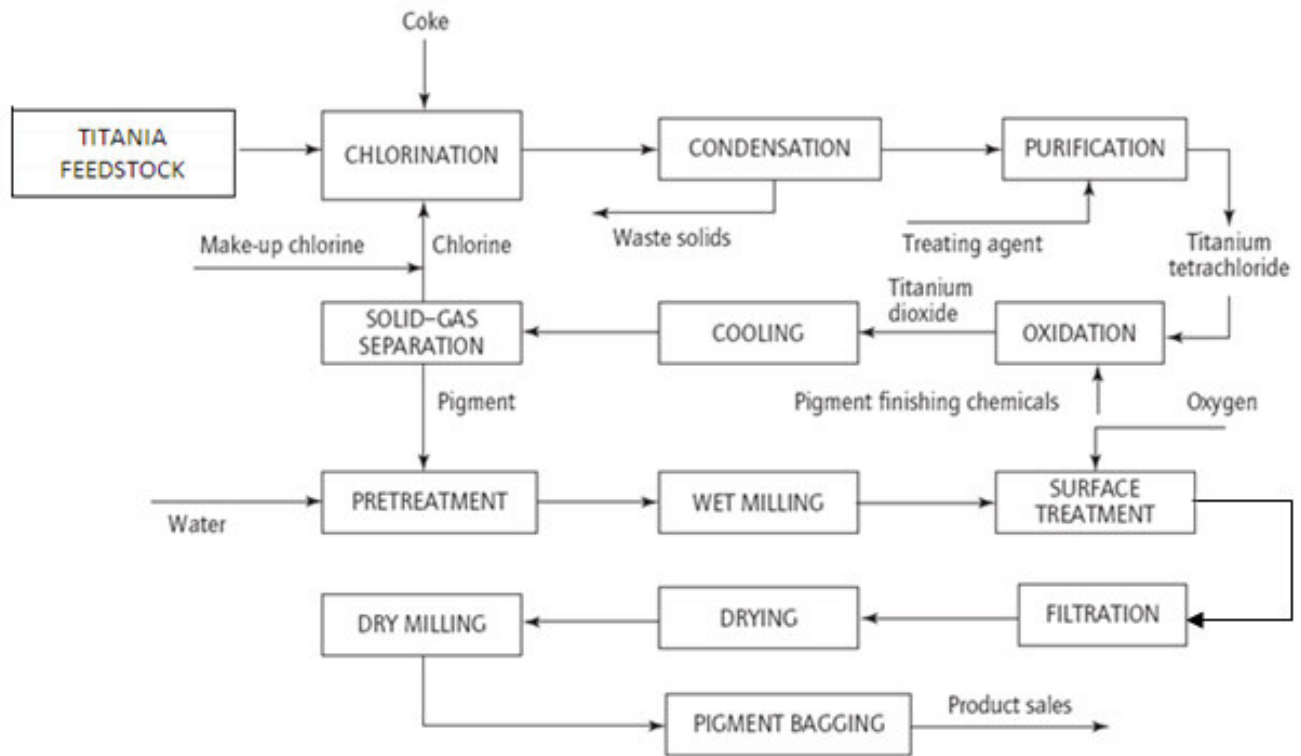


Figure 1: Chloride Process Flowsheet (Burger and Rabe, 2007)

Disregarding intermediate steps the most important chlorination reactions are (Bergholm 1961):



Reactions 1 and 2 are exothermic and reaction 3 is endothermic. The overall reaction is exothermic so an external heat supply is not required, however air or oxygen is supplied to chlorinators to maintain reaction temperature (Youn and Park, 1989).

1.1.2.1.1 Process description

The chlorinator is a long, brick lined steel reactor, with a gas chamber and gas distributor at the bottom and a feed port and product discharge line at the top. The industrial process is continuous, with the feedstock and coke charged from the top of the reactor. Chlorine velocities four times the minimum fluidizing velocity are usually used to fluidise and react with the bed. As the chlorination reactions proceed, CO is produced by the endothermic reaction of carbon with carbon dioxide and thus oxygen is added to the reactor to maintain temperature between 800 and 1000°C (Habashi, 1997). According to Reeves and Reeves (1997),

most industrial scale chlorinators are limited to 1000°C because of bed sintering and refractory damage that occurs at higher temperatures.

Calcined petroleum coke is used as the reducing agent because it has extremely low ash content and low volatile content. Coke consumption per ton TiO₂ is 250 – 300 kg and the mean particle size of coke particles is usually 5 times the size of the titania feedstock (Habashi, 1997). Large coke size fractions are used as the terminal velocity of the coke is lower than that of the feedstock's and if small size fractions are used they will be blown out of the chlorinator.

TiCl₄ gas together with other volatile metal chlorides and non-reacted or partially reacted solids exits the chlorinator top. As ore and coke particles react and diminish in size, they become entrained in the exiting gas and are carried out of the chlorinator.

The gas stream from the chlorinator is directly/indirectly cooled with liquid TiCl₄ to less than 300°C. At this low temperature, the chlorides are separated from TiCl₄ by condensation or sublimation. The cooled gaseous product stream is transferred through a series of separation steps to recover the TiCl₄ from the other chlorides i.e. fractional condensation, double distillation and chemical treatment. The conversion of TiO₂ to TiCl₄ is 95 – 100% and is dependant on reactor design and chlorine velocity. In the next stage of the process, the purified TiCl₄ is oxidised to TiO₂ at 985 °C (Reaction 4). Aluminium chloride is added in this step to promote/catalyse the formation of TiO₂. Chlorine gas is liberated during this reaction and recycled to the fluidised bed reactor. The resulting TiO₂ particles of this stage are known as raw pigment.



In the final stage of the process, the raw pigment is milled to the required particle size, treated with chemicals (i.e. sodium aluminate and sodium silicate) to enhance surface properties, dry milled and then packaged.

1.2 JUSTIFICATION

Rutile, is the preferred feedstock for the chlorination process but today due to dwindling reserves different feedstock's (i.e. slag, rutile, synthetic rutile, UGS etc) and blends are fed to chlorinators. Though the TiO_2 content maybe the same, the mineralogy and physical characteristics of the feedstock's differ. The aim of this study is to physically and chemically characterise the feedstock's and determine how these differences affect chlorination rates, carryover and chlorination mechanism. Full characterisation of the feedstock will provide valuable insight to gaining the best understanding of the process. Especially when considering chlorination of feedstock blends of material is a new subject, full characterisation becomes necessary to explain experimental results.

Numerous studies were completed on the chlorination of slag, rutile and synthetic rutile however no literature was found on the chlorination of feedstock blends. Since producers now feed a blend of feedstocks to the chlorinator it becomes important to understand how this affects chlorinator performance.

Mineralogical analysis of the chlorination bed residue will provide additional information of the chlorination mechanism.

Two titania slags with different TiO_2 contents will be compared in this study. Slag B has a TiO_2 content that is closer to that of rutile, it will be interesting to note if this slag behaves as a rutile particle.

1.3 PROBLEM STATEMENT

Due to the cost and availability of rutile (*i.e.* the feedstock of choice for the chloride process) a number of chloride producers are now forced to feed a blend of feedstocks to the chlorinator. Although the TiO_2 content of the feedstocks may be the same, the different feedstocks (*i.e.* slag, rutile, synthetic rutile and ilmenite) vary in TiO_2 content, impurity content and physical properties (*i.e.* size distribution, density and shape factor). These factors can have a significant effect on chlorinator performance; process stability, throughput, elutriation figures (*i.e.* blowover from the chlorinator), waste generation and thus influence the design of the chlorination circuit. For the purpose of the study, individual feedstocks and a blend of two feedstocks (*i.e.* slag and rutile) were chlorinated.

The study aims to highlight the differences in chlorination mechanism between rutile and slags, compare chlorination of different TiO_2 content slags and behaviour of the blend. The effect of the physical behaviour of blend material is an unknown and was also investigated.

1.4 HYPOTHESIS

- The chlorination mechanism for rutile and slag differs. Chlorination of iron leaves behind a porous matrix with a larger surface area for reaction, this means that slag chlorination will be faster than rutile
- It is expected that the blend (i.e. a mixture of 50wt% Slag and 50wt% Rutile) behaviour will not be as simple as lying between that of its individual components. Shape factor, particle size distribution, average density and bed voidage are parameters that will change in the mixed bed. Minimum fluidising velocity, terminal velocity, entrainment and elutriation will be affected by a change in these factors. The combination of these changes will most likely result in a non linear change in chlorination behaviour.

1.5 OBJECTIVES OF THE RESEARCH

The aim of this research is to:

- Determine physical and hydrodynamic properties of the various feedstocks (*i.e.* density, particle size distribution, shape factor, minimum fluidising velocity, terminal velocity and elutriation constants). Feedstock's included in this study were rutile, slag and blends of rutile and slag.
- Compare reaction rates of various titania feedstocks
- Investigate behaviour of blend material in the chlorinator
- Investigate the chlorination behaviour of individual species
- Investigate the chlorination behaviour of Ti_2O_3
- Compare with published reaction rate
- Characterize chlorination products through chemical analysis, Scanning Electron Microscopy(SEM)

1.6 LAYOUT OF THESIS

Based on the background information as described in Chapter 1, the investigation into the chlorination of slag and rutile was conducted as follows:

Chapter 2 consists of a literature review of titania feedstocks, chlorination investigations of rutile, ilmenite, synthetic rutile and titania slag. Kinetic data on the various feedstock's are listed; this will be used for comparison purposes in Chapter 5. The latter half of the Chapter is dedicated to reviewing fluidisation theory.

Chapter 3 describes the detail of the experimental set up and methodology of the fluidisation and batch chlorination experiments. The techniques employed for analysis of the chlorination products are also discussed in this chapter.

Chapter 4 discusses the results obtained from the chlorination experiments as well as the product analysis. The chemical results and SEM work are included. The effect of time, temperature, blending of feedstock and comparison of reaction kinetic with previous studies are also presented in this chapter.

The research report was concluded in Chapter 5 which contains the conclusions and recommendations for future work.

CHAPTER 2

2. LITERATURE REVIEW

The literature review is divided into 3 sections i.e. feedstock production, chlorination, and fluidisation principles.

Background information on the feedstock's used in the chlorination process is supplied. This provides some perspective on the differences between the production techniques of the various feedstocks which will in turn explain the difference in physical properties and behaviour in the chlorinator.

The second part of the chapter is a review of literature on chlorination. Studies have been completed on rutile, synthetic rutile, ilmenite and slag. No investigations into the behaviour of a feedstock consisting of a blend of two feedstocks have been reported.

Since the chlorination process is carried out in a fluidised bed reactor, it is important for the purposes of this study to understand fluidisation theory and the effect of particle physical properties on chlorinator performance. Currently combinations of feedstock's are fed to commercial chlorinators and though the TiO_2 content of the feed may be the same the behaviour of the material in the beds can be very different as mineralogy, morphology, density and particle size distribution of rutile, synthetic rutile, ilmenite and slag varies.

2.1 TITANIA FEEDSTOCKS FOR THE PIGMENT INDUSTRY

Titanium (Ti) is the ninth most abundant element on earth and occurs mainly in a form that can be mined as ilmenite ($\text{FeO}\cdot\text{TiO}_2$) and rutile (TiO_2) minerals (Sahu et al., 2006). Other titanium bearing minerals include anatase, brookite and leucosene. Figure 2 illustrates the various processing routes that the titania minerals can follow to reach final products (*i.e.* pigment or titanium sponge).

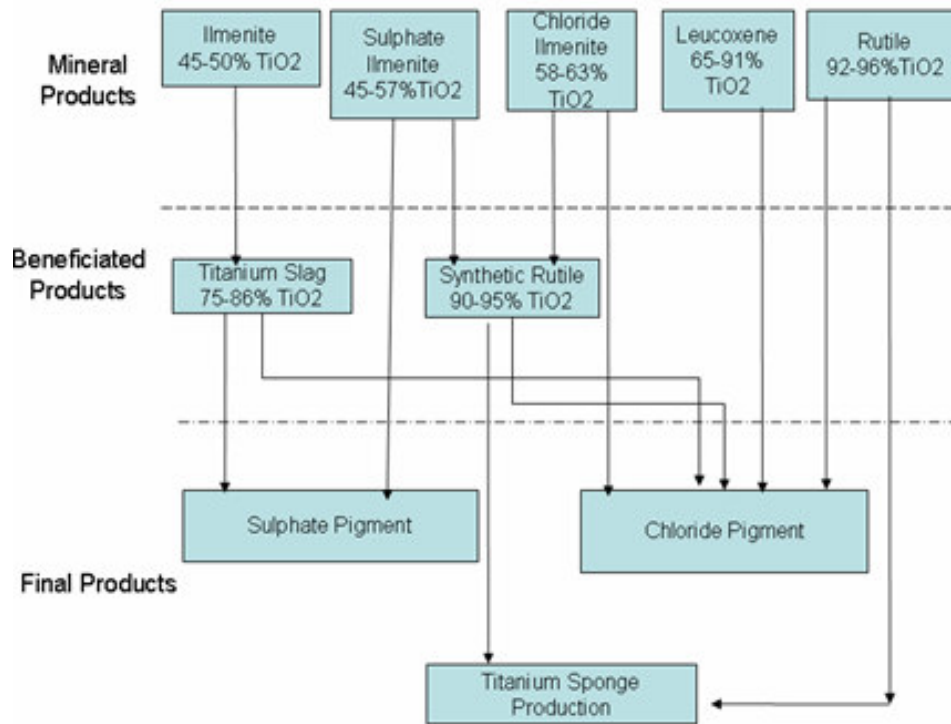


Figure 2: Process Routes in the Ti/TiO₂ industry (Murty et al., 2007)

Since the study focuses on the chlorination of rutile and slag, a product of ilmenite smelting, only these feedstocks will be discussed further.

2.1.1 Rutile

Rutile (93-95% TiO₂) is the purest naturally occurring form of TiO₂. Natural rutile is the preferred feedstock for chlorination because it contains low amounts of problem causing impurities, is readily chlorinatable to high purity TiCl₄ and presents minimal operational and waste disposal problems (Stanaway 1994). Rutile is insoluble in sulphuric acid and is therefore not used in the sulphate process.

2.1.2 Processed Ilmenite as Feedstock

Ilmenite (FeTiO_3) is the most abundant titania bearing mineral and contains between 45 and 60% TiO₂. The largest deposits of ilmenite are found in South Africa, Norway, India and Canada. Unlike rutile, ilmenite can't

be used directly in pigment production processes and has to be treated in order to upgrade the TiO_2 content. Existing commercial processes for upgrading ilmenite is electro-smelting to produce a titania rich slag and synthetic rutile production which involves leaching of the iron fraction. Figure 3 shows the various technologies (commercial and development) available for the upgrading of ilmenite.

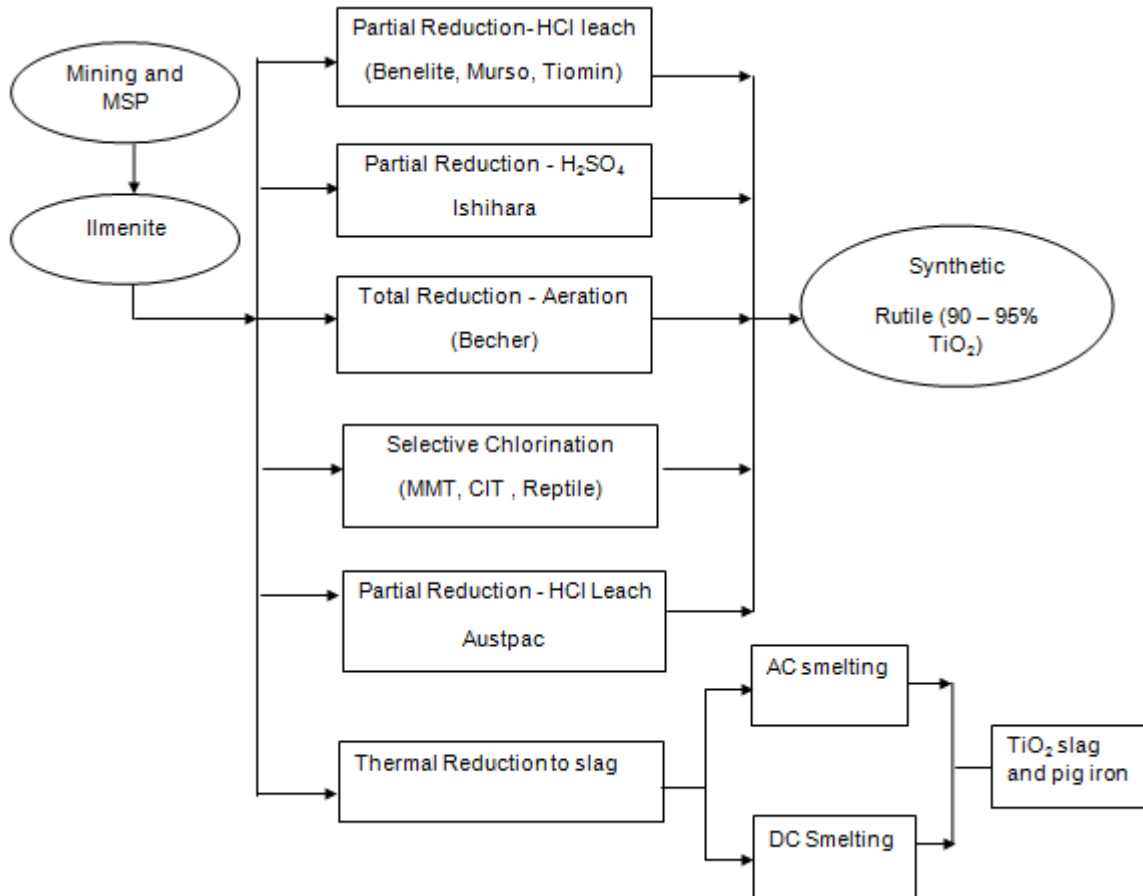


Figure 3: Technologies for upgrading of ilmenite (Murty et al., 2007)

2.1.2.1 Titania Slag Production

Ilmenite is smelted in an electric furnace with a carbonaceous reductant to yield TiO_2 rich slag as the primary product and pig iron and CO rich gas as by-products. The process flow is illustrated in Figure 4. Ilmenite pre-reduction and pre-heating are variables in the process flowsheet. Pre-reduction and pre-heating reduce the amount of electric energy required for the smelting process. Ilmenite pre-reduction is currently only employed at the Tinfos plant in Norway.

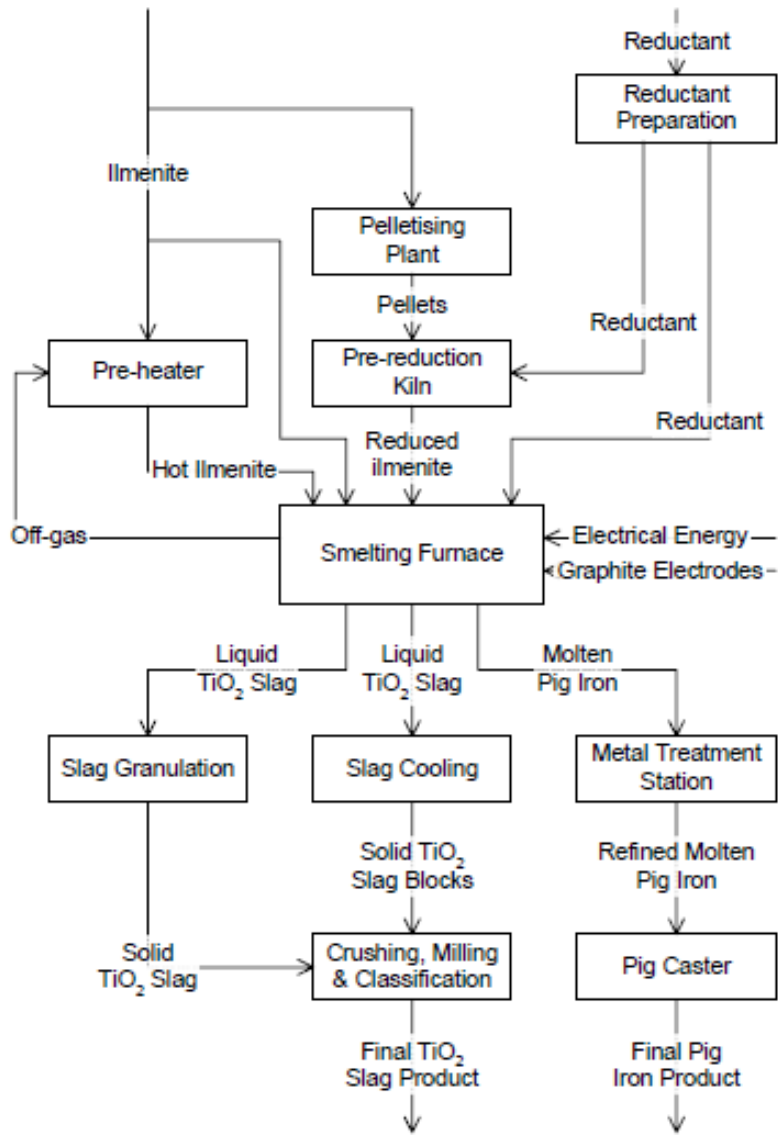


Figure 4: Ilmenite Smelting (Zietsman, 2004)

The final slag quality is dependant on the ilmenite and reductant quality since virtually all impurities (*i.e.* MnO, MgO, CaO, Al₂O₃ and SiO₂) report to the slag. These impurities make up about 6 % (by mass) of the slag chemistry (Pistorius and Le Roux, 2002). The chloride process is very sensitive to impurities (*i.e.* CaO and MgO) so good quality reductant is required for the smelting process. Anthracite is normally used. Table 2 shows typical slag qualities of the various slag producers.

Table 2: Typical Slag Qualities (Murty et al., 2007)

Quality (%)	TiO ₂ slag from Indian Ilmenite	RBM - Chloride Slag	Namakwa - Chloride Slag	Tinfos - Sulphate Slag	QIT -Sulphate Slag
TiO ₂	88.00	85.50	86.00	80.00	80.00
Fe(t)	10.00	10.60	9.00		
Al ₂ O ₃	1.30	1.30	1.40	1.70	2.90
SiO ₂	1.70	2.10	1.80	4.50	2.40
MnO	0.60	1.70	1.70		0.25
Cr ₂ O ₃	0.08	0.17	0.08	0.13	0.17
V ₂ O ₅	0.28	0.44	0.40		0.57
MgO	1.20	1.10	0.70	5.50	5.00
CaO	0.03	0.17	10.60		0.60
S					0.06
U (ppm)	17	15-30	10		
Th(ppm)	130	15-30	10		

FeO acts as a flux in the process and as FeO content decreases and TiO₂ content of the slag increases, higher operating temperatures are required for smelting. This places a limit on the minimum level of FeO that can be present in a typical slag. In the process of reducing the FeO some TiO₂ is reduced to Ti₂O₃ (Figure 5 depicts the relationship). Ti₂O₃ is not highly desired as it does not increase the equivalent TiO₂ content of slag but consumes more electrical energy and carbon (Pistorius, 2001). The chlorination reaction of Ti₂O₃ is also highly exothermic and cause hotspots in the chlorinator bed which can lead to sintering.

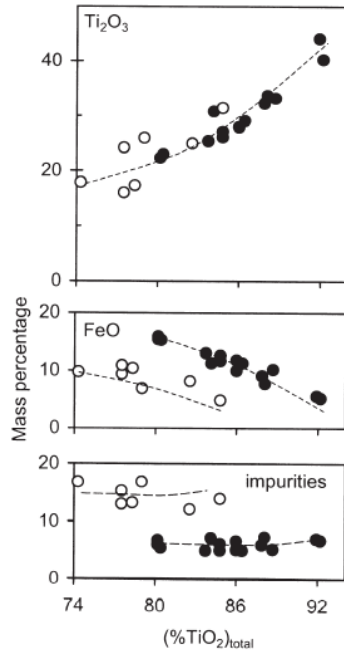


Figure 5: Changes in FeO and Ti₂O₃ content of ilmenite smelter (Zietsman and Pistorius, 2004)

Filled circles indicate slags produced from South African ilmenite and empty circles indicate slags produced from Canadian ilmenite

There are three titania slag producers in South Africa i.e. Richards Bay Minerals (RBM), KZN Sands and Namakwa Sands. The KZN Sands and Namakwa Sands plant utilise DC smelting technology. RBM has rectangular six inline AC furnaces.

2.1.2.1.1 Slag Mineralogy

There are four mineralogical phases (i.e. solid solution, rutile, metallic iron and glassy) present in high titania slags (Bessinger et al., 1997). The major phase is a solid solution referred to as the M₃O₅ phase. This phase is a solid solution of the end members FeTi₂O₅, Ti₃O₅, MnTi₂O₅, MgTi₂O₅, Cr₂TiO₅, Al₂TiO₅ and V₂TiO₅ (Kotze, 2007).

The second most prominent phase is the glassy phase. The SiO₂ and CaO form separate silicate phases between the M₃O₅ phases.

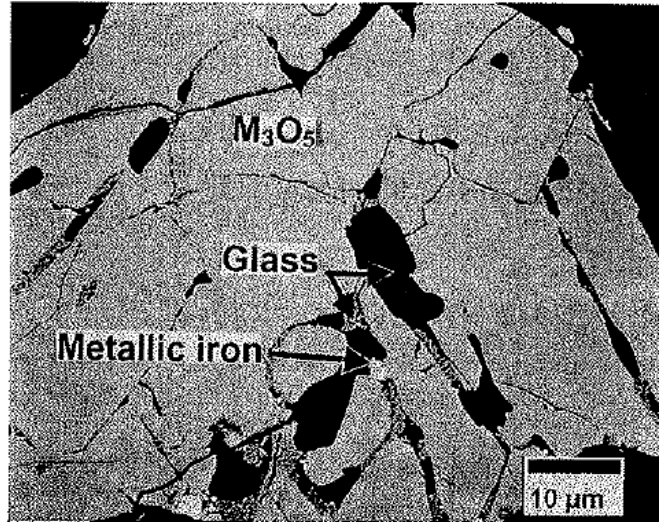


Figure 6: Micrograph of slag indicating the M_3O_5 , glassy and metallic iron phases (van Dyk and Pistorius, 1999)

2.1.2.2 Synthetic Rutile Production

In synthetic rutile production, the feedstock (ilmenite/leucoxene) is upgraded by partial or total reduction of iron followed by leaching to remove iron. The result is synthetic rutile, which contains 90 – 94% TiO_2 and has a suitable grain size for the fluidised bed chlorinator. The chemical composition of synthetic rutile is similar to natural rutile but differs in physical form. Two technologies that reached commercialisation are the Becher and Kerr McGee processes.

2.1.3 Feedstock requirements for the chloride process

The feedstock requirements are dependant on the producer's chlorination and purification process and their ability to dispose of the waste streams arising from the process. It is estimated that about thirteen kilograms less waste is generated/ton feedstock treated for every percentage point increase in TiO_2 feedstock (Burger et al., 2009).

The chloride process has very stringent feedstock requirements:

- CaO and MgO content of the feedstock is normally restricted to 0.2 and 1.2% respectively as these compounds form chlorides ($CaCl_2$ and $MgCl_2$) with high boiling points (See Figure 7) which can liquefy in the chlorinator and causes operational problems such as stickiness and defluidization. CaO is also problematic because it reduces TiO_2 chlorination by forming $CaO \cdot TiO_2$ (Minkler and Baroch, 1981). The abovementioned specifications for CaO and MgO are negotiated with each customer and thus variances between suppliers may occur.
- Restrictions are also placed on the SiO_2 content as certain forms of silica (i.e. alpha quartz) do not react in the chlorinator but merely accumulate in the bed and must be periodically removed. The

more SiO_2 , the more frequent the bed drains and the greater the plant downtimes. SiO_2 also coats the TiO_2 particles and prevents the reaction with chlorine (Stanaway, 1994)

- Low FeO is desired as to minimise waste generation (i.e. iron chlorides) and chlorine consumption.
- Arsenic levels must be low. Although arsenic chlorinates readily, it is difficult to separate from TiCl_4 as boiling points are close (See Figure 7)
- For environmental reasons low levels of uranium and thorium are required for both sulphate and chloride route.
- Aluminium is undesirable because it consumes chlorine at a higher rate than other metals. Aluminium trichloride is soluble in TiCl_4 and causes corrosion problems in the plant because it attacks carbon steel.
- The feedstock has to have sufficient grain size and bulk density to minimize blowover in the chlorinator. Slag and rutile have an advantage over synthetic rutile since the latter has a porous structure (Stanaway, 1994). Coarser particles are required for chloride process; this decreases entrainment and blowover.

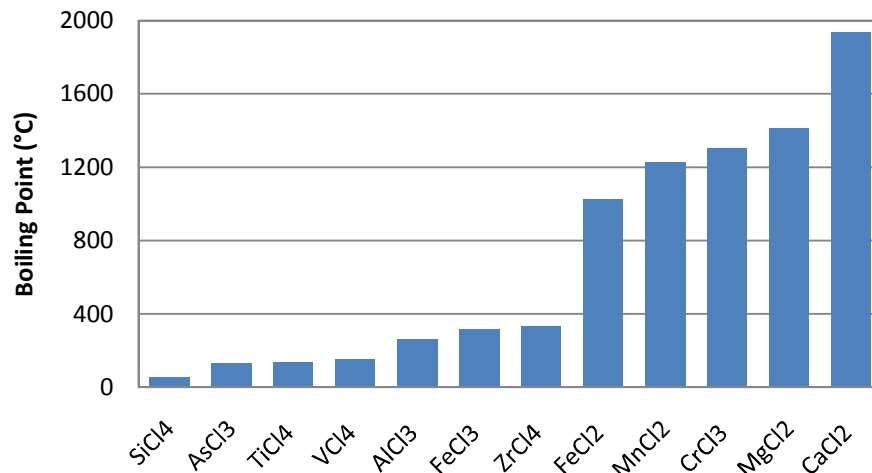


Figure 7: Boiling Points of Metal Chlorides

2.2 CHLORINATION

2.2.1 Effect of Carbon and CO

Den Hoed and Nell (2002), Dunn (1979) and Bergholm (1961) studied the chlorination of titania feedstocks with carbon and CO and found that the presence of carbon significantly improved the reaction rate. Also demonstrated was that intimate contact between carbon particles and the feedstock is required for good reaction rates or the reactions proceed as if there was no carbon in the bed. Barin and Schuler's (1980) investigation of the chlorination of TiO₂ tablets placed alongside carbon concluded that chlorination rate is 40 to 50 times faster with carbon than without and that rate of chlorination decreases with increasing distance between carbon and TiO₂.

Den Hoed and Nell (2002) noted that the degree of chlorination increased with increasing carbon content but levelled off at 15% carbon. At carbon levels lower than 15wt%, availability of carbon is the rate limiting step but once the stoichiometric requirement is exceeded the reaction proceeds unhindered. Dunn (1979) showed that reaction rate increases linearly with increasing carbon content until 25wt%.

Den Hoed and Nell (2002) also investigated the effect of the CO on the reaction rate with carbon in the bed and showed that the absence of CO only slightly decreases reaction rate. According to den Hoed and Nell (2002), good rates of chlorination are attainable at 1000°C in a vigorously fluidized bed containing 20% solid carbon and 35% Cl₂. Den Hoed and Nell (2002) compared chlorination results of coke to more reactive carbons i.e. carbon black and activated carbon and found that reductant reactivity played a small role in reaction kinetics.

Dunn (1979) found through chlorination of rutile with carbon and carbon monoxide that small amounts of CO does not affect the reaction rate significantly but large additions tend to have a sharp negative effect on reaction kinetics. The effect becomes more serious as carbon particle size decreases and the authors suspect that the CO absorbs onto the carbon surface preventing the other reagents from reaching the surface.

Bergholm (1961) chlorinated Australian rutile with CO and then carbon and found that carbon activity and distance between carbon and rutile particles had a significant effect on reaction kinetics.

2.2.2 Chlorination Mechanism

The chlorination mechanism of slag, rutile and synthetic rutile has been widely investigated and it is generally accepted that mechanism differs for the various feedstocks. This is due to the difference in FeO content.

Zhou et al., (1996) chlorinated slag and rutile with petroleum coke and CO and examined the microstructure of chlorination products. The authors found that the iron oxide content of the titania feedstock contributes significantly to the manner in which the solid changes during the chlorination reaction. When slag is chlorinated, the rapid chlorination of the iron oxide creates porosity that extends deep within the particles and thus there is a much greater surface area on which the chlorination reaction can occur. With rutile, the particle is attacked from the outside and mechanism is expected to follow the shrinking core model. Therefore the rate of chlorination of titania slag per unit area for slag is expected to be higher than rutile. Chlorination of rutile occurs exclusively on the surface of the particle at a rate proportional to the receding surface area (Morris and Jensen, 1976)

Pistorius and Le Roux (2002) chlorinated titania slag with CO and within the first five minutes of the reaction, over 95% of the Fe and Mn was chlorinated (Figure 8).

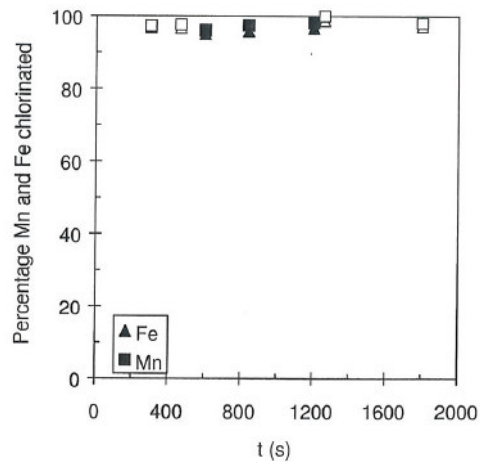


Figure 8: Fe and Mn removal during first few minutes of chlorination (Pistorius and Le Roux, 2002)

The chlorinated iron and manganese leave behind pores in the particles which increases the surface area for subsequent reaction. The chlorination of TiO_2 proceeds at a much slower rate compared to the chlorination of Fe and Mn.

Den Hoed and Nell (2003) investigated chlorination of various titania feedstocks with CO and solid carbon (27% of the charge) at $1000^{\circ}C$ and found that ilmenite chlorinates faster than titania slag and slag chlorinates faster than rutile (Figure 9). The rate of chlorination is proportional to the iron content of the feedstock. The relationship exists because:

- FeO is chlorinated more readily than TiO_2
- Chlorination of FeO leaves behind a porous structure with a larger surface area.

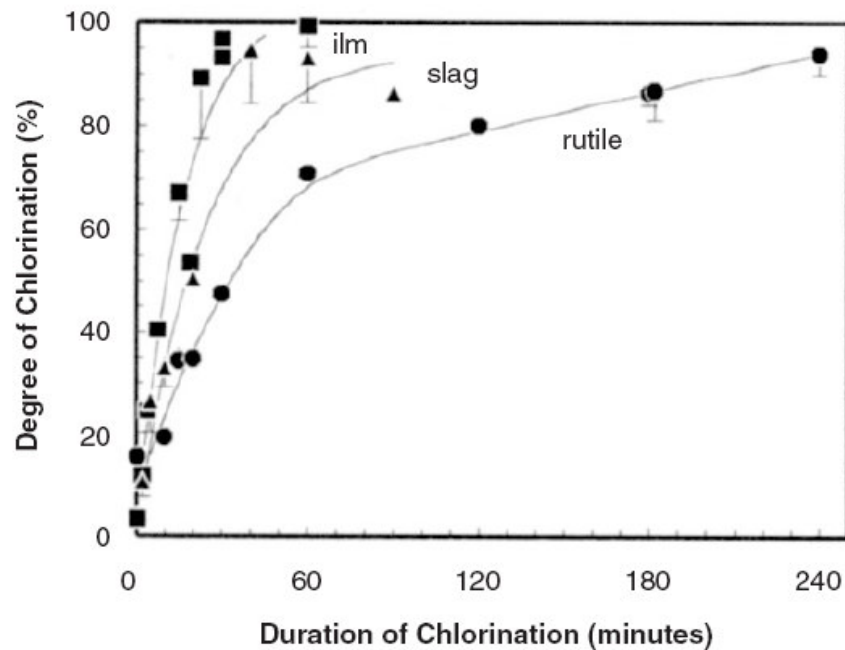


Figure 9: Rates of chlorination (Den Hoed and Nell, 2003)

Although increasing FeO content improves chlorination kinetics, too much FeO is undesirable as large amounts of waste must be disposed off.

Zhou et al (1996) found that the final products on the surface layer of partially chlorinated rutile were TiO_2 , TiO and a small amount of Ti_3O_5 .

Morris and Jensen (1976) has suggested the formation of $TiOCl_2$ and $TiCl_2$ (relatively stable chlorination products) that coat the surface of the TiO_2 particles and limits the access of Cl_2 and CO to the particle

2.2.3 Chlorination of Ti^{3+}

In ilmenite smelting, some TiO_2 is reduced to Ti_2O_3 . Typically as the FeO content of the slag decreases, the Ti_2O_3 content increases. Den Hoed and Nell (2003) and Le Roux (2001) have given some attention to the chlorination of Ti_2O_3 in recent years.

Den Hoed and Nell (2002) argued that Ti_2O_3 chlorinates within the first few minutes of reaction. The argument is substantiated by an observed increase in bed temperature (Figure 10) which they associated with the chlorination of Ti_2O_3 . Ti_2O_3 chlorination (Reaction 5) is more exothermic than that corresponding to TiO_2 chlorination (Reaction 6).

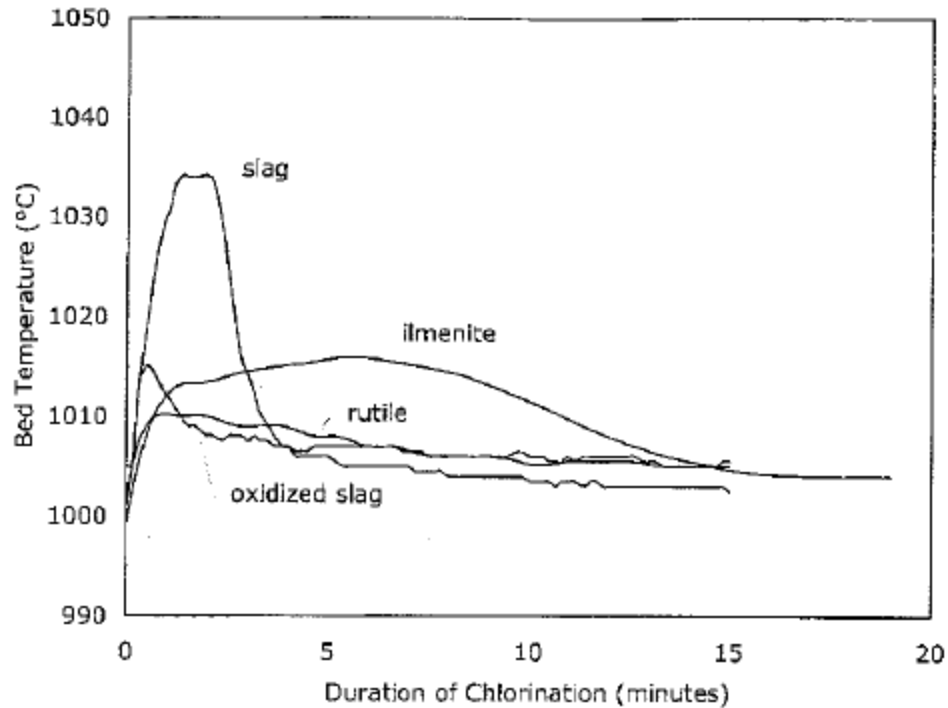
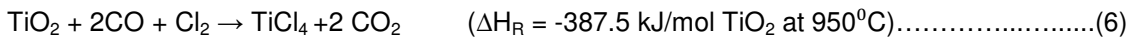
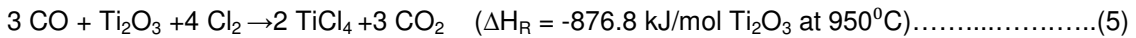
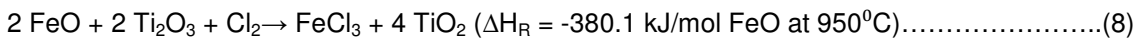
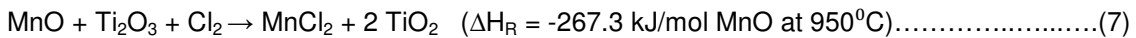


Figure 10: Bed temperature during first few minutes of chlorination (den Hoed and Nell, 2002)



When oxidised slag and ilmenite were chlorinated, a smaller temperature increase was observed; this further substantiates the idea that the chlorination of Ti_2O_3 causes the spike in bed temperature.

Le Roux (2001) chlorinated slag in the absence of reductant (i.e. no coke and/or CO) and found that chlorination reactions still took place albeit to a lesser extent. Le Roux (2001) demonstrated by mass balance methods that there was enough Ti_2O_3 to act as a reductant for the chlorination of FeO and MnO according to Reaction 7 and 8.



This suggestion was supported by the increase in bed temperature (Reaction 7 and 8 are exothermic). An energy balance revealed that the temperature increase could not solely be attributed to Reaction 7 and 8 and that a portion of Ti_2O_3 was chlorinated in the process.

2.2.4 CHLORINATION REACTIONS

Dunn (1979) discovered the autocatalytic nature of $TiCl_4$ and proposed that small amounts of $TiCl_4$ are generated through Reaction 9 to start the chlorination process. Thereafter $TiCl_4$ and TiO_2 react under equilibrium to form gaseous titanium oxychloride, which diffuses out of the boundary layer of the rutile particle and is transported by diffusion to the carbon particle surface. The oxygen from the titanium oxychloride and the carbon reacts to form carbon oxides, chlorine is absorbed and $TiCl_4$ is formed.



Knudsen cell mass spectrometry has since identified $TiOCl_2$ as an intermediate reaction product not $TiOCl_2 \cdot TiCl_4$ (Nell and den Hoed (2003)).

The observations made by Nell and den Hoed (2003) support Dunn's (1979) theory. Nell and den Hoed (2003) propose that gaseous titanium oxychlorides (possibly $TiOCl_2$) form at reduced surface sites on the titanium oxide particle. Gaseous titanium oxychlorides is adsorbed onto carbon particles where reaction with chlorine results in formation of gaseous $TiCl_3$. The liberated oxygen reacts with carbon to form CO. $TiCl_3$ reacts with Cl_2 to form $TiCl_4$. In the absence of carbon, $TiOCl_2$ reacts with Cl_2 gas to form oxygen and $TiCl_3$, the oxygen reacts with CO to form CO_2 , but the conversion of CO to CO_2 is inhibited by the presence of Cl_2 and thus so is the formation of $TiCl_3$. This explains the need to have carbon intimately mixed with the titanium particles. At a temperature of $1000^{\circ}C$ and in the presence of Cl_2 , solid carbon is a superior scavenger of O_2 than CO thereby promoting the formation of Ti_2O_3 surface sites and the formation of $TiCl_3$ (Nell and den Hoed, 2003).

Rhee and Sohn (1990) studied the chlorination of ilmenite with CO and proposed that the iron in ilmenite reacts with Cl_2 first and the liberated O_2 is removed by carbon monoxide. The reaction proceeds rapidly initially but then slows down. The authors propose that this is due to the formation of high boiling liquid phases which block the particle pores and prevent reaction gases from reacting with the particle.

Jena et al., (1998) chlorinated TiO_2 powder and graphite powder (20 – 25wt %) and proposed the following chlorination mechanism:



2.2.5 Kinetic Models

Several studies were conducted on the carbo-chlorination of rutile, ilmenite and slag with various models being formulated to predict and explain the kinetic behaviour of these feedstock's during chlorination. However, chlorination kinetics has remained a relatively poorly understood process with results of the models differing from each other. Although no kinetic model is proposed in this study, results from the experimental work are compared to models discussed here.

Chlorination mechanism will affect the reaction kinetics. As discussed earlier, the mechanism for the various feedstock's differ because of the different physical and chemical properties of the feedstocks. In slag and ilmenite the FeO is chlorinated rapidly leaving behind a porous particle with a large surface area for reaction. Once the FeO has been removed, the chlorination of the remaining TiO₂ is essentially the chlorination of rutile. Synthetic rutile is porous and therefore should chlorinate faster than natural rutile.

Dunn (1960) chlorinated several titaniferous feedstock's (i.e. ilmenite, Canadian slag, and Australian rutile) with CO and Cl₂ and found the chlorination rate for rutile to be linearly dependant on Cl₂ and CO partial pressure and proportional to the weight of the ore.

Morris and Jensen (1976) studied the chlorination of Australian rutile in a CO-Cl₂ and C – Cl₂ system and proposed empirical equations for both systems. The authors found the activation energy for a C-Cl₂ system was much less than the CO system (45.2 vs 158 kJ/mol). Coke was a far better chlorination promoter than CO and at 1000°C the chlorination rate with carbon was 19 times greater than with CO.

Sohn et al., (1998) investigated the fluidised bed chlorination of natural rutile in CO-Cl₂ mixtures. A rate equation was determined for the temperature range 950°C – 1150°C.

Sohn and Zhou (1998) studied the chlorination kinetics of titania slag with chlorine gas and petroleum coke. A rate equation which incorporates the effects of temperature, chlorination partial pressure and initial particle size was established.

Sohn and Zhou (1999) proposed a rate equation for the chlorination of beneficiated ilmenite (i.e. synthetic rutile) in a CO, Cl₂ atmosphere. Since synthetic rutile is more porous than natural rutile, reaction kinetics for the two feedstocks were expected to differ. The shrinking core model was not applicable for this feedstock as pore diffusion occurred simultaneously with chemical reaction inside the particle. Sohn and Zhou (1999) compared the kinetics of beneficiated ilmenite to a previous study of natural rutile and found that beneficiated ilmenite chlorinated much faster than natural rutile. This is mainly due porous nature of synthetic rutile.

Le Roux (2001) studied the chlorination rate of titania slag in a fluidised bed reactor. The effects of CO and Cl₂ partial pressure, particle size and temperature were examined and a rate model was proposed. The model is only valid to explain the first 20% of TiO₂ chlorination.

A summary of the reaction condition and rate equations for the above-mentioned studies is illustrated in Table 3.

Table 3: Summary of kinetic studies conducted on TiO₂ feed stocks

Author	Materials	Temp °C	PSD μm	Partial pressures kPa	Activation energy (kJ/mol)	Rate Equation
Morris and Jensen(1976)	Rutile CO Cl ₂	870-1038	149-177	CO: 25.33-50.65 Cl ₂ : 25.33-50.65	158	$1 - (1 - X)^{1/3} = 6065(p_{CO} p_{Cl_2})^{0.665} \exp\left(\frac{-1.90 \times 10^4}{T}\right) t$
Morris and Jensen(1976)	Rutile Coke Cl ₂	955-1033	149-420	Cl ₂ 25.325-50.65	45.2	$1 - (1 - X)^{1/3} = 0.294 \exp\left(\frac{-10.820}{RT}\right) \cdot p_{Cl_2}^{0.692} d_c^{-0.55} \left(\frac{coke}{ore}\right)^{0.376} t$
Sohn et al (1998)	Rutile CO Cl ₂	950-1150	38-250	CO and Cl ₂ 0.9-57	175	$1 - (1 - X)^{1/3} = 2.87 \times 10^4 d_p^{-1} p_{CO}^{0.55} p_{Cl_2}^{0.74} \exp\left(\frac{-2.10 \times 10^4}{T}\right) t$
Sohn and Zhou (1998)	Slag (84.6% TiO ₂) Coke Cl ₂	950 - 1120	53 - 300	17 - 86	29	$1 - (1 - X)^{1/3} = 2.93 \times 10^{-4} d_p^{-0.2} p_{Cl_2}^{1.5} \exp\left(\frac{-3488}{T}\right) (t - t_0)$ with $t_0 = 0.042 \exp\left(\frac{6900}{T}\right)$ and $X = 0$ for $0 \leq t \leq t_0$
Le Roux (2001)	TiO ₂ Slag (86 - 89%TiO ₂) CO Cl ₂	910-950	106-850	CO: 25.8-60.2 Cl ₂ : 8.6-25.8	28.8	$X_T = X_{TiO_2}^{init} + \left(2.45 \times 10^3 d_p^{-0.14} p_{CO}^{0.84} p_{Cl_2}^{0.47} \exp\left(\frac{-28.8 \times 10^3}{RT}\right) t \right) (1 - X_{TiO_2}^{init})$ where $X_{TiO_2}^{init} = 7.9 \times 10^3 p_{CO}^{0.21} p_{Cl_2}^{0.09} N^{1.9} \exp\left(\frac{-66.5 \times 10^3}{RT}\right) t$ and $X_T \leq 0.2$
Sohn and Zhou (1999)	Beneficiated ilmenite/SR (92% TiO ₂) Coke Cl ₂	900-1050	63-252	CO: 9.6-57.4 Cl ₂ 9.6-57.4	156	$\lambda \left[\exp\left(\frac{X}{\lambda}\right) - 1 \right] - b = 69 \exp\left(\frac{-18800}{T}\right) p_{CO}^{0.82} p_{Cl_2}^{1.05} t$ Where $b = 3.32 d_p^{-0.8}$ and $\frac{1}{\lambda} = 1.32 \times 10^3 d_p^{0.36} \exp\left(\frac{-11700}{T}\right)$

It is clear from literature that the chlorination rates of slag, rutile, synthetic rutile and ilmenite is expected to be different since the physical properties of the material differ. Using the models presented in Table 3, Figure 11 to Figure 14 were plotted for the following conditions:

- $P_{Cl_2} = 60.2 \text{ kPa}$
- $P_{CO} = 25.4 \text{ kPa}$
- Particle size = $150 \mu\text{m}$
- Temperature = 1000°C
- Coke/ore ratio = 0.2

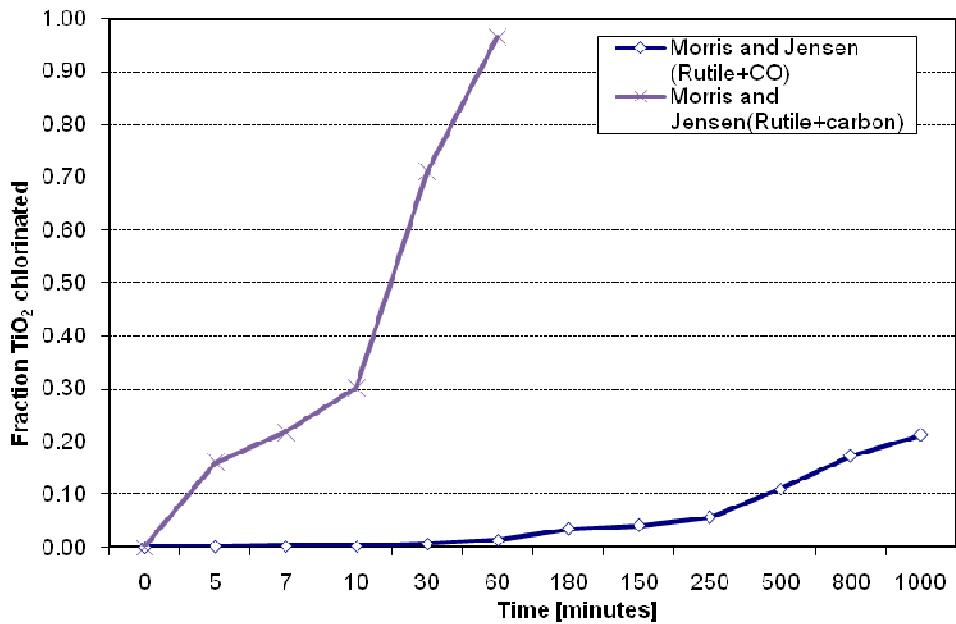


Figure 11: Chlorination of Rutile (C-Cl₂ system vs CO-Cl₂ system)

Morris and Jensen (1976) proposed rate equations for the C-Cl₂ and CO-Cl₂ systems, Figure 12 shows that the presence of carbon dramatically increases the chlorination rate.

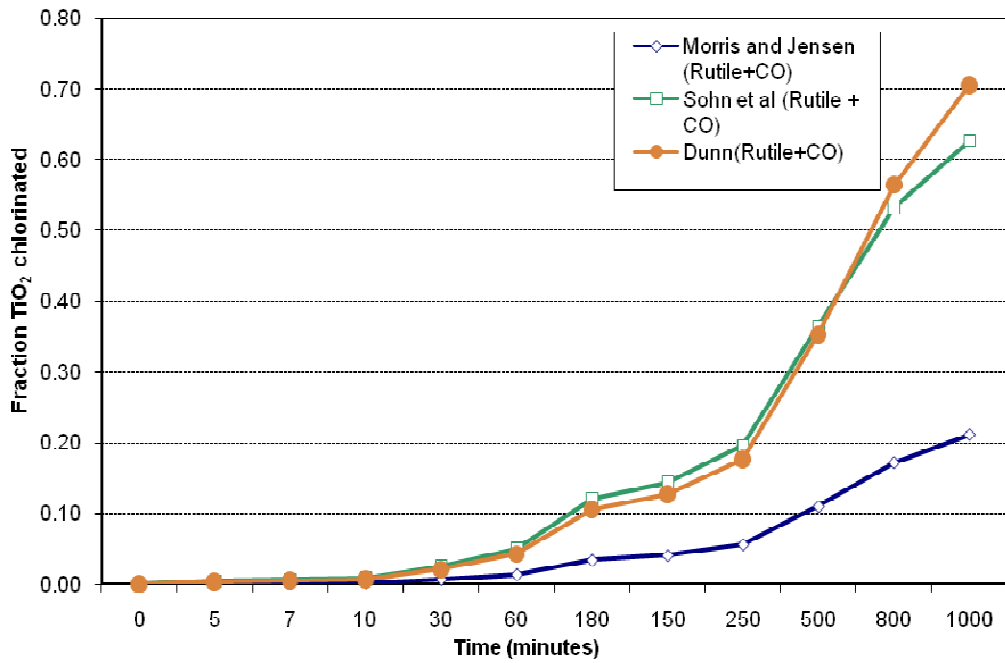


Figure 12: Chlorination of Rutile (CO-Cl₂ system)

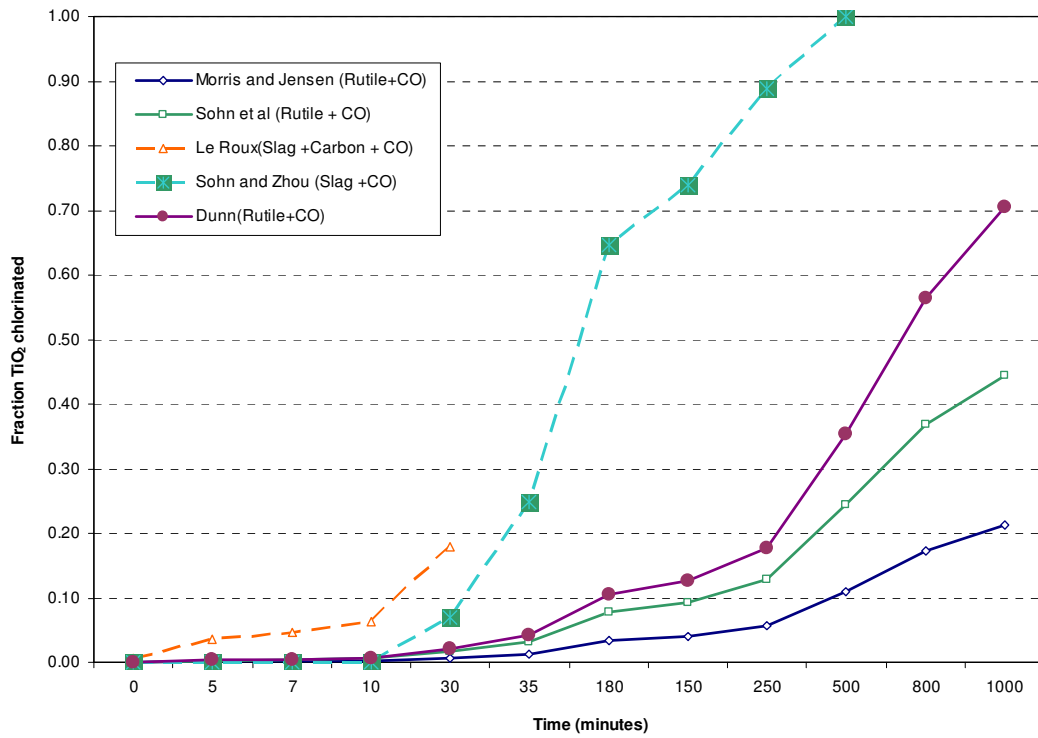


Figure 13: Chlorination of rutile vs slag (CO-Cl₂ system)

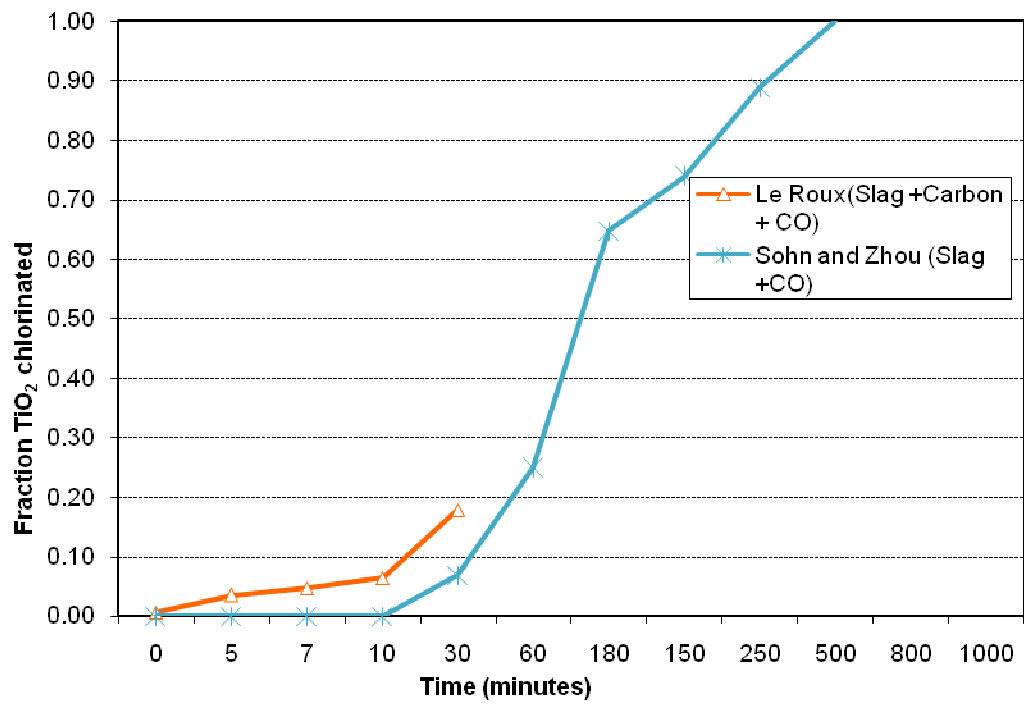


Figure 14: Chlorination of Slag (C-CO- Cl_2 system vs CO- Cl_2 system)

2.3 FLUIDISATION BACKGROUND

2.3.1 Fluidisation principles

A fluidised bed is a packed bed through which fluid flows at such a high velocity that the bed is loosened and the particle fluid mixture behaves as though it is a fluid (Kunii and Levenspiel (1969)). The fluid can either be a gas or liquid and should be sufficient to suspend the particles but not large enough to transport particles out of the reactor. Elutriation is the process in which fine particles are carried out of the fluidised bed due to the fluid flow rate passing through the bed (Chase, 2010). The material that is elutriated is known as blowover/carryover.

Feedstock fines (<106µm) are undesirable as this material is elutriated and re-circulates through the reactor, decreasing the chlorinator capacity and leading to lower chloride gas efficiencies. Occurrence of fine particles in the chlorinator is as a result of (Chase, 2010):

- Introduction through the feed material,
- Reacting and shrinking particles,
- Mechanical attrition of larger particles and
- Temperature stress cracking of particles.

In order to understand the phenomenon proposed by Kunii and Levenspiel (1969), consider what happens when fluid is passed through a tube with a porous plate supporting solid particles. When fluid flows through the bed, a drag force is exerted on the particles resulting in a pressure drop across the bed. As fluid velocity is increased the pressure drop increases, drag force increases and the bed expands. The particles arrange themselves to offer less resistance to fluid flow. At a certain fluid velocity, the point is reached where the drag force is sufficient to support the weight of the particles in the bed and the bed is said to be fluidized.

$$\left(\begin{array}{l} \text{Weight of} \\ \text{solids particles} \end{array} \right) = \left(\begin{array}{l} \text{Drag force on the particles} \\ \text{from upward moving gas} \end{array} \right)$$

Or

$$A_B \Delta P = A_B L_{mf} (1 - \epsilon_{mf}) g (\rho_s - \rho_g) \dots \dots \dots (14)$$

- A_B cross section area of bed, cm²
- g acceleration due to gravity, cm/s²
- mf subscript meaning “at minimum fluidizing conditions”
- ρ_s density of solids particles, g/cm³

L length of fluidized bed,cm

The frictional pressure drop through a fixed bed L containing a single size solid of screen size d_p , has been correlated by Ergun in Equation 15:

$$\frac{\Delta P}{h} = \rho_g U^2 \left[\frac{150 (1 - \epsilon)}{Re_p \phi_s} + \frac{7}{4} \right] \frac{1 - \epsilon}{\phi_s d_p \epsilon^3} \dots\dots\dots (15)$$

Where:

- L length of fluidized bed, cm
- ΔP pressure drop across depth L , Pa
- ϵ porosity of the bed
- μ gas viscosity, g/cm.s
- U superficial gas velocity, cm/s
- Φ_s particle shape factor
- d_p particle diameter, cm
- ρ_g gas density, g/cm³
- h bed height, cm
- Re_p Reynolds number

Re_p is the dimensionless Reynolds number given by the following equation:

$$Re_p = \frac{\rho_g d_p U}{\mu} \dots\dots\dots (16)$$

Particle sphericity (Φ_s) is defined as the ratio of the surface area of a sphere to the surface area of a particle having the same volume. The value of sphericity particle falls between 0 and 1. The following values are given in Kunii and Levenspiel (1991) for sphericity:

$$\Phi_s = \frac{[(\text{surface of sphere})/(\text{surface of particle})]_{\text{of same volume}}}{\dots\dots\dots} \dots\dots\dots (17)$$

Φ_s (round sand particles i.e. rutile) = 0.86

Φ_s (slag) = 0.66

Crushed slag particles are irregular in shape whereas naturally occurring rutile is smooth and round therefore Φ_s is higher.

The velocity at which the bed is just fluidised is known as the minimum fluidisation velocity (U_{mf}). The pressure drop across the bed, ΔP , then remains constant (even with further increase in the fluid velocity) and equal to the effective weight of the bed per unit area. The minimum velocity can be calculated by combining Equation 14 and 15

$$\frac{1.75}{\phi_s \epsilon_{mf}^3} \left(\frac{d_p u_{mf} \rho_g}{\mu} \right)^2 + \frac{150(1 - \epsilon_{mf})}{\phi_s^2 \epsilon_{mf}^3} \left(\frac{d_p u_{mf} \rho_g}{\mu} \right) = \frac{d_p^3 \rho_g (\rho_s - \rho_g) g}{\mu^2} \dots\dots\dots(18)$$

or

$$\frac{1.75}{\epsilon_{mf}^3 \phi_s} \text{Re}_{p,mf}^2 + \frac{150(1 - \epsilon_{mf})}{\epsilon_{mf}^3 \phi_s^2} \text{Re}_{p,mf} = \frac{d_p^3 \rho_g (\rho_s - \rho_g)}{\mu^2} \dots\dots\dots(19)$$

Solving quadratic Equation 19, For $\text{Re}_{p,mf} < 20$

$$u_{mf} = \frac{(\phi_s d_p)^2}{150 \mu} [g(\rho_s - \rho_g)] \frac{\epsilon_{mf}^3}{1 - \epsilon_{mf}} \dots\dots\dots(20)$$

2.3.2 Fluidisation Stages

Figure 15 illustrates the various stages of fluidisation. The fixed bed and minimum fluidisation velocities have already been discussed so bubbling fluidisation; slugging and lean phase fluidisation will be covered in this section.

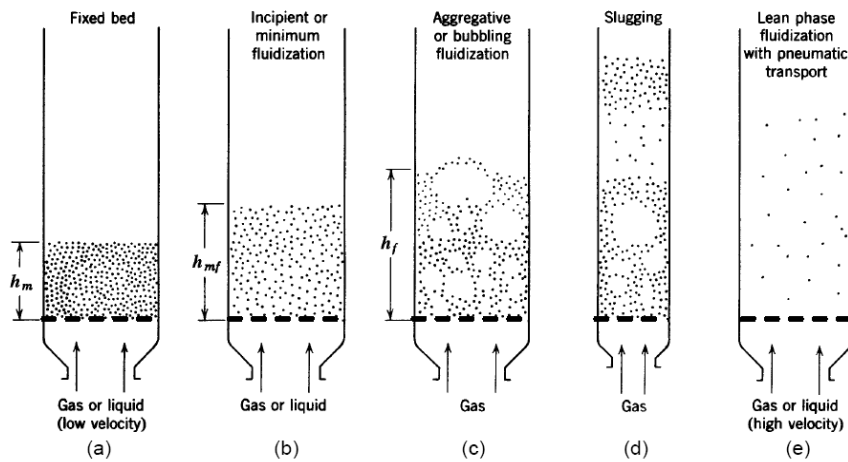


Figure 15: Fluidisation stages (Kunii and Levenspiel, 1969)

When the fluid velocity is increased above the minimum fluidising velocity (U_{mf}), unstable bubbles form and channelling is noticeable. The bubble like cavities promotes particle circulation in the bed. The bed is said to be a bubbling fluidised bed.

Slugging occurs when gas bubbles coalesce and grow as they rise through the vessel. The bubble can grow to reach a size where it occupies the entire cross sectional area of the tube. The large bubbles push the solid particles ahead of it. Slugging is undesirable as it increases entrainment and elutriation and lowers the vessel's performance.

Finally when fluid velocity exceeds the terminal velocity of the solids, the solids are carried out of the tube with the fluid (i.e. elutriation). Terminal velocity is calculated using Equation 21.

$$u_t = u_t^* \left(\frac{\mu(\rho_s - \rho_g)g}{\rho_g^2} \right)^{\frac{1}{3}} \dots\dots\dots(21)$$

$$u_t^* = \left[\frac{18}{(d_p^*)^2} + \frac{2.335 - 1.744\phi_s}{(d_p^*)^{0.5}} \right]^{-1} \dots\dots\dots(22)$$

$$d_p^* = d_p \left[\frac{\rho_g(\rho_s - \rho_g)g}{\mu^2} \right]^{\frac{1}{3}} \dots\dots\dots(23)$$

Minimum fluidising velocity and terminal velocity are functions of the materials physical characteristics. The setpoint for the superficial fluid velocity through the fluidised should be between the minimum and terminal velocity setpoints. U_{mf} and U_t can be calculated using Equations 20 and 21.

2.3.3 Geldart Classification

Geldart (1973) proposed a graph (Figure 16) to classify the fluidisation behaviour of solid particles when fluidised by a gas/liquid at ambient conditions. Material is classified into 4 groups based on density and particle size i.e.:

- Group A – Aeratable
- Group B – Sandlike bubbling
- Group C – Cohesive
- Group D – Spoutable

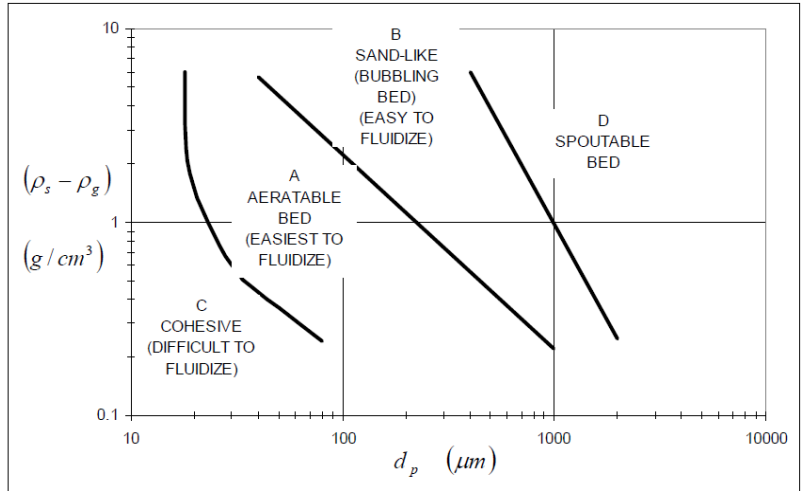


Figure 16: Geldart Group Classification

2.3.4 Elutriation

Elutriation refers to the separation or removal of fines from a gas-solid mixture (Kunii and Levenspiel, 1991). In a bubbling fluidized bed reactor, solids are thrown into the freeboard area via one of three ways i.e. from the roof of a bursting bubble, from the bubble wake and from the wake of a trailing bubble just as it coalesces with its leading bubble (Kunii and Levenspiel, 1991). This is illustrated in Figure 17.

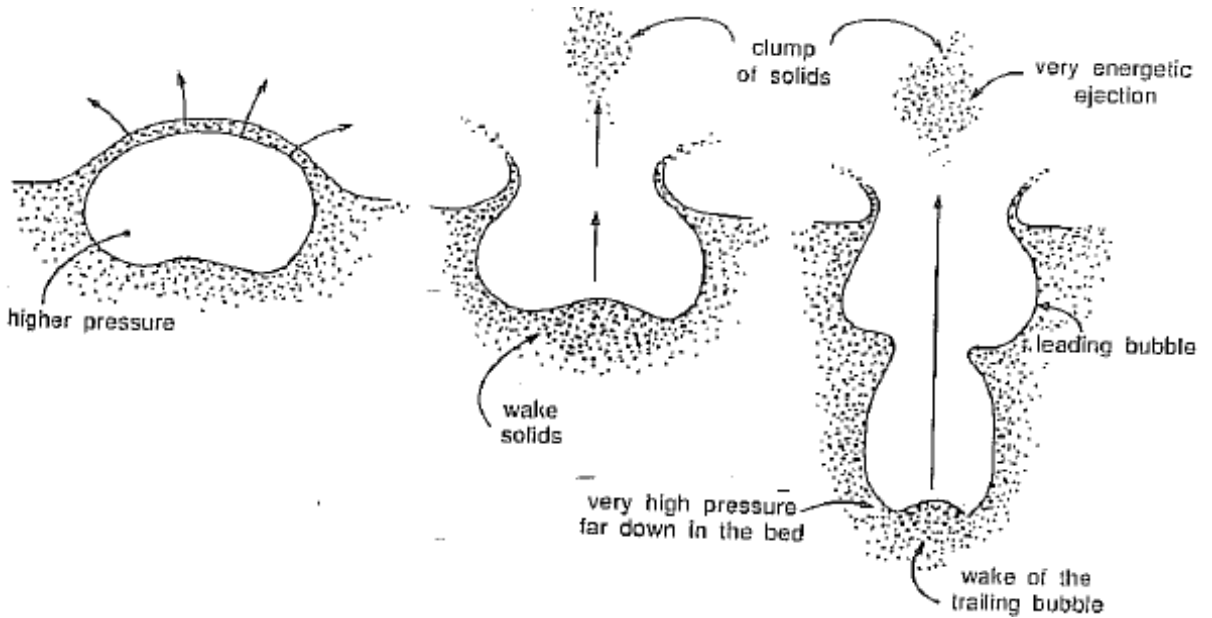


Figure 17: Bubble behaviour in a fluidised bed (Kunii and Levenspiel, 1991)

A high elutriation rate translates to a shorter residence for particles in the fluidised bed which in turn negatively affects conversion efficiencies. This is one of the reasons why it is important to determine elutriation rates.

Carryover can be measured by means of a value called the elutriation constant (k_i^*). Kunii and Levenspiel (1991) describe a method to determine elutriation constants by doing batch experiments. Assuming that the flux rate of any particular size of solid i is proportional to its weight x_i in the bed, all other factors being constant, the flux of particles out of the fluidised bed may be written as (Kunii and Levenspiel, 1991)

$$-\frac{1}{A} \frac{dW_i}{dt} = k_i^* x_i = k_i^* \left(\frac{W_i}{W} \right) \dots\dots\dots(24)$$

If the total mass of the sample does not change much during the experiment (i.e. < 20%), then integration of Equation 24 gives:

$$\frac{W_i}{W_{i0}} = \exp\left(-\frac{k_i^* A t}{W}\right) \dots\dots\dots(25)$$

- W_{i0} = initial weight of mass fraction i
- W_i = final weight of mass fraction i
- W = total weight of sample before fluidisation
- A = area of reactor (m^2)
- t = time (s)
- k_i^* = elutriation constant ($kg/m^2.s$)

The elutriation constant can be calculated using Equation 25 provided that the particle size distribution of the initial bed and some time after is known.

2.3.5 Bubbling Fluidised beds

The simplest description of the expansion of a bubbling fluidized bed is derived from the Two-Phase Theory of fluidization of Toomey and Johnstone (1952). This theory considers the bubbling fluidized bed to be composed of two phases; the bubbling phase (the gas bubbles) and the particulate phase (the fluidized solids around the bubbles). The particulate phase is also referred to as the emulsion phase. The theory states that any gas in excess of that required at incipient fluidization will pass through the bed as bubbles. Thus, in bubbling fluidization, bed expansion at velocities beyond minimum bubbling velocity is due to the presence of bubbles. Bubbles are excellent for particle circulation and promote heat and mass transfer but a negative aspect is that the bubbles contain most of the gas. In order to maximise conversion, the mass transfer from the gas phase to dense phase has to be as high as possible.

This simplified model is generally accepted in literature and has formed the basis for many studies (McAuley et al., (1994), Wen and Chen (1982), and Hoffmann et al., (1993)). Kunii and Levenspiel (1969) proposed a three phase model and suggested that the existence of cloud phase between the bubble and the emulsion provides the main resistance to mass transfer between the two phases (See Figure 18). According to McAuley et al., (1994) the only mechanism by which mass can be transferred from the bubbles to the emulsion phase is by diffusion through the bubble clouds

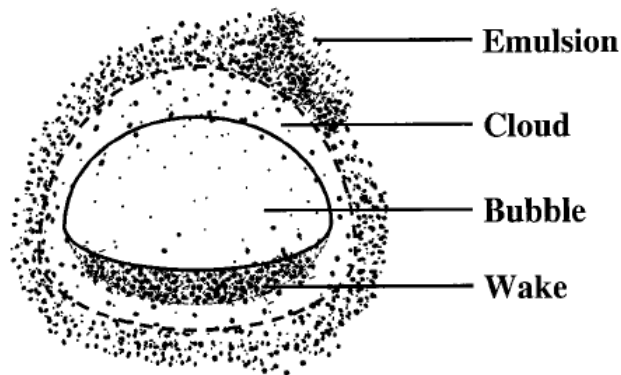


Figure 18: Kunii and Levenspiel Model (1991)

Mass transfer is largely affected by the bubble size, as bubble size decreases, the interfacial area between the bubble and the emulsion phase's increases leading to smaller resistance to heat and mass transfer (McAuley et al., 1994). The increase in bubble size results in poorer gas solid contact, hence in order to maintain good fluidisation, gas bubbles should be kept as small as possible and interchange of gas should take place between the bubble phase and dense phase (Mohanty et al., 2008).

The ultimate size of the bubbles formed depends upon the size of the fluidised bed, gas velocity, relative density of the gas and the solid, gas entry configuration and the size of the solid (Mohanty et al., 2008). Of the abovementioned, the only factor that changes significantly in the current experimental set up is the particle size distribution of the feedstocks so only this aspect will be discussed further.

Beetstra et al., (2009) demonstrated by manipulating the particle size distribution of alumina powder, the bubble size could be reduced by up to 40%, the addition of fines to a given particle size distribution also decreases the bubble diameter up to 40%. Spectral decomposition method and optical probes were used to measure bubble size. The authors concluded that there was no singular explanation as to why the effect of fines has an effect on the bubble size but various interparticle forces, for example Van der Waals forces and collision properties, are expected to influence the bed behaviour. It is often speculated that the fines act as a lubricant and lowers the apparent viscosity of the dense phase leading to smaller voids and more uniform gas distribution (Beetstra et al., 2009). Beetstra et al., (2009), showed that when bubble diameter is decreased from 10cm to 6cm, conversion increases from 53% to 75% (Figure 19).

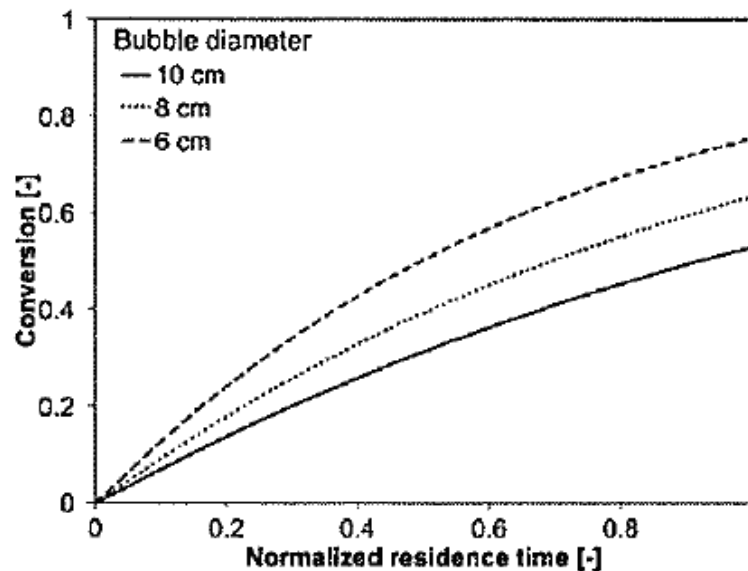


Figure 19: The effect of bubble size on the conversion of reactants in a fluidised bed, based on Kunii and Levenspiel model (Beetstra et al., 2009)

Singh and Majumder (2010) studied mass transfer in fluidised beds and illustrated through MATLAB simulation that if the increase in bubble diameter is large, mass transfer between the gas and liquid phase will change drastically. Presence of the larger bubbles led to an overall decrease in gas holdup and thus mass transfer decreases. Gas hold up refers to the fraction of volume of the gas phase occupied by the gas bubble inside the bubble column reactor and is the most important factor characterising the column parameters (Singh and Majumder, 2010).

Sharma and Pugsley (2007) showed through CFD simulations that particle size distribution has an effect on conversion of ozone. Figure 20 shows that a wider PSD led to better ozone conversion.

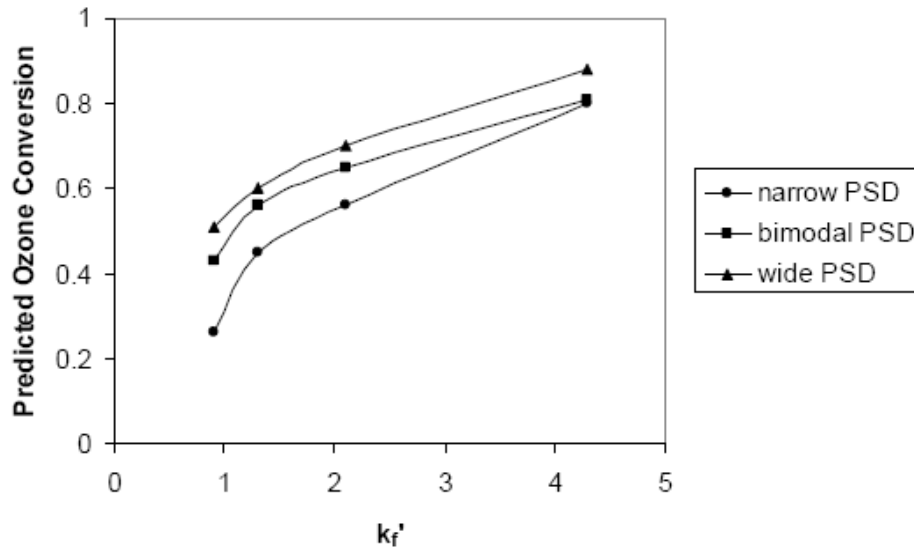


Figure 20: CFD predictions of ozone conversion as a function of dimensionless rate constant for the three different size distributions (Sharma and Pugsley, 2007)

Sun and Grace (1990) tested the effects of varying catalyst particle size distribution (i.e. wide, narrow and bimodal) on ozone conversion. The wider particle size distribution led to a higher conversion whilst the narrow mixture gave the lowest. The authors suggested that this effect was due to an increased amount of fines in the dilute phase compared to the dense phase. The authors concluded that the performance of fluidised bed particles depends not only on the quantity of fines but also on their nature and overall particle size distribution.

Grace and Sun (1991) proposed the following as an explanation to why a wider particle size distribution leads to smaller bubbles:

- The wider PSD results in more expanded dense phase which in turn leads to more gas passing through the dense phase and to a reduced effective viscosity
- Associated with the lower effective dense phase viscosity, voids or bubbles tend to be smaller with a wider PSD. This leads to improved interphase mass transfer and better gas solid contacting
- In beds with wide PSD, voids are smaller so that they rise less quickly on average, resulting in greater bed expansion and increased gas residence time

- There are more particles present in the voids with the wider PSD. These particles enhance reactor efficiency since they are in intimate contact with relatively unconverted gas in the dilute phase
- Transition to the turbulent fluidisation regime occurs sooner for a wide size distribution than for a narrow one. This leads to partial breakdown of the two phase behavior which characterizes the bubbling and slugging regimes and hence to better overall gas solid contacting

Various correlations for estimating bubble diameter has been proposed in literature (Mori and Wen, 1975):

$$D_B = 1.6\rho_s d_p \left(\frac{u_o}{u_{mf}} - 1 \right)^{0.63} h \quad \text{Yasui et al.,(1958).....(26)}$$

$$D_B = 1.4\rho_s d_p \left(\frac{u_o}{u_{mf}} \right) h + D_{BO} \quad \text{Park et al.(1999).....(27)}$$

$$D_B = 33.3d_p^{1.5} \left(\frac{u_o}{u_{mf}} - 1 \right)^{0.77} h \quad \text{Kato and Wen (1969).....(28)}$$

In McAuley et al., (1994), correlations for maximum bubble size based on terminal velocity for a given particle size is given:

$$D_{\max} = \frac{2U_t^2}{g} \quad \text{(Davidson and Harrison, 1963).....(29)}$$

$$D_{\max} = \frac{2U_t^2}{g} \quad \text{(Grace,1986a).....(30)}$$

Grace (1986a) postulated the same equations but used instead the terminal velocity of a particle of $2.7d_p$, resulting in a larger stable maximum bubble size. Equation 29 and 30 show that the smaller the particle, the smaller the terminal velocity, and the smaller the bubble size.

2.3.5.1 Effect of Particle Size Distribution on Elutriation

Bubbles carry particles as they move through the bed, when the bubble reaches the surface, it bursts and material is thrown into the freeboard area (Baeyens et al., 1992, Wen and Chen (1982), George and Grace (1978)). Smaller bubbles carry less material which leads to lower entrainment rates.

Wen and Chen (1982) correlated the rate of particles ejected at the bed surface to bed hydrodynamic parameters such as bubble size and excess gas velocity above minimum fluidisation velocity

$$\frac{F_B}{A} = D_B (3.07 * 10^{-9} \frac{\rho_g^{3.5} g^{0.5}}{\mu^{2.5}} (u_o - u_{mf})^{2.5} \dots\dots\dots (31)$$

Where,

- F_B total entrainment rate at bed surface (kg/m²s)
- A cross sectional area of the column (m²)
- D_B bubble diameter at the bed surface (m)
- u_{mf} minimum fluidising velocity (m/s)
- u_o actual velocity (m/s)
- μ viscosity (kg/ms)
- ρ_g density gas (kg/m³)

George and Grace (1978) investigated the volume of ejected particles as a function of bubble size and found that volume of elutriated particles increases with increasing bubble size. The experiments were carried out on silica sand (i.e. 210 to 500μm) and Ballotini glass particles (i.e. 250 – 297 μm).

Controlling the bubble size to avoid large and fast bubbles that bypass the bed and increase the elutriation is an important task (Sobrino et al., 2009).

Contrary to the belief that an increase in fines will results in increased blowover, Baeyans et al., 1992 found that elutriation constants increased with decreasing particle size and then levelled off below a critical size, Li et al., (2004) found that elutriation rate decreases with an increase in weight fraction of fines and Shin et al., (2007) fluidised fine carbon black particles and alumina particles in an inert medium and showed that entrainment rate decreased as the content of fine powders (<40μm) in the mix increased.

The literature indicates that the benefit of smaller bubbles is two fold:

- Better interaction between the gas and solid particles leading to higher conversion rates
- Lower rates of elutriation

CHAPTER 3

3. EXPERIMENTAL

3.1 SAMPLES

The experimental testwork consists of two phases i.e. fluidisation experiments to determine the blowover and chlorination experiments. The four titania samples under investigation are listed below:

- Slag A
- Slag B
- Rutile
- Blend consisting of 50 wt% rutile and 50wt% Slag A

Slag A and rutile were from a South African source whereas Slag B was sourced from an international ilmenite smelting operation. Petroleum coke was utilised as reductant in the chlorination experiments.

Elemental analysis of the feedstocks was determined through Induced Coupled Plasma Analysis – Optical Emission Spectroscopy techniques. Forms of titanium were determined by wet chemical analysis. The chemical composition of the titania feedstocks is given in Table 4.

Table 4: Feedstock Chemical Analysis

	Slag A	Slag B	Rutile	Blend
	Wt%			
SiO₂	1.64	1.49	1.44	1.36
Al₂O₃	1.02	1.64	0.31	0.78
FeO	8.60	1.96	0.49	4.52
Fe(metallic)	0.00	1.03	0.00	0.00
TiO₂(equivalent)*	87.46	95.02	95.69	91.55
Ti₂O₃	23.42	38.80	0.00	9.99
TiO₂	61.92	51.90	95.69	80.45
CaO	0.22	0.26	0.08	0.15
MgO	0.73	0.25	0.01	0.34
Na₂O	0.02	0.03	0.00	0.00
K₂O	0.03	0.01	0.00	0.00
MnO	1.90	2.80	0.01	1.03
P₂O₅	0.18	0.10	0.00	0.00
ZrO₂	0.17	0.16	0.92	0.55
Nb₂O₅	0.16	0.08	0.00	0.00
Cr₂O₃	0.09	0.14	0.11	0.06
V₂O₅	0.46	0.21	0.49	0.29

*TiO₂ equivalent denotes all forms of Tiⁿ⁺, expressed as TiO₂

Slag B is more reduced than Slag A and therefore has a lower FeO content and higher Ti₂O₃ content. The Blend is a combination of Slag A (50wt %) and rutile (50wt %). A high quality (i.e. low impurity) reductant is required for the chlorination process. The ultimate and proximate analysis results of the petroleum coke used for these experiments are listed in Table 5.

Table 5: Coke Analysis

	Ultimate Analysis (%)
%C (Air Dried)	94.70
%H (Air Dried)	0.54
%N (Air Dried)	1.42
%O (Air Dried)	0.45
	Proximate Analysis (%)
% Inherent moisture content (Air Dried)	0.20
% Ash content (Air Dried)	1.60
% Volatile Matter (Air Dried)	1.30
%Fixed carbon (calculation) (Air Dried)	96.90
% Total sulphur (Air Dried)	1.08

Screen sieves of size 850, 600, 425, 300, 212, 150, 106, 90, 75, and 56 μm were used to determine particle size distribution of the titania feedstocks. The results of the sieve analysis of the feedstocks and the petroleum coke are displayed in Figure 21 and Figure 22. Table 6 gives the calculated d_{50} of the feedstocks which was calculated by interpolation.

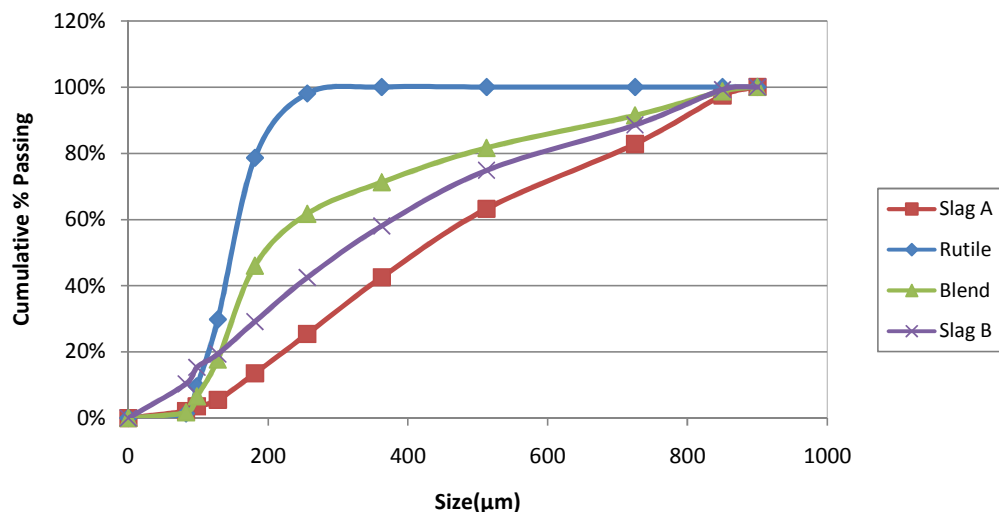


Figure 21: Particle size distribution of Feedstock's

Table 6: Feedstock d_{50}

Feedstock	$d_{50}(\mu\text{m})$
Slag A	294
Slag B	217
Rutile	110
Blend	141

Rutile is finer than the two slags's and has a particle top size of 300 μm . The slag top size is 850 μm with Slag A being coarser than Slag B. Slag blocks are milled and therefore tends to have a wider particle size distribution than the naturally occurring rutile.

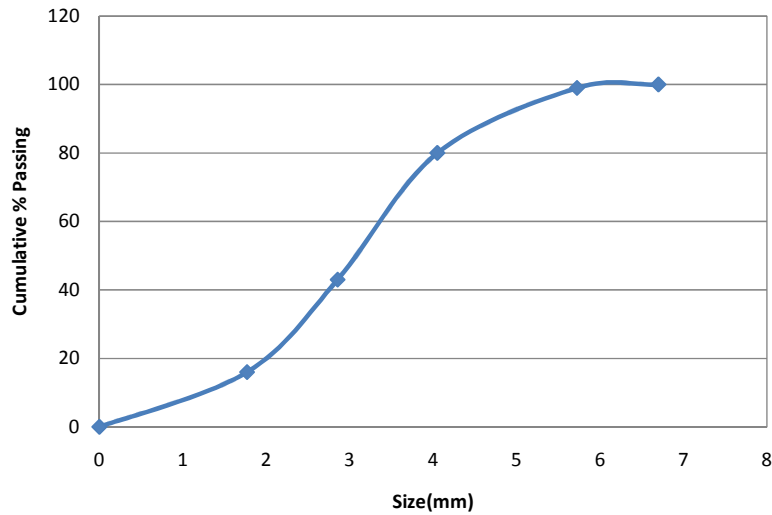


Figure 22: Coke particle size distribution

Feedstock density (g/cm^3) was determined by helium pycnometry, results are presented in Table 7. Rutile is less porous than slag and has a higher TiO_2 content, hence has the highest density.

Table 7: Feedstock Density

Feedstock	Density(g/cm^3)
Slag A	4.03
Slag B	4.05
Rutile	4.16
Blend	4.10

3.2 FLUIDISATION TESTWORK

Elutriation is the process by which fine particles are carried out of the fluidised bed due to the fluid flow rate passing through the bed (Chase, 2010). Elutriation rate affects the particle residence time in the reactor and inevitably conversion rates. For this reason, it is important to compare blowover tendencies of the various feedstocks prior to the chlorination experiments. Carryover can be measured by means of a value called the elutriation constant (k_i^*) which is determined during batch scale experiments. The elutriation constant (k_i^*) can be calculated using Equation 32 provided that the particle size distribution of the initial bed and sometime after is known.

$$\frac{W_i}{W_{i0}} = \exp\left(-\frac{k_i^* At}{W}\right) \dots\dots\dots(32)$$

- W_{i0} = initial weight of mass fraction i
- W_i = final weight of mass fraction i
- W = total weight of sample before fluidisation
- A = area of reactor (m^2)
- t = time (s)
- k_i^* = elutriation constant ($kg/m^2.s$)

3.2.1 Experimental Sample

The elutriation experiments were performed on Slag A, Slag B, rutile and the blend sample. Each of the feedstock bulk samples were split into 10kg samples. The 10 kg samples were further split into 1 kg samples using a rotary splitter. If smaller samples were required for analysis or experiments then the 1kg sample was split further using the rotary splitter illustrated below in Figure 23. If larger samples were required then the 100g samples were combined.



Figure 23: Rotary Splitter used for 2nd and 3rd stage sample splitting

3.2.2 Experimental Apparatus

A silica reactor (i.e. 110mm diameter and 1100mm height) connected to a crossover duct; cyclone and two collection flasks was used for the elutriation testwork (See Figure 24). The crossover duct provides a passage for the gas and elutriated particles to leave the silica reactor. The elutriated particles settle in the collection flask whilst the gas is vented to the atmosphere. The silica reactor is encased in an electrically heated furnace. The dimensions of the furnace are a height of 1350mm, breadth of 900mm and width of 80mm. A porous distributor plate divided the silica reactor into two zones and allowed for the passage of gases for

fluidisation of the sample. The fluidising agent was nitrogen, the supply was from a cylinder and the flowrate was controlled by rotameters. The furnace temperature was controlled by a K type thermocouple (Pt, Rh), which measured temperature in the bed.

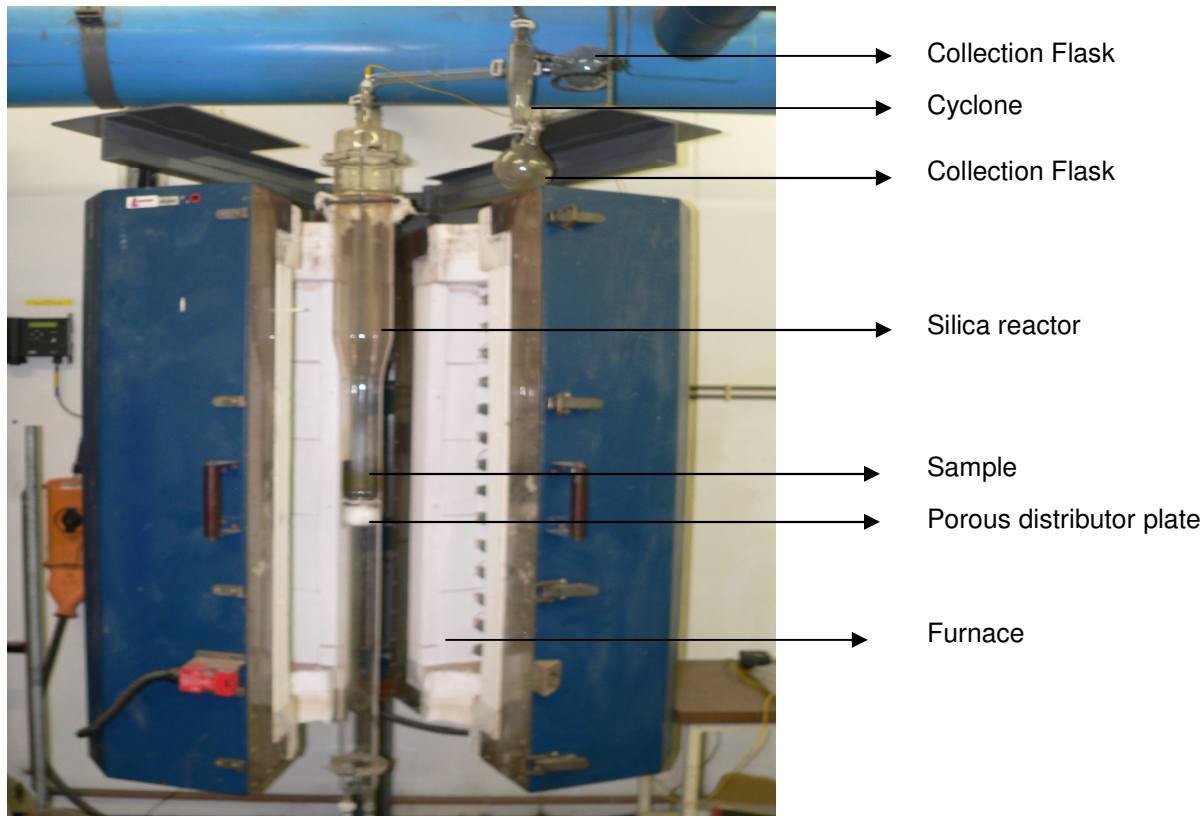


Figure 24: Photograph of the Fluidisation set-up

3.2.3 Experimental Procedure

Following the sample splitting and screening procedures described above, 600g of material was collected for each experiment. The sample was lowered into the dismantled reactor and onto the distributor plate. The remaining components of the reactor were carefully assembled and the completed assembly was placed vertically into the furnace. The nitrogen gas line entered through the silica reactor bottom and had to be connected prior to the start of each experiment and disconnected at the end. With the installation of the nitrogen line the equipment set up was complete and the furnace was switched on. Nitrogen gas with a superficial velocity of 0.19m/s fluidised the titania sample.

Gases exited at the top of the reactor and carried with it a fraction of the finer, lighter material. The elutriated solids are separated from the gas through the action of the cyclone. The solids settled out in the round bottom flask whilst the gases pass through the offgas duct and are vented from the system. After 30 minutes of fluidisation at 1000°C, the furnace was switched off and sample was allowed to cool to room temperature.

Upon cooling, the remaining bed sample and the elutriated fines were collected, weighed and screened. The results are discussed in Chapter 4.

3.2.4 Experimental Technique

Upon conclusion of the fluidisation test, the bed sample and carryover was collected, weighed and particle size distribution was determined. Screen sizes 200, 150, 100 and 75 μm were used for particle size distribution determination.

3.3 CHLORINATION TESTWORK

The feedstocks identified as Slag A, Slag B, rutile and blend (i.e. a mixture of Slag A (50wt%) and rutile (50 wt%) were subjected to carbochlorination at temperatures varying from 800 $^{\circ}\text{C}$ to 1000 $^{\circ}\text{C}$. Petroleum coke and CO gas were used as reductants. The experimental setup followed was similar to that proposed in literature (Le Roux (2001), Sohn et al., (1998), Dunn (1960))

Oxygen is used in the commercial chlorination process but is not used in laboratory experiments as it becomes difficult to control the bed temperature. Lack of oxygen lowers CO generation which is undesirable as gas composition in the lab scale chlorinator then differs from the commercial chlorinator. In order to simulate commercial scale conditions, many investigators added CO as a reagent. It was noted that in previous investigations into the chlorination of titania feedstocks that three reductant combinations were used:

- CO (Bergholm (1961), Dunn (1960), Le Roux (2001))
- CO and carbon (Den Hoed and Nell (2003), Dunn (1979)) and
- Carbon (Jena et al., (1998), Sohn and Zhou (1998), Youn and Park(1989))

3.3.1 Experimental sample

In order to minimise the effects of particle size on the chlorination experiments and establish a common basis for comparison, a common size fraction was screened and used in the experiments. Rutile is the finer material and has a top size of 300 μm , hence 300 μm was selected as upper limit for the chlorination experiments. The hydrodynamic study revealed that particles below 106 μm have a high tendency to be blown out of the reactor, a higher carryover was undesirable for the chlorination tests so particles smaller than 300 μm but greater than 106 μm were selected. Fine material (i.e. < 106 μm) is not fed to industrial chlorination scale chlorinators due to the high entrainment rates.

3.3.2 Experimental Apparatus

The fluidised bed reactor system used for the experiments consists of a silica reactor, furnace, K type thermocouple, crossover tube, blow-over collector flask, off gas duct and scrubber system as illustrated in Figure 25. The silica reactor (80mm in diameter and 1100 mm in length) stood vertically in an electrically

heated furnace (900 mm height, 600mm breadth, 550mm width) for the chlorination trials. The furnace and silica reactor are shown in Figure 26 and Figure 27 and the control panel in Figure 28. The sample rested on a porous silica disc. The disc served two functions i.e. supported the charge and allowed for the even distribution of fluidizing and chlorination gases in the sample area. Gas flow (i.e. Cl_2 , CO and Ar) was controlled by rotameters to give a superficial gas velocity of 39.8 cm/s. The flow rates of Cl_2 and CO gas were maintained at 8NI/min and 4NI/min respectively. The total gas pressure inside the fluid bed reactor was approximately 85kPa with the partial pressure of Cl_2 gas in the fluid bed reactor approximately 57kPa.

Bed temperature was controlled by a thermocouple (K type) which lay in the middle of the sample bed. The crossover duct allowed for the passage of the product gases from the silica reactor into the round bottom flask, where the solids settled out. The gases then passed into a perspex pipe, into the offgas duct and finally into the scrubber system.

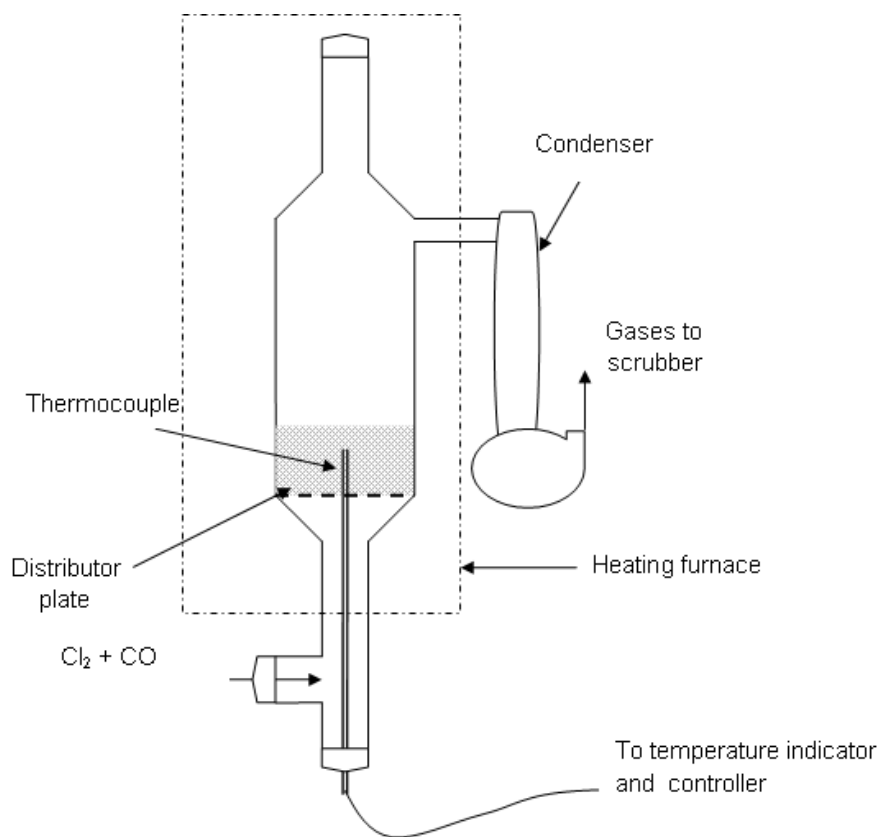


Figure 25: Schematic of experimental set up for chlorination experiments (Kale and Bisaka, 2010)



Figure 26: Furnace used for chlorination experiments

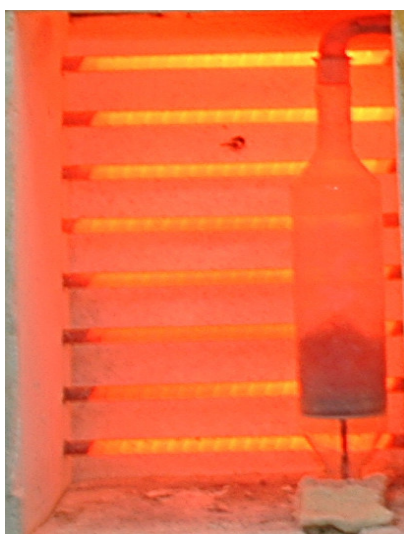


Figure 27: Photograph of heated furnace with silica reactor



Figure 28: Control Panel

3.3.3 Experimental Procedure

The screened feedstock (-300 + 106 μm) and coke (-5mm + 1.5mm) samples were combined to yield a homogeneous mixture. The minimum fluidising velocity of petroleum coke (-300 + 106 μm) is significantly lower than titania feedstock so larger coke particles was selected to minimise the coke blowover. The charge (i.e. 200g feedstock and 40g coke) was loaded into the reactor and onto the distributor disc. Den Hoed and Nell (2002) found that at carbon levels lower than 15wt%, availability of carbon is the rate limiting step but once the stoichiometric requirement is exceeded the reaction proceeds unhindered. In this experimental procedure, 20wt% coke was added.

The reactor was placed vertically in the furnace and the crossover duct and round bottom flask were connected. The gas line for CO, Cl₂ and Ar was connected. The sample was fluidised with argon for the duration of the heat up period. Once the desired temperature was reached, the Ar flow was switched to CO (33 vol %) and Cl₂ (67 vol %), this marked the start of the test.

The gases exited the silica reactor through the crossover duct. Elutriated material passed through the crossover duct and settled out in the round bottom flask. Upon reaching the test duration, the flow of CO and Cl₂ was switched off and the sample was cooled in Ar atmosphere. Once the reactor reached room temperature, the remaining bed sample was removed, the crossover duct and round bottom flask cleaned and blowover collected. The large carbon particles were screened out of the bed sample. The blowover and bed sample was washed with water and dried at 105 °C for 2 hrs. Thereafter the material was roasted at 900 °C for 2 hours to burn off fine coke particles. Samples were then screened, weighed and sent for chemical analysis.

It took approximately 1.5 hours to heat the sample to the desired reaction temperature. A dry run (without chlorine gas) showed a mass loss of 1.5 - 2% of ore and 1.5 -2.6% of coke from the bed. This was elutriated from the reactor during the heatup. This mass is considered to be insignificant compared to the amount chlorinated and thus was reported in the blowover fraction

Table 8: Sample Mass Before and After Heat Up

	Slag A	Rutile	Blend
Ore in (g)	200	200	200
Ore out (g)	197	197.24	196.08
Mass change	-3	-2.76	-3.92
% change	-1.50%	-1.38%	-1.96%
Pet coke in (g)	40	40	40
Pet coke out (g)	39.42	38.98	39.1
Mass change	-0.58	-1.02	-0.9
% change	-1.45%	-2.55%	-2.25%

Sintering of particles and bed defluidisation can be problematic during high temperature fluidisation. A stationery bed affects chlorination rate so several checks were done on the bed during the heat up. If the bed was stationery, a gentle tap of the reactor and slight increase on the inert gas velocity fluidized the bed again.

The chlorine flow rate (8 NI/min), carbon monoxide flow rate (4NI/min), mass of ore (i.e. 200g) and the quantity of reductant (40g) were kept constant throughout the experiments. The chlorination tests and conditions are listed in Table 9.

Table 9: Test Plan for Chlorination Experiments

Feedstock	Chlorination time (minutes)	Temperature (°C)
Slag A	1,30, 60, 180	1000
Slag A	180	900
Slag A	180	800
Slag B	30, 60, 180	1000
Slag B	180	900
Slag B	180	800
Rutile	30, 60, 180	1000
Rutile	180	900
Rutile	180	800
Blend (-300+106µm) (50 wt % Slag A, 50wt% Rutile)	30, 60, 180	1000
Blend (-300+106µm) (75wt% Slag A, 25wt% Rutile)	180	1000
Blend (-150+106µm) (50wt% Slag A, 50wt% Rutile)	180	1000
Blend (-212+150µm) (50wt% Slag A, 50wt% Rutile)	180	1000

3.3.4 Experimental Technique

3.3.4.1 Chemical Analysis

Compositions of the bed samples were determined through Inductively Coupled Plasma (ICP) analysis. The carbon and sulphur values were determined through LECO analysis.

3.3.4.2 Mineralogical Analysis

Scanning Electron Microscope (SEM) and Quantitative Evaluation of Minerals by Scanning Electron Microscopy (QEMSCAN) were used for mineralogical characterisation of the feed samples and the chlorinated bed samples.

QEMSCAN is a combination of a scanning electron microscope (SEM) and a data processing software package that enables the user to obtain mineralogical and textural information. The advantage of QEMSCAN

software is that the data can be converted into quantitative information and compared to each other. Particles are set in a resin mixture which is polished to expose the grains. QEMSCAN analyses approximately 3500 grains by the Particle Mineral Analysis (PMA) technique on a 5µm by 5µm grid/2µm by 2µm grid.

The SEM utilises Energy Dispersive Spectrometers (EDS), an analytical technique used for elemental analysis and chemical characterisation of a sample. The investigation was carried out using a QemSem E430, Zeiss EVO50 SEM platform, fitted with Bruker AXS XFlash, X275HR, detectors. The analytical conditions used for SEM/EDS analyses included an acceleration voltage of 15kV, beam current of 11 µA, specimen current of 5nA, 90 000cps pulse processor and at a working distance of 22.5 mm. The quantification software and hardware are calibrated using the copper standard. The quantification Bruker Quantax Esprit v1.8.2 software was used. High resolution backscatter electron (BSE) images were collected with an acceleration voltage of 25kV.

X-Ray diffraction is used to identify phases as each crystalline phase has a unique crystalline pattern. Therefore one can distinguish between compounds utilising the diffraction methods sensitivity to structure and not just composition. Due to this sensitivity it is possible to differentiate between polymorphic forms of the same compound. The mineralogical composition of the samples was determined by matching the best fitting patterns from the ICDD database to the measured diffractogram using Panalytical XPert HighScore analytical software. Quantification was by means of the relative intensity method (RIR) of the PanAnalytical HighScore software.

3.3.4.3 Factsage

The thermodynamic tool Factsage v 6.1 was used to calculate the change in Gibbs free energy for the chlorination reactions. Factsage consists of a series of databases (i.e. both solution and pure compounds) and numerous calculation modules. More information on Factsage is available on www.factsage.com. The Reaction module of Factsage was used for the calculation of the Gibbs energy in this study.

3.3.4.4 Porosity

Porosity of the feed and the bed samples were measured using the QEMSCAN. There is no built-in function in QEMSCAN to determine porosity, for this QEMSCAN study porosity was defined as:

$$\% \text{ Porosity} = (\text{Pore area} / \text{Total Particle area}) \times 100 \% \dots\dots\dots (33)$$

Pore area is identified as area of the particles that was filled with resin, which the QEMSCAN identifies as background

3.4 SAFETY, HEALTH AND ENVIRONMENTAL

3.4.1 Chlorine

Exposure to chlorine either by inhalation, swallowing or skin contact is dangerous so every precaution was taken to reduce the risk of contact during the experiments. Contact through inhalation is the most harmful route of exposure. The severity of the health effects depends on the dosage and duration, common symptoms are: respiratory tract irritation, a sore throat, coughing, chest tightness, eye irritation, skin irritation, chemical pneumonitis and pulmonary edema.

Safety measures:

- Prior to the start of the experiment, the pipes and connections were tested for leaks
- The lab was equipped with chlorine detectors for early detection of leaks. When unsafe levels of chlorine were detected the chlorine feed would automatically shut down.
- All staff working on the chlorination experiments attended chlorine gas handling gas.
- Chlorine has a very distinct and pungent odour so leaks were quickly and easily detected. Staff would evacuate immediately and return with breathing apparatus to fix the problem.

3.4.2 Carbon monoxide

Carbon monoxide (CO) is a colourless, odourless and tasteless gas. CO enters the bloodstream through the lungs and displaces the oxygen. Early symptoms of carbon monoxide poisoning are irritated eyes, headache, nausea, weakness and dizziness. Prolonged exposure to low concentrations or very short exposure to high concentrations can lead to death.

Safety Measures:

- Operators wore portable CO monitors
- The lab was equipped with a fixed CO monitor
- If CO was detected, the experiment was stopped and area evacuated

3.4.3 Chlorine leaks

Blockages of the exhaust pipe and chlorine leaks were experienced during the longer experiments. The exhaust pipe blockages usually occurred in the first thirty minutes as the amount of fumes and liquefied TiCl_4 was the greatest during this period. A gentle tapping of the pipe usually unblocked the pipe but on a few occasions, the pipe had to be replaced.

The various pipe connections downstream of the reactor provided escape points for the reaction gases if they were not sealed properly. Checks were done prior to the start of the experiment but the leaks weren't completely evaded.

3.4.4 Fumes

Dark brown fumes signifying iron chlorination were produced almost immediately after Cl_2 and CO were introduced to the system for Slag A and Slag B and the blend. The intensity of the brown fumes decreased after a few minutes and was gradually replaced by white fumes. After approximately 3 minutes, liquefied TiCl_4 could be seen in the exhaust pipe.

CHAPTER 4

4. RESULTS AND DISCUSSION

The results of the fluidisation and chlorination experiments are presented in this chapter. The fluidisation experiments were conducted on the complete feedstock sample whilst a narrower size range (-300+106µm) was selected for the chlorination experiments.

4.1 FLUIDISATION

4.1.1 Geldart Classification

The feedstock's d_{50} (i.e. of the unscreened sample) were plotted onto the Geldart group classification graph, all feedstocks lie in Group B and are classified as easy to fluidise according to Geldart classification. Figure 75 to Figure 77 (Appendix 2) are plots of the various size fractions of the feedstocks on the Geldart graph. When plotted on the Geldart curve, 85% of Slag A particles fall in group B range but 15% fall in Group D (larger particles) and thus will be difficult to fluidise (Figure 75). Slag B has a wide size distribution and thus is spread over three Geldart classes i.e. A, B and D (Figure 76). The portion that lies in Group A will be prone to elutriation whilst that in Group D will be difficult to fluidise. All the rutile particles fall into Group B and hence are the easiest to fluidise (Figure 77).

At operating temperatures and pressures above ambient, the material may appear in a different group from that which it occupies at ambient conditions, this is due to the change in gas properties.

4.1.2 Minimum Fluidising Velocity and Terminal Velocity

The velocity that marks the onset of fluidisation is termed the minimum fluidising velocity. This velocity can be calculated using Equation 34. The theory related to fluidisation and derivation of Equation 34 is described in Chapter 2.

$$u_{mf} = \frac{(\phi_s d_p)^2}{150\mu} [g(\rho_s - \rho_g)] \frac{\epsilon_{mf}^3}{1 - \epsilon_{mf}} \dots\dots\dots (34)$$

Minimum fluidising velocity is a function of particle diameter (d_p), density of material (ρ_s), density of gas (ρ_g), sphericity of material (Φ_s), viscosity of gas (μ), voidage at minimum fluidization (ϵ_{mf}).

The minimum fluidising velocity for the feedstocks were calculated based on the average particle size. The results are presented in Table 10.

Table 10: Minimum fluidisation velocity

Material	Average Particle size(μm)	Average particle density (kg/m ³)	Sphericity [*]	Temperature (°C)	Air Density(kg/m ³) at 1000°C [‡]	Air Viscosity (kg/m.s) At 1000°C [‡]	Voidage [†]	U _{mf} (m/s) at 1000°C
Slag A	294	4030	0.67	1000	0.27	0.0000491	0.41 [†]	0.024
Slag B	218	4045	0.67					0.013
Rutile	110	4196	0.86					0.006
Blend	141	4113	0.77					0.008

^{*} Value obtained from Kunii and Levenspiel, 1991, (pp62)

[†] Value obtained from Kunii and Levenspiel, 1991, (pp68)

[‡] Value obtained from http://www.engineeringtoolbox.com/dry-air-properties-d_973.html

The average particle size of Slag A is larger than the other feedstocks and consequently minimum fluidising velocity is higher.

Terminal velocity (U_t) for the various size fractions was determined using Equation 35; results are presented in Table 11. At gas velocities higher than the terminal velocity, particles will be blown out of the bed.

$$u_t = u_t^* \left(\frac{\mu(\rho_s - \rho_g)g}{\rho_g^2} \right)^{\frac{1}{3}} \dots\dots\dots(35)$$

Table 11: Terminal Velocity of different feedstocks

Particle size (μm)	Slag A (m/s)	Slag B (m/s)	Rutile (m/s)	Blend (50wt% Slag A, 50wt% Rutile) (m/s)
300	2.34	2.35	2.66	2.50
212	1.41	1.41	1.54	1.48
150	0.80	0.81	0.85	0.83
106	0.44	0.44	0.45	0.45

The gas velocity used in the chlorination experiments should be a value above the minimum fluidising velocity but below the terminal velocity of the smallest particles.

4.1.3 Elutriation Constants

The elutriation constant (kg/m².s) gives an indication of the tendency of a particular material or size fraction to be blown out of the reactor. Following the experimental procedure described in Chapter 3, the values

presented in Table 12 to Table 15 were obtained for the initial PSD and the PSD after 30 minutes of fluidisation.

Table 12: Experimental data for Slag A elutriation calculation

Initial weight of sample = 600 grams		Blowover = 18 grams	
Particle size distribution		Particle size distribution	
Size(μm)	Mass(grams)	Size(μm)	Mass (grams)
-212 + 150	77.8	-212 + 150	0.75
-150 + 100	55.7	-150 + 100	3.80
-106 + 75	26.5	-100 + 75	4.80
-75	16.5	-75	8.50

Table 13 : Experimental data for Slag B elutriation calculation

Initial weight of sample : 600 grams		Blowover : 24.5 grams	
Particle size distribution		Particle size distribution	
Size(μm)	Mass(grams)	Size(μm)	Mass (grams)
-212 + 150	79.8	-212 + 150	0.7
-150 +100	59.1	-150 +100	3.9
-106 + 75	54.0	-100 + 75	4.1
-75	61.2	-75	15.9

Table 14: Experimental data for Rutile elutriation calculation

Initial weight of sample : 600 grams		Blowover : 1.5 grams	
Particle size distribution		Particle size distribution	
Size(μm)	Mass(grams)	Size(μm)	Mass (grams)
-212 + 150	116.2	-212 + 150	0.06
-150 +100	293.0	-150 +100	0.3
-106 + 75	170.4	-100 + 75	0.4
-75	8.1	-75	0.7

Table 15: Experimental data for Blend elutriation calculation

Initial weight of sample : 600 grams		Blowover : 2 grams	
Particle size distribution		Particle size distribution	
-212 + 150	94.0	-212 + 150	-
-150 +100	170.4	-150 +100	0.130
-106 + 75	95.4	-100 + 75	0.300
-75	10.2	-75	1.600

Figure 29 compares the blowover percent for the various feedstocks' after the 30 minute fluidisation experiment. The highest carryover was experienced with Slag B, followed by Slag A, the blend and then rutile. Slag B had the highest mass of fine material (i.e. < 212µm) at the start so it isn't a surprise that the blowover was the highest.

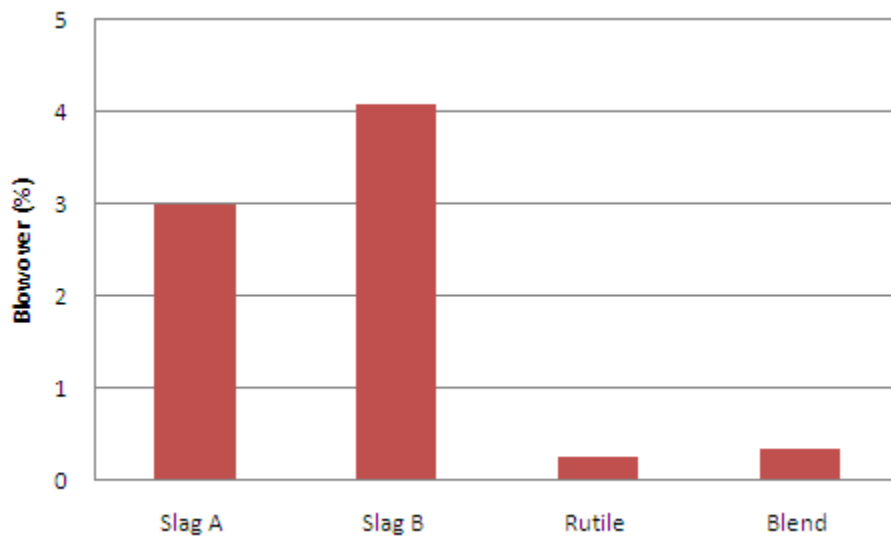


Figure 29: Blowover from elutriation experiment as a percentage of the initial mass of feed

Blowover from the rutile sample is significantly lower than Slag A or Slag B. The finer material (i.e. < 75µm) had the highest tendency to be elutriated. A small fraction of the particles in -212 +150 µm size range was also elutriated; particles larger than 212 µm were not elutriated.

The blowover of the blend sample is significantly lower than Slag A. The results indicate that the addition of rutile changes the hydrodynamic properties of the bed, improving the overall performance. With the combination of feedstocks, there is bound to be a difference in the physical properties of the bed (e.g. shape factor, density, bed voidage), the most obvious being the difference in particle size distribution and the

average particle size (i.e. d_{50}). The d_{50} of Slag A is 294 μm and the d_{50} of rutile is 110 μm (PSD presented in Figure 21 and d_{50} in Table 6), by combining the feedstocks the distribution is widened.

From the literature, it is clear that particle size distribution (Sun and Grace (1990), Grace and Sun (1991), Sharma and Pugsley (2010), Beetstra et al., (2009)) and fines content (Yates and Newton (1986), Li et al., (2004), Shin et al., (2007), Baeyans et al., (1992)) have an effect on fluidisation behaviour. However, the effect of PSD and the effect of fines are not easy to quantify, it is dependent on a number of factors, differs from material to material, depends on the fines fraction, the size of the fines, etc. Sun and Grace (1990), fluidised materials having the same d_{50} but varying PSD (i.e. bimodal, narrow and wide) within the same size range (i.e. -130 + 20 μm). The wide particle size distribution yielded the highest conversion rate, smallest voids, and largest bed expansion. Beetstra et al., (2009) demonstrated that the bubble diameter could be reduced by 40% by manipulating the particle size distribution.

Sun and Grace (1990) concluded that a wider particle size distribution leads to more expanded dense phase with smaller voids which results in smaller bubble generation. According to Baeyans et al., (1992) and George and Grace (1978), particle entrainment is the result of bursting bubbles at the bed surface. Smaller bubbles generate lower entrainment rates. Wen and Chen (1982) correlated the rate of particles ejected at the bed surface in terms of hydrodynamic properties of the bed such as bubble diameter and excess gas velocity above minimum fluidising velocity. George and Grace (1978) correlated the volume of particles ejected at the freeboard as a function of particle diameter.

In summary, particle size distribution has an effect on the fluidised bed performance, literature indicates that the bubble size is reduced with a wider distribution, entrainment is lowered with smaller bubbles and this offers an explanation as to why the blend has a lower blowover. It will be interesting to see if this trend with the blend is observed during the chlorination experiments because this will improve chlorination.

Elutriation constant was determined with Equation 36; the calculated values are presented in Table 16.

$$\frac{W_i}{W_{io}} = \exp\left(-\frac{k_i^* A t}{W}\right) \dots\dots\dots(36)$$

- W_{io} = initial weight of mass fraction i
- W_i = final weight of mass fraction i
- W = total weight of sample before fluidisation
- A = area of reactor (m^2)
- t = time (s)

k_i^* = elutriation constant ($\text{kg/m}^2 \cdot \text{s}$)

Elutriation constant is proportional to the amount of material that is removed from the chlorinator. Intuitively smaller size fractions are more likely to be elutriated and this is illustrated by the results. Elutriation constant for particles less than 75 μm particles is more than 3 times greater than the next highest size range. The elutriation constants of the blend is lower than the average of the rutile and Slag A elutriation constants, the values are close to that of rutile's indicating that the slag blowover is significantly reduced in the blend.

Table 16: Elutriation Constants

Elutriation Constants ($\text{kg/m} \cdot \text{s}$)				
Size Fraction	Slag A	Slag B	Rutile	Blend
	$\times 10^{-3}$			
-212 +150	0.3	0.3	0.019	0.000
-150 + 106	2.5	2.4	0.04	0.027
-106 + 75	7	2.8	0.08	0.110
-75	25.6	10.6	3.2	5.861

4.2 CHLORINATION

Four titania samples were chlorinated with coke and CO as per the experimental procedure described in Chapter 3. The mineralogical characterisation of the feed material and bed samples as well as the mass balance are presented in this section.

4.2.1 Mineralogical Characterisation of Feed Material

The titania feedstocks and bed samples were examined by Scanning electron microscopy (SEM)/EDS and XRD to determine the phases present in the feed material and bed samples. SEM analysis is available in Appendix 3 and XRD analysis is presented in Appendix 6.

SEM images (Figure 30 to Figure 32) clearly show that the rutile particles are far more evenly sized and rounded than the slag particles. The slag particles also appear to have more cracks and defects; these provide ideal sites for the chlorination reaction and points for breakage. The slag has been milled hence has a wider particle size and a more irregular shape than the naturally occurring rutile.

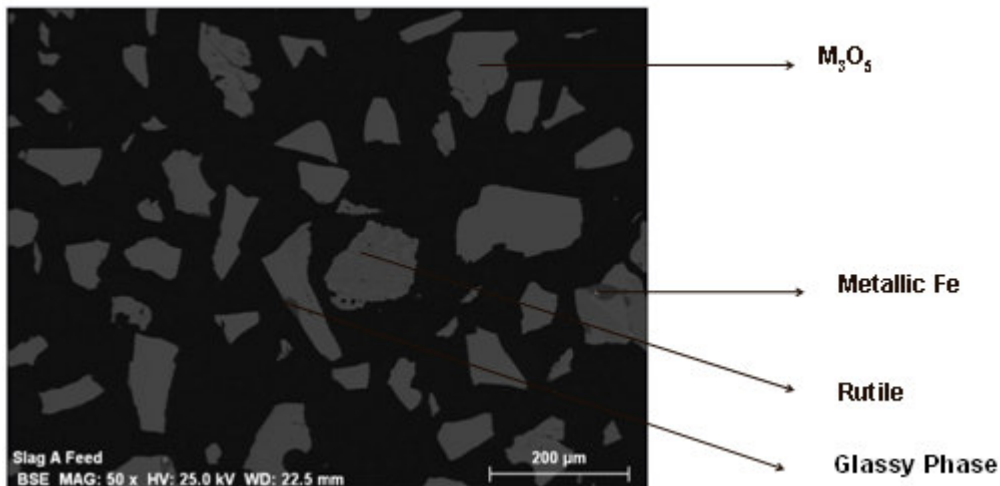


Figure 30: BSE Image of Slag A

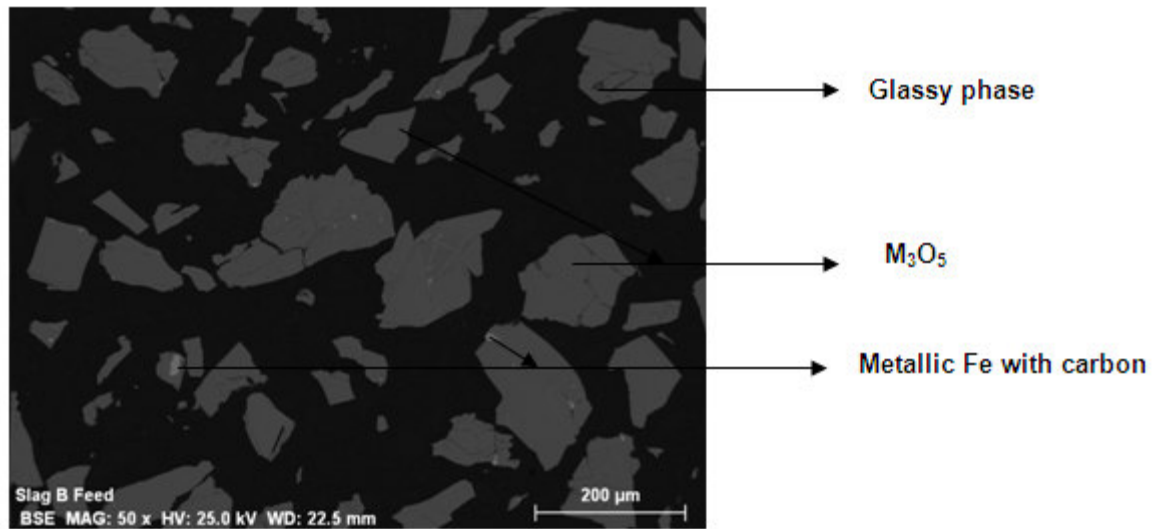


Figure 31: BSE Image of Slag B

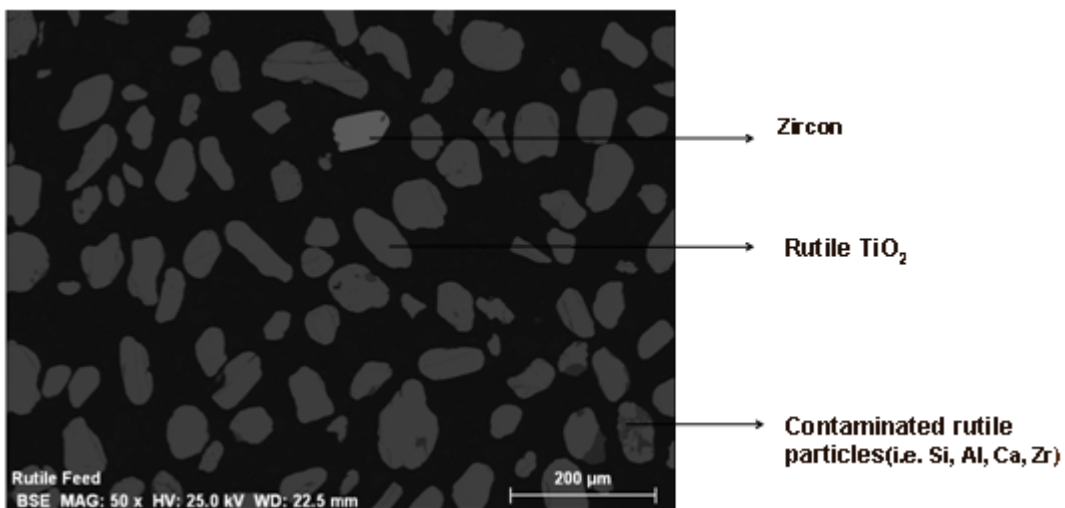


Figure 32: BSE Image of Rutile Feed

4.2.1.1 Slag A

Identification and characterisation of the phases were done by EDS point analysis, a back scattered electron image illustrating the various phases is given in Figure 33 . Several samples were analysed, the bulk analysis is available in Appendix 3.

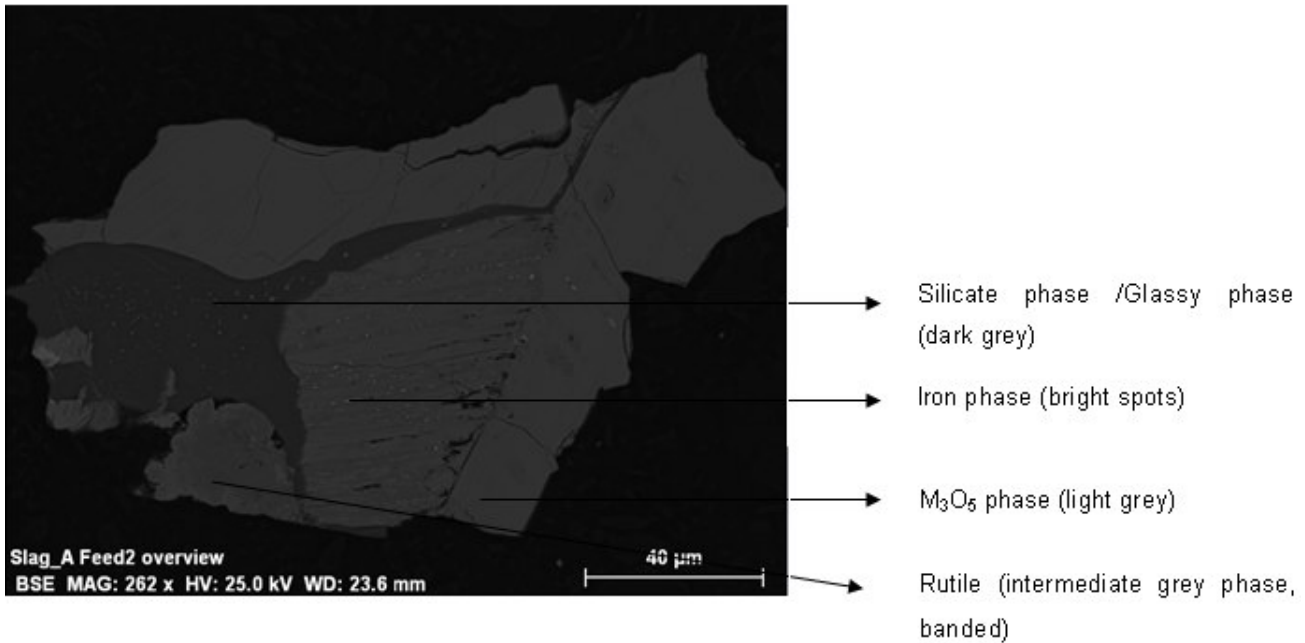


Figure 33: BSE image of Slag A particle

The solid solution phase (i.e. M₃O₅ phase) was identified as the major phase in the Slag A samples by XRD, the second most predominate phase was a glassy silicate followed by rutile with precipitated Fe (Figure 34). The average compositions of the various phases are given in Table 17 to Table 20. Fe droplets are very small and difficult to analyse without background interference from the matrix. The M₃O₅ phase composition was calculated by normalising the SEM point analysis in order to obtain the number of cations for every five oxygen atoms. The calculated M₃O₅ phase is given in Table 17. There are a total of 3.35 cations for every 5 oxygen atoms; this ratio is higher than what is expected for the M₃O₅ phase. Since M₃O₅ was identified as the major phase by XRD analysis, this suggests that there is some error in the oxygen analysis determined by the SEM analysis. In order to balance the charges, the Ti³⁺ fraction (as a fraction of the total Ti in moles) of the M₃O₅ phase was found to be over 0.8, which is too high, this also suggests that there is an error in the oxygen analysis as determined by SEM analysis.

The tabular lath like rutile crystals is accompanied by abundant fine grained metallic iron precipitates. Bessinger (2000) and Toromanoff and Habashi (1984) also found metallic iron to be present in the rutile phase. According to Toromanoff and Habashi (1984), the precipitates nucleated during the cooling of the slag as a result of the following reaction:



The glassy phase is present in various shapes and sizes throughout most of the slag particles and consists of mainly of SiO₂, with smaller amounts of Al₂O₃ and TiO₂.

Table 17: Average composition of the M₃O₅ phase in Slag A (Point analysis)

	O	Mg	Al	Si	Ti	Mn	Fe
	(wt%)						
M₃O₅ phase	32.53	0.84	0.89	0.09	56.06	1.45	8.14

Average composition: Mg_{0.08}Al_{0.07}Ti_{2.83}Mn_{0.06}Fe_{0.32}O₅(M_{3.35}O₅)

Table 18: Average composition of the Glassy phase in Slag A (Point analysis)

	O	Na	Mg	Al	Si	K	Ca	Ti	Mn	Fe	Zr	Nb
	(wt%)											
Glassy phase	50.62	1.53	0.12	4.27	35.49	1.6	1.69	3.81	0.11	0.42	0.19	0.15

Table 19: Average composition of rutile and iron in Slag A (Point analysis)

	O	Si	Ti	Fe
	(wt%)			
Rutile + Fe phase	6.49	0.08	27.03	66.4

Table 20: Average composition of the rutile phase in Slag A (Point analysis)

	O	Ti	Mn	Fe
	(wt%)			
Rutile phase	38.00	60.08	0.37	0.97

Calculated composition (normalising O to 5): Ti_{1.1}O₂

4.2.1.2 Slag B

Similarly to Slag A, M₃O₅ was identified as the predominant phase by XRD analysis. The M₃O₅ phase appears to be made up of a number of different phases, namely an Mn-rich phase which can be equated to kennedyite ((Fe,Ti,Mn)Ti₂O₅), an Fe-Ti phase which can be related to amalcolite ((Fe,Ti)Ti₂O₅) and pseudobrookite (Fe₂TiO₅). These phases belong to a solid solution series where M can consist of variable amounts of Fe, Ti, Mg or Mn. The glassy phase and metallic iron was identified in the SEM analysis. No rutile was identified in the SEM analysis, although 4% was picked up by XRD. The average composition of the major phases in Slag B is presented in Table 21 to Table 23. The iron droplets present in Slag A were between 1 and 2 μm whereas in Slag B it is approximately 20μm and associated with carbon. The chemistry and size of the iron droplets indicate that they were trapped in a viscous slag and didn't precipitate out during cooling as with Slag A. Slag B has a higher TiO₂ content than Slag A. The composition of the silicate phase of the two slag's also differ, Slag B has significantly higher Ca and Mn in the silicate phase.

The calculated M_3O_5 phase composition is given in Table 21. Similarly to Slag A, the cations to oxygen ratio is high suggesting that there is an error in the oxygen content as determined by SEM analysis.

Table 21: Average Composition of the M_3O_5 phase in Slag B Feed Material (Point analysis)

	O	Al	Si	Ti	Mn	Fe
	(wt%)					
M_3O_5 phase	33.93	1.21	0.03	61.70	1.85	1.28

Calculated composition (normalising O to 5): $Al_{0.09}Ti_{2.98}Mn_{0.07}Fe_{0.05}O_5(M_{3.2}O_5)$

Table 22: Average Composition of the glassy phase in Slag B Feed Material (Point analysis)

	O	Na	Al	Si	S	K	Ca	Ti	Mn	Fe	Zr	Nb
	(wt%)											
Glassy Phase	48.98	1.39	4.72	25.26	0.12	0.38	3.73	4.05	10.18	0.13	0.56	0.4

Table 23: Average Composition of the Fe phase in Slag B Feed Material (Point analysis)

	C	Si	Ti	Cr	Mn	Fe	Nb
	(wt%)						
Fe	2.81	0.89	1.46	0.23	0.69	93.83	0.10

4.2.1.3 Rutile

Majority of the particles are clean rutile particles but a few do show signs of contamination with impurities (i.e. Si, Al, Fe, Ca). A few free lying zircon particles were also identified. The average analysis of the rutile, zircon and iron silicate phase is given in Table 24 to Table 26.

Table 24: Average Composition of rutile phase

	O	Al	Si	Ti	Nb	Zr
	(wt%)					
Rutile	38.02	0.45	0.16	61.23	0.05	0.08

Table 25: Average Composition of Zircon in rutile

	O	Si	Zr
	(wt %)		
Zircon	32.2	15.69	52.12

Table 26: Average composition of iron silicate phase

	O	Na	Mg	Al	Si	K	Ti	Fe	Ca
	(wt%)								
Iron silicate	49.33	0.78	2.00	3.50	24.15	1.19	2.39	15.96	0.70

4.2.2 Mineralogical characterisation of Bed Samples

After the 30, 60 and 180 minute experiments, the remaining bed sample was collected and prepared for SEM analysis. The SEM images provided vital information for understanding the difference in the chlorination mechanism of slag and rutile. No particle agglomeration was observed in the bed samples. Figure 34 to Figure 36 show a porous slag matrix depleted of Fe and Mn whilst the rutile is still very much solid with chlorination taking place at the boundaries and on cracks and other particle defects. Figure 34 is an image of a Slag A particle after 1 minute of chlorination; porosity is evident even at this early stage. Figure 35 shows the images of the bed samples after 30 minutes of chlorination whilst Figure 36 shows images after 180 minutes of chlorination. It is clear from these images that the slag becomes more porous as chlorination time increases whilst rutile remains solid.

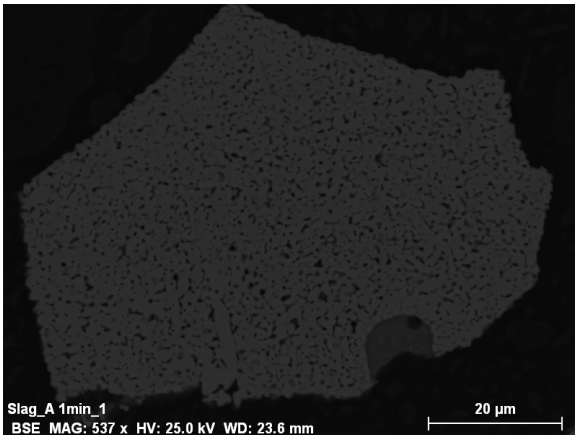
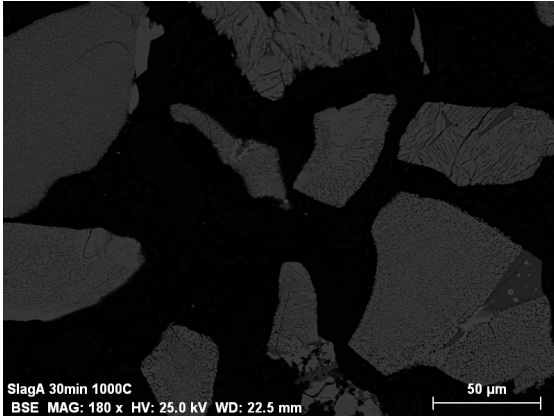
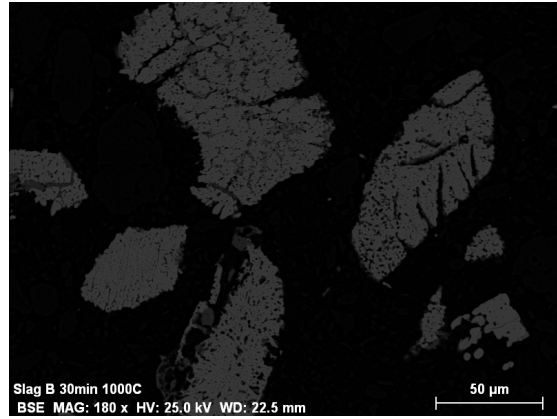


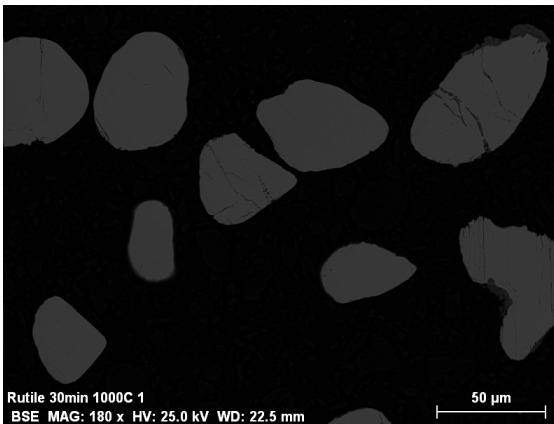
Figure 34: BSE image of Slag A after 1 minute of chlorination



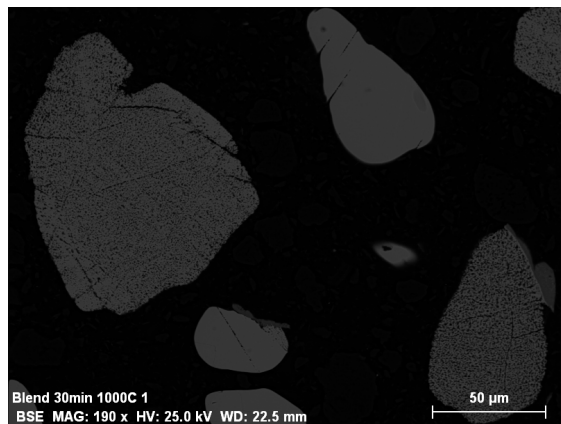
a.



b.

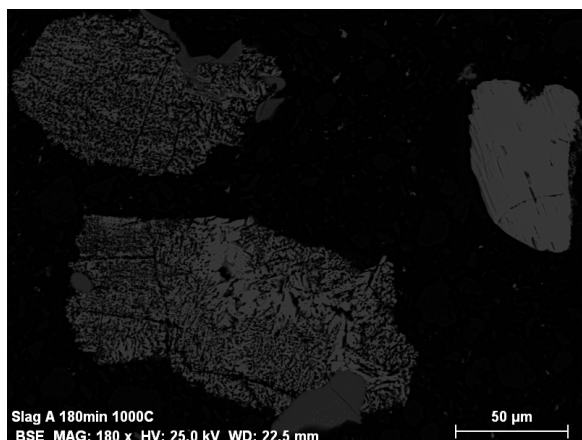


c.

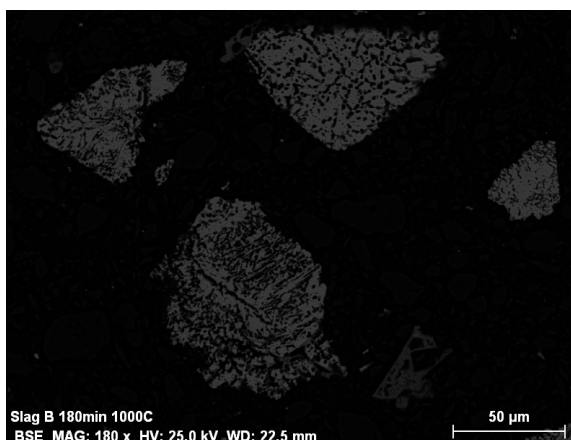


d.

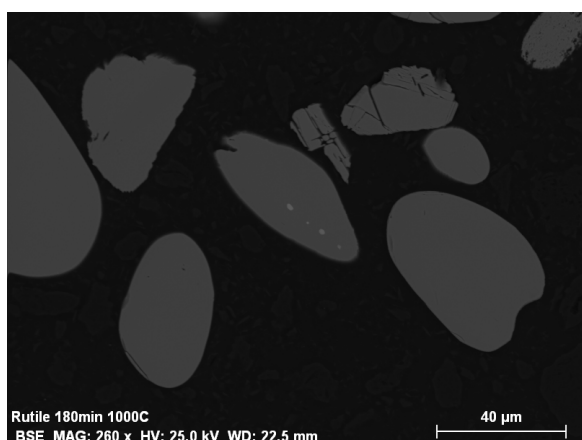
Figure 35: BSE image of bed samples after 30 minutes of chlorination at 1000°C, (a) Slag A, (b) Slag B, (c) Rutile, (d) Blend (a mixture of 50wt % rutile and 50wt% Slag A)



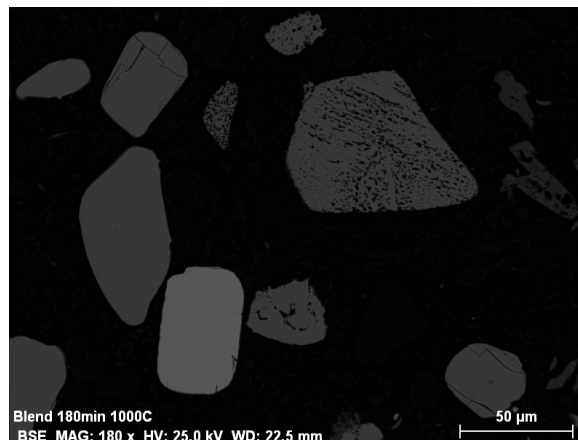
a.



b.



c.



d.

Figure 36: BSE image of bed samples after 180minutes of chlorination at 1000°C, (a) Slag A, (b)Slag B, (c) Rutile, (d) Blend (a mixture of 50wt % rutile and 50wt% Slag A)

The phase composition of the titania bed sample products as determined by XRD is given in Table 62 to Table 65. Diffractograms are available in Appendix 6. XRD analysis identified rutile as the major phase in the chlorinated bed samples.

SEM images of chlorinated rutile and slag particles are given in Figure 37 to Figure 42. EDS point analysis was done on selected points in each sample; the normalised results are given in Table 27 to Table 32. The analysis of the points of interest are presented in this section of the report, the full point analysis is available in Appendix 5. With the exception of samples that were chlorinated for 1 minute, rutile was identified as the major titania phase in all the bed samples, this analysis is supported by the XRD results.

With EDS point analysis small amounts of chlorine (maximum 3.97%) was identified on the slag samples (Figure 37 to Figure 41). These points were usually identified in porous areas of the particle and were not

restricted to the edge of the sample as with rutile. Small amounts of chlorine were also identified on the silicate phases (Figure 41 and Table 31). With rutile, evidence of chlorination was only found on the boundary of the particle, close to a crack (Figure 42).

The images confirm that with the early chlorination of iron and manganese the slag becomes porous and the area for subsequent reaction increases whereas with rutile chlorination is limited to the surface of particle. More SEM images and point analysis results are available in Appendix 4.

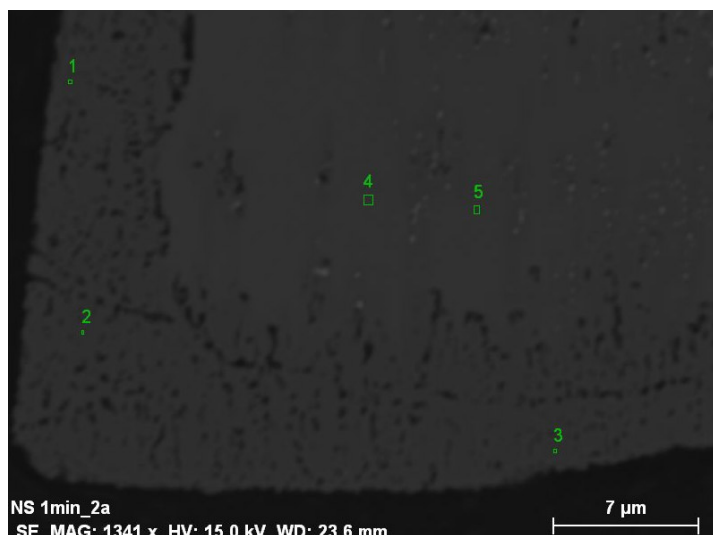


Figure 37: BSE image of Slag A after 1 minute of chlorination at 1000°C – Sample 1

Table 27: Normalised Point analysis of Slag A – Sample 1

	O	Mg	Al	Si	Cl	Ca	Ti	Mn	Phase
	(%)								
1	36.85	0.12	0.35	0	0.32	0.47	61.88	0	$M_3O_5-Mg_{0.01}Al_{0.03}Ca_{0.03}Ti_{2.81}O_5$
2	35.74	0.00	0.32	0	1.62	0.52	60.75	1.04	$M_3O_5-Al_{0.03}Ca_{0.03}Ti_{2.84}O_5$
3	36.3	0.00	0.45	0	0.19	0.45	62.62	0	$M_3O_5-Al_{0.04}Ca_{0.03}Ti_{2.9}O_5$

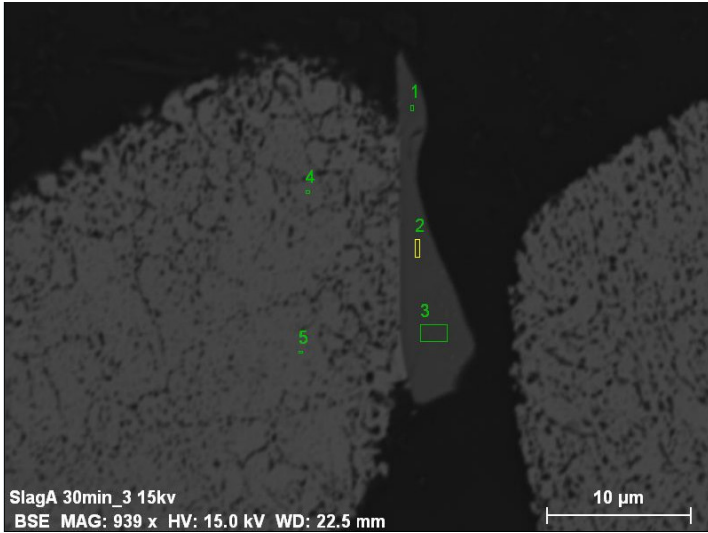


Figure 38: BSE image of Slag A after 30 minutes of chlorination at 1000°C – Sample 2

Table 28: Normalised Point analysis of Slag A –Sample 2

	O	Mg	Al	Si	Cl	Ca	Ti	Phases
	(%)							
1	57.21	0.23	3.26	34.55	0.00	2.17	2.57	Glassy phase
2	56.88	0.00	3.26	35.27	0.00	2.10	2.50	Glassy phase
3	57.80	0.00	2.96	34.13	0.00	2.27	2.84	Glassy phase
4	37.59	0.52	0.10	0.00	2.48	0.00	59.32	Rutile –Ti _{1.05} O ₂
5	37.33	0.81	0.00	0.00	3.97	0.00	57.89	Rutile –Ti _{1.03} O ₂

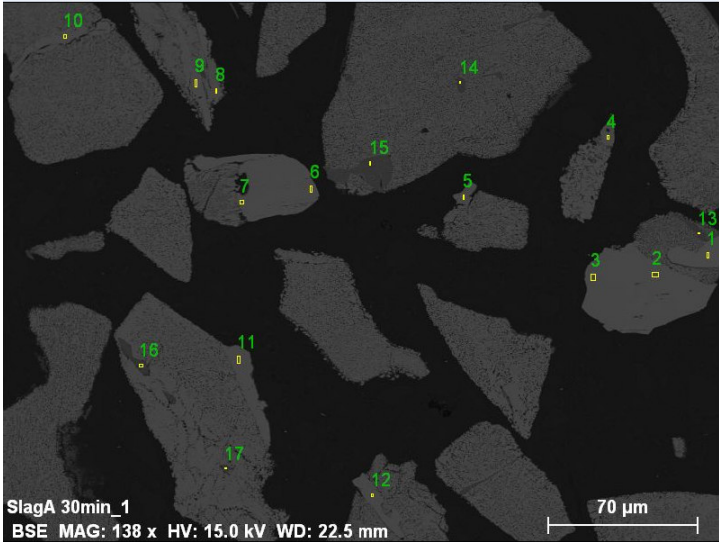


Figure 39 : BSE image of Slag A after 30 minutes of chlorination at 1000°C – Sample 3

Table 29: Normalised Point analysis of Slag A – Sample 3

	O	Mg	Al	Si	Cl	Ca	Ti	Mn	Fe	Phase
	(%)									
13	56.71	0.90	3.85	33.59	0.24	1.69	3.03	0.00	0.00	Glassy phase
14	56.39	0.00	2.95	35.00	0.00	1.88	3.77	0.00	0.00	Glassy phase
15	57.93	0.00	3.20	31.62	0.00	4.32	2.93	0.00	0.00	Glassy phase
16	50.86	0.47	3.18	36.97	0.64	1.83	4.33	0.60	1.11	Glassy phase
17	54.30	2.28	4.39	34.33	0.67	0.69	3.35	0.00	0.00	Glassy phase

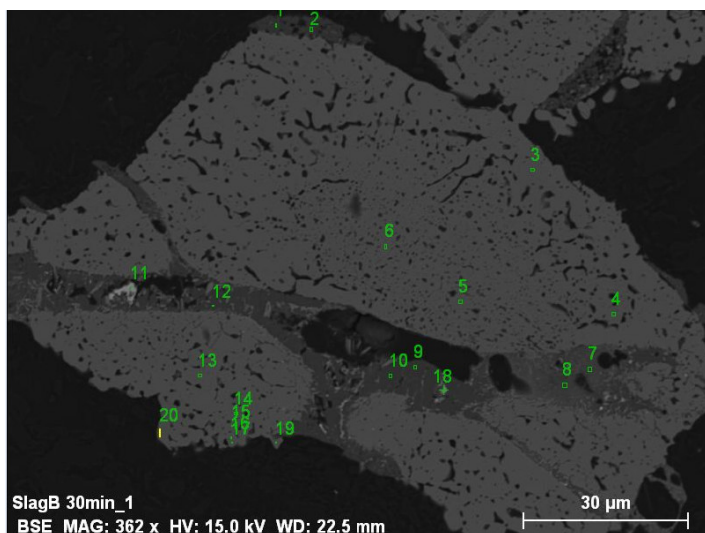


Figure 40: BSE image of Slag B after 30 minutes of chlorination at 1000°C – Sample 4

Table 30: Normalised Point analysis of Slag B – Sample 4[‡]

	O	Na	Al	Si	Cl	Ca	Ti	Phase	
	(%)								
1	55.36	1.08	2.02	38.27	0.00	0.55	2.72	Glassy Phase	
2	54.90	1.31	1.93	37.66	0.00	0.94	3.27	Glassy Phase	
3	39.18	0.00	0.00	0.00	0.00	0.00	60.82	Rutile –Ti _{1.04} O ₂	
4	39.57	0.00	0.00	0.00	0.43	0.00	59.99	Rutile –Ti _{1.01} O ₂	
16	40.12	0.00	0.00	0.00	0.76	0.24	58.88	Rutile –Ti _{1.00} O ₂	
17	38.16	0.00	0.00	0.00	0.00	0.00	61.84	Rutile –Ti _{1.08} O ₂	
19	37.91	0.00	0.34	0.00	0.00	0.00	61.76	Rutile –Ti _{1.08} O ₂	
20	41.00	0.00	0.17	0.12	0.00	0.00	58.71	Rutile –Ti _{1.00} O ₂	

[‡] Full analysis available in Appendix 5

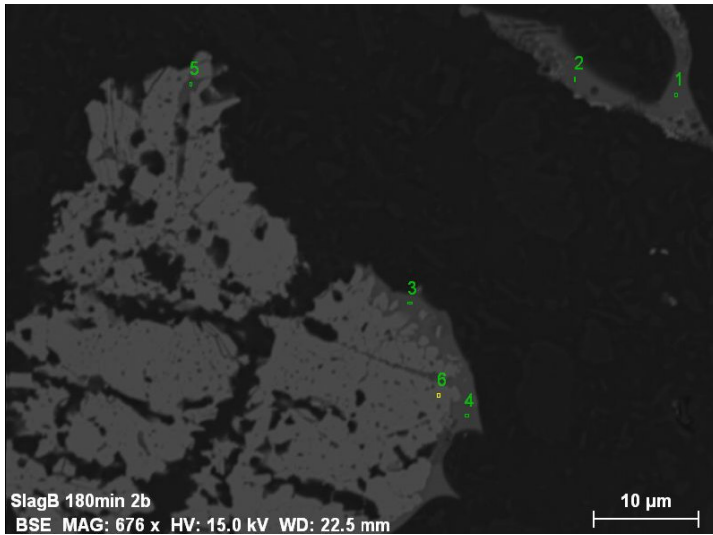


Figure 41: BSE image of Slag B after 180 minutes of chlorination at 1000°C – Sample 5

Table 31: Normalised Point analysis of Slag B – Sample 5

	O	Al	Si	Cl	Ca	Ti	Zr	Nb	Phase
	(%)								
1	57.59	4.85	27.57	0.93	2.26	6.81	0.00	0.00	Glassy phase
2	58.34	3.56	28.76	0.63	1.77	6.53	0.00	0.41	Glassy phase
3	54.94	6.17	27.17	1.25	4.70	5.62	0.00	0.14	Glassy phase
4	57.21	5.84	26.38	1.08	4.52	4.88	0.00	0.09	Glassy phase
5	54.38	4.54	28.33	0.93	3.21	8.35	0.00	0.28	Glassy phase
6	38.03	0.19	0.10	0.00	0.00	61.22	0.47	0.00	Rutile –Ti _{1.08} O ₂

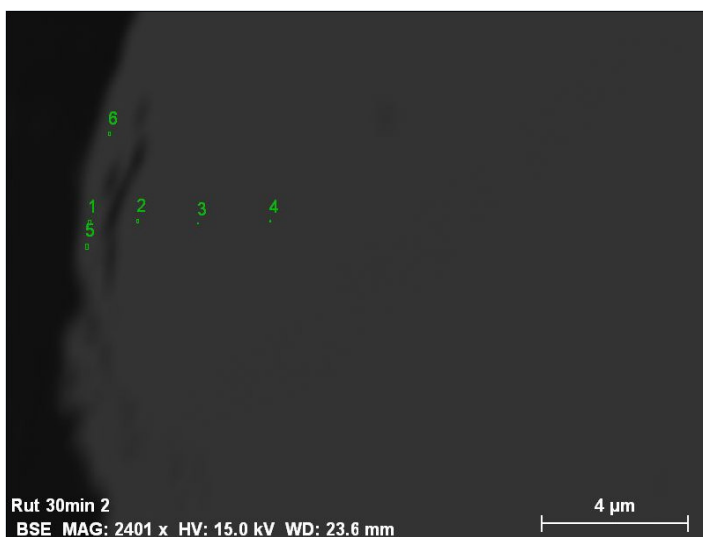


Figure 42: BSE image of rutile particle after 30 minutes of chlorination at 1000°C – Sample 6

Table 32: Normalised Point analysis of rutile particle – Sample 6

	O	Al	Cl	Ti	Phases
	(%)				
1	40.36	0.00	0.10	59.53	Rutile –Ti _{0.98} O ₂
2	38.79	0.17	0.00	61.04	Rutile –Ti _{1.05} O ₂
3	38.84	0.06	0.00	61.1	Rutile –Ti _{1.05} O ₂
4	38.98	0.11	0.00	60.92	Rutile –Ti _{1.04} O ₂
5	41.66	0.00	0.10	58.24	Rutile –Ti _{0.93} O ₂
6	39.75	0.06	0.07	60.12	Rutile –Ti _{1.01} O ₂

4.2.3 Mass Balance

Four titania samples were chlorinated with coke and CO as per the experimental procedure described in Chapter 3. Upon completion of the experiment, the bed residues and the blowover were weighed and analysed. Using these masses, the degree of conversion of solid material to gaseous chlorides was determined. No gas analysis was completed during the experiment, and the mass balance was completed assuming that the difference between the initial mass and the remaining mass (i.e. bed residue plus blowover) was the mass that was chlorinated.

One of the aims of this research project was to determine the rate of chlorination for each feedstock, due to the significant blowover after 180 minutes of chlorination; it was not possible to do so and therefore a new parameter was defined i.e. degree of conversion. If the blowover for a test is significant, the rate of chlorination is falsely lowered, however it would also be incorrect to exclude the blowover mass as these particles are partially chlorinated.

Mass chlorinated or degree of conversion (%) is defined as:

$$D_c = \frac{M_{chlorinated}}{M_{initial}} \times 100\% \dots\dots\dots(38)$$

$$M_{chlorinated} = M_{initial} - M_{bed} - M_{blowover} \dots\dots\dots(39)$$

where,

- D_c = degree of conversion or mass chlorinated (%)
- $M_{chlorinated}$ = mass chlorinated (g)
- $M_{initial}$ = mass of initial feedstock (g)
- M_{bed} = mass of feedstock remaining in bed (g)
- $M_{blowover}$ = mass of blowovers(g)

Using Equation 38, the degree of conversion was calculated for each feedstock based on experiments carried out with petroleum coke (20 wt% of the feedstock mass), Cl₂ (67 vol %), CO (33 vol%) and feedstock particles greater than 106 μm and less than 300μm. The results are presented Appendix 4, Table 51 to Table 54 together with the detailed mass balance of the major elements. In the mass balance, Ti is expressed as Ti₂O₃, TiO₂ and TiO₂ (equivalent) in the results. TiO₂ equivalent is the total Ti (i.e. Ti³⁺ and Ti⁴⁺) expressed as TiO₂.

4.2.4 Chlorination as a function of temperature

To test the effect of temperature, Slag A, Slag B and rutile was chlorinated for 3 hours with 20 wt% petroleum coke in a CO and Cl₂ environment at 800°C, 900°C and 1000°C. The results are presented in Figure 43 below.

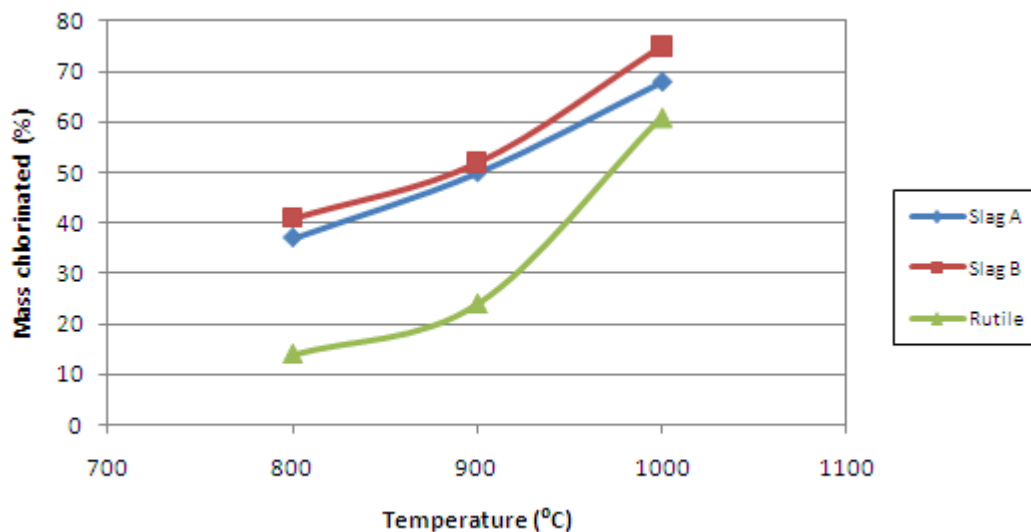


Figure 43: Chlorination as a function of temperature for 180 minutes

Temperature has a significant effect on the overall chlorination rate with the chlorination of rutile especially hindered at lower temperatures. Slag B shows the highest degree of chlorination, with Slag A following closely behind. At 800°C only 15% of rutile is chlorinated compared to 60% at 1000°C. It is clear to see why the commercial chlorination process is carried out at 1000°C.

Figure 43 shows the dependence of overall conversion rate on temperature, delving deeper into the chlorination of the individual elements, Figure 44 to Figure 46 show that MgO, Al₂O₃ and TiO₂ chlorination significantly increases with increasing temperatures. TiO₂ chlorination is especially hindered at low temperatures; at 800°C the chlorination of TiO₂ in rutile was 15% whilst at 1000°C it was 62%. With increasing temperature, the gap in TiO₂ chlorination between rutile and the slags is narrowed. At 800°C, rutile TiO₂ chlorination was more than 20% less than Slag B, whilst at 1000 °C it is down to 12%.

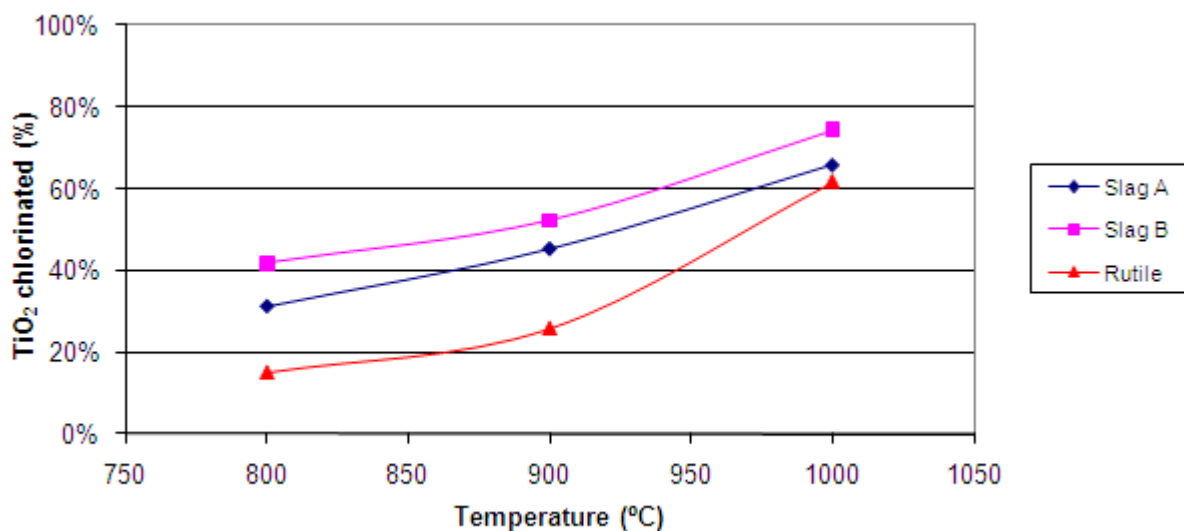


Figure 44: TiO₂ chlorination as a function of temperature for 180 minutes

Al₂O₃ conversion to AlCl₃ significantly improves with increasing temperature (Figure 45); there is a 40% improvement in Al₂O₃ chlorination when temperature is increased from 800°C to 1000°C. Al₂O₃ chlorination in rutile is lower than the titania slags.

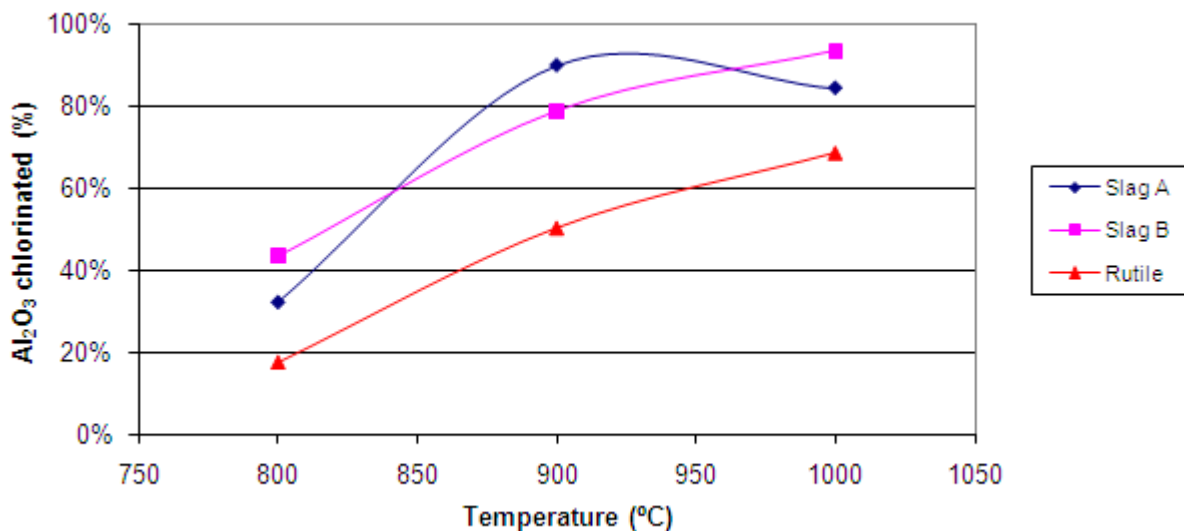


Figure 45: Al₂O₃ chlorination of as a function temperature for 180 minutes

MgO chlorination (Figure 46) in the Slag A and Slag B improves with increasing temperature. Complete MgO chlorination is achieved in the rutile sample at 800°C.

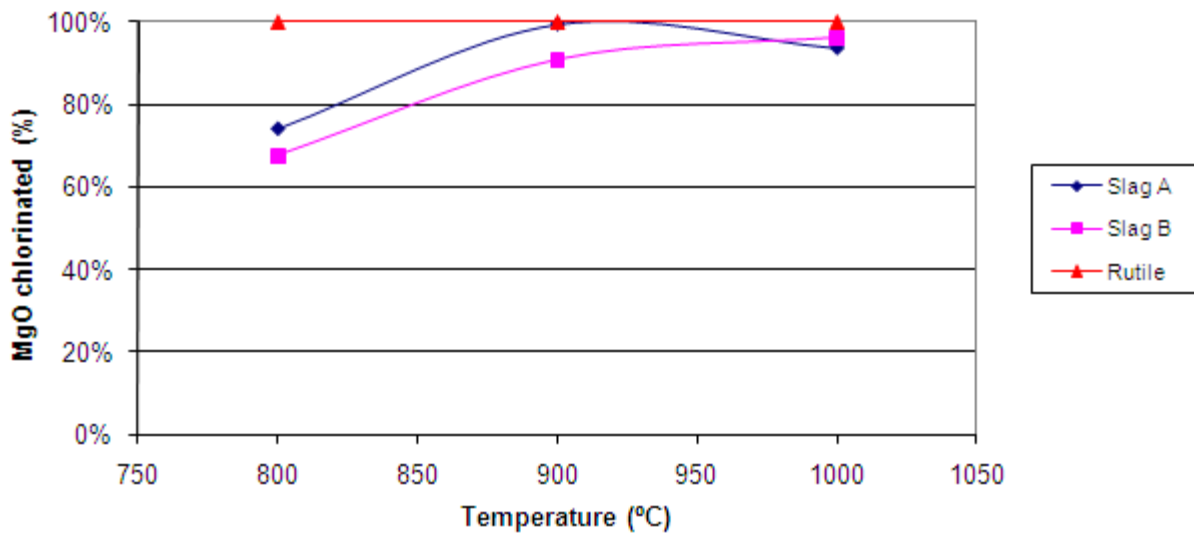


Figure 46: MgO Chlorination as a function of temperature for 180 minutes

The chlorination of FeO (Figure 47) in rutile is slightly hindered at 800°C, whilst that of Slag A and B is largely unaffected.

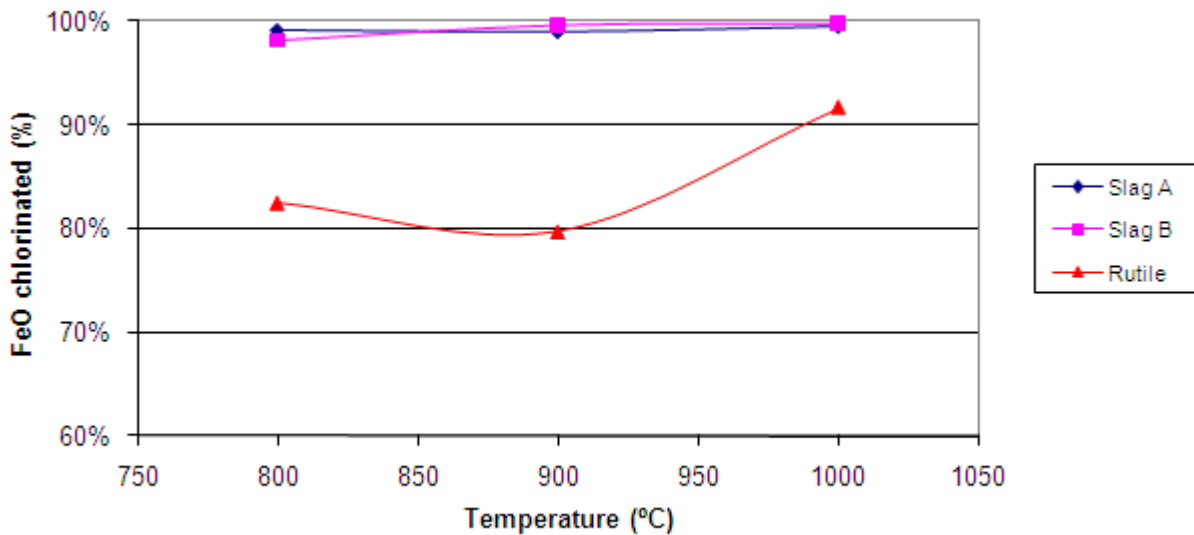


Figure 47: FeO chlorination as a function of temperature for 180 minutes

MnO chlorination (Figure 48) of the slags is above 90% at 800 °C, but was 5% lower than the 1000°C experiment. Complete MnO chlorination is achieved in the rutile sample at 800°C.

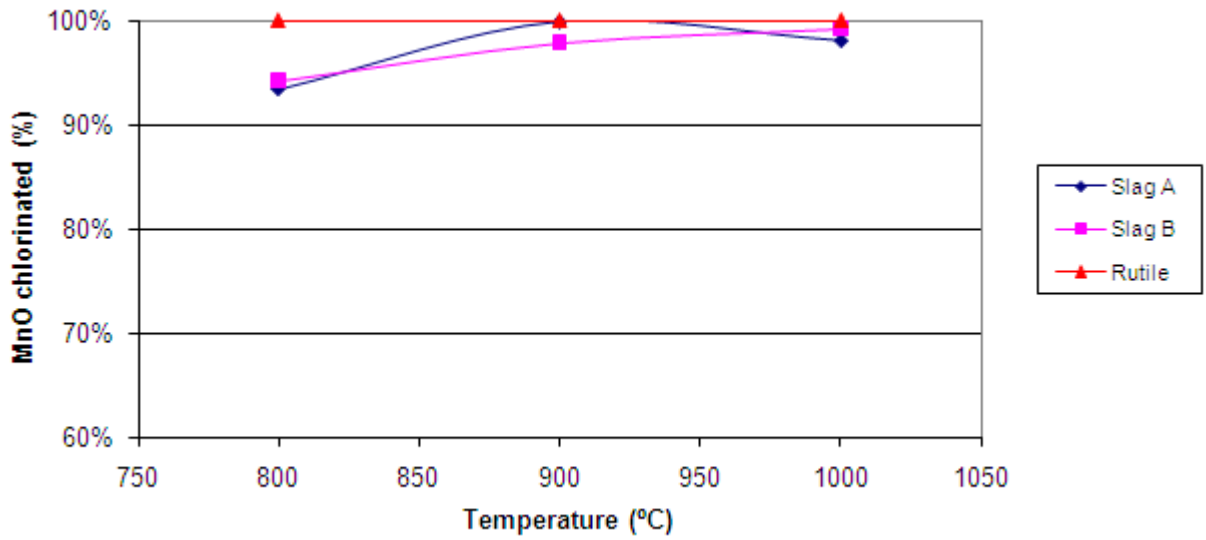


Figure 48: MnO chlorination as a function of temperature for 180 minutes

The SiO₂ content (%) of the bed sample is higher than the initial feed analysis. The mass balance shows that there is more SiO₂ in the bed sample than at the start of the reaction; this difference is approximately 1g to 2g and is considered insignificant compared to the total sample mass. This is probably due to analytical error. This indicates that SiO₂ does not chlorinate significantly during the experiment.

4.2.5 Chlorination as a function of time

Using Equation 38, the relative degree of conversion of Slag A, Slag B, rutile and the blend (i.e. a mixture of 50wt% rutile and 50wt% slag) to chloride gas was plotted in Figure 49. The curves are based on the experiments carried out with petroleum coke (20 wt% of the feedstock mass), Cl₂, CO and feedstock particles greater than 106 μm and less than 300μm.

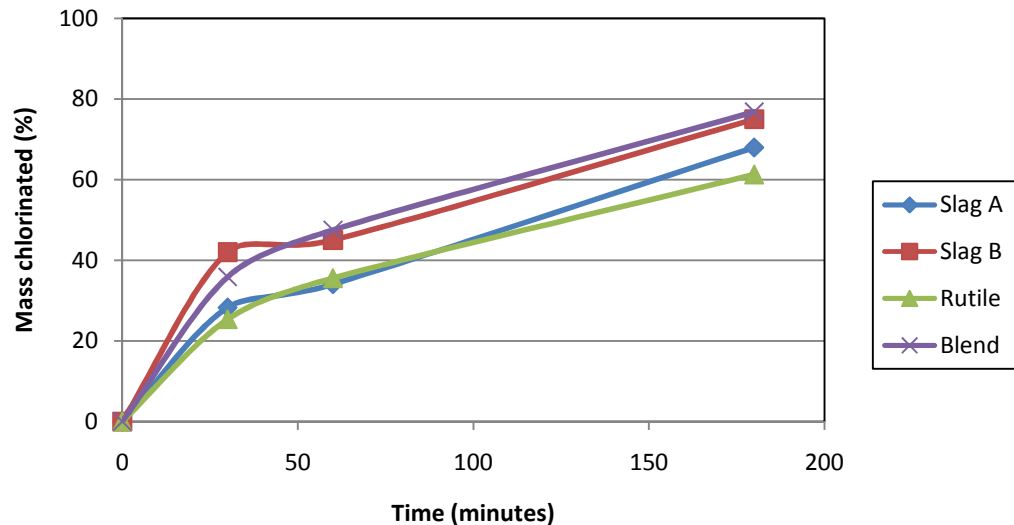


Figure 49: Mass chlorinated at 1000°C

At 1000°C, the highest degree of conversion was achieved with the blend (i.e. 77%), whereas that of rutile was 61% and Slag A was 68%. These results are inconsistent with the findings of Nell and den Hoed (2003) who noted that the rate of chlorination was proportional to the iron content of the feedstock. If this was the case, then Slag A should have chlorinated the fastest. However the Nell and den Hoed (2003) experiments were conducted at lower gas velocities (10 – 24 cm/s) than the current experiments (39cm/s) and therefore blowover was lower and didn't have a significant effect on the chlorination rate.

Although degree of conversion for Slag A is only 68% after 180 minutes of reaction, only 10g of feedstock was left in the bed compared to the other feedstocks which had approximately 40g left over in the bed. Degree of conversion of Slag A was lowered because 52g of partially reacted feedstock was blown out of the reactor after the 180 minute experiment. See Table 33 and Figure 51 for blowover and bed residue values. The slag porosity increases to the extent that the superficial gas velocity exceeds the particle terminal velocity and the partially chlorinated material is blown out before it has a chance to fully react. This illustrates the impact that high blowover can have on process efficiencies.

The blowover of the blend is significantly lower than its individual components (i.e. rutile and Slag A) and this has an impact on the mass chlorinated. With a lower blowover, there is more material available for chlorination, hence the highest conversion was achieved with the blend. The factors that affect blowover will be discussed later in the report.

Table 33: Blowover after 180 minutes of chlorination at 1000°C

Feedstock	Blowover(g)
Slag A	52.8
Slag B	2.8
Rutile	30.2
Blend	6.0

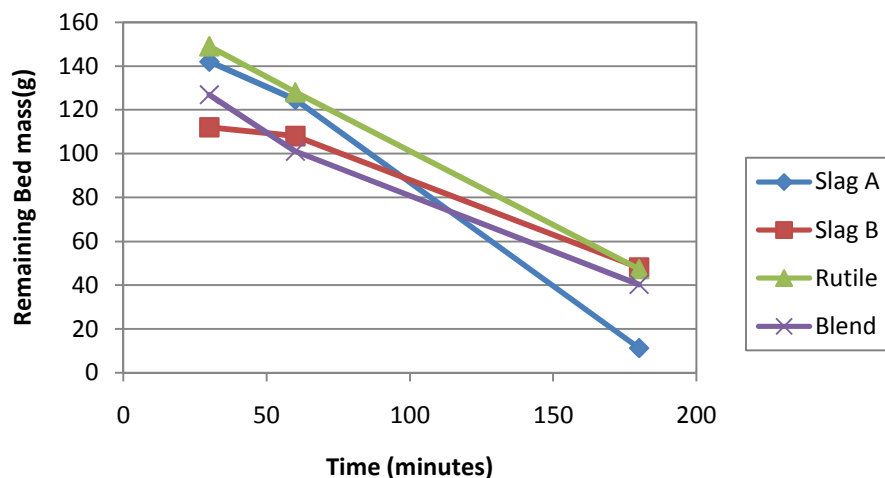


Figure 50: Bed residue after chlorination at 1000°C

Figure 51, and Figure 54 to Figure 57 consider the chlorination behaviour of the major species (i.e. TiO_2 , FeO , MnO , MgO and Al_2O_3).

As the impurities (i.e. Fe and Mn etc) are chlorinated the remaining matrix becomes enriched with titania, hence the increase in TiO_2 percentage of the bed analysis. The chlorination rate of TiO_2 (equivalent), is not as fast as Fe and Mn and is strongly affected by the reaction temperature especially that of rutile. The chlorination of TiO_2 is plotted in Figure 51. The highest TiO_2 chlorination was achieved with the blend (i.e. 80%).

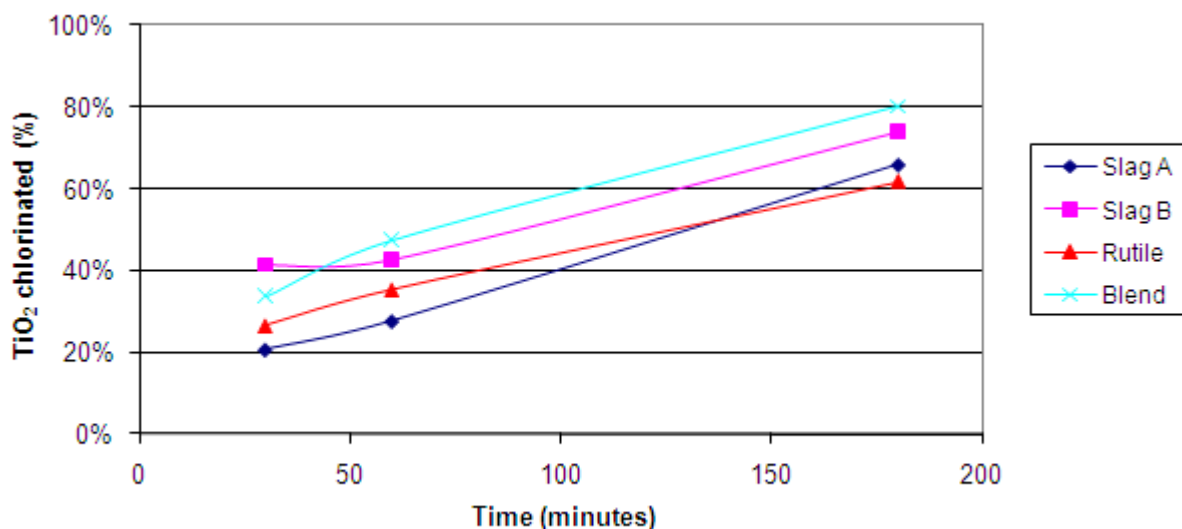
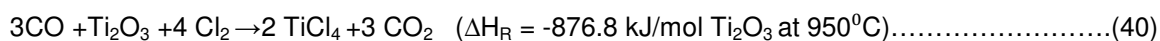


Figure 51: TiO₂ chlorination as a function of chlorination time

4.2.5.1 Effect of Ti₂O₃

After 30 minutes of chlorination, the highest degree of TiO₂ chlorination is achieved with Slag B (i.e. 41%); at the same stage the chlorination of TiO₂ in Slag A is only 20%. The chlorination of Ti₂O₃ is highly exothermic (i.e. Reaction 40), den hoed and Nell (2002) suggest that this reaction takes place within the first few minutes of the experiment; the argument is substantiated by the spike in the bed temperature.



A 1 minute chlorination experiment was conducted with Slag A to determine what happens to the Ti₂O₃ during the initial stages of the reaction. The results are presented in Table 34. The blowover from this short experiment was less than 2g and considered to be negligible for the mass balance.

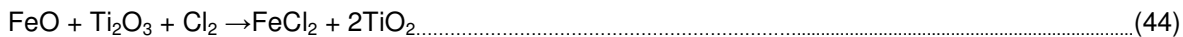
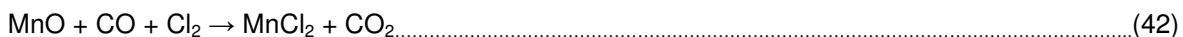
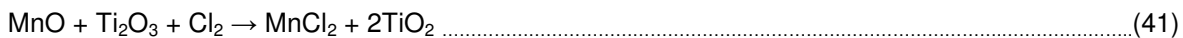
Table 34: Mass Balance for 1 minute chlorination of Slag A

Elements	Initial Material (200g)		Bed Sample (178.70g)		Mass chlorinated(g)	% Chlorinated
	Analysis %	Mass(g)	Analysis %	Mass(g)		
Ti (tot)	52.42	104.83	55.9	99.89	4.94	5%
Ti ⁽³⁺⁾	15.51	31.02	1.89	3.38	27.64	89%*
Ti ⁽⁴⁺⁾	36.91	73.81	53.98	96.46	-22.65	-31%
Ti ₂ O ₃	23.42	46.83	2.84	5.08	41.75	89%
TiO ₂	61.92	123.85	90.15	161.1	-37.25	-30%
Fe(tot)	7.01	14.02	2.82	5.04	8.98	64%
Fe(met)	0.31	0.62	0.06	0.11	0.51	82%
FeO	8.60	17.20	1.89	3.38	13.82	80%
Al ₂ O ₃	1.02	2.04	0.97	1.73	0.31	15%
SiO ₂	1.64	3.28	1.92	3.43	-0.15	-5%
CaO	0.22	0.44	0.12	0.21	0.23	52%
MgO	0.73	1.46	0.4	0.71	0.75	51%
MnO	1.90	3.80	0.78	1.39	2.41	63%

*Ti³⁺ is not chlorinated but oxidised to Ti⁴⁺

Slag A feed contains Ti in the form of Ti³⁺ and Ti⁴⁺; however after 1 minute of chlorination, the chemical analysis indicates that most of Ti in the bed is present as Ti⁴⁺. Initially the sample contained 31 g of Ti³⁺, after 1 minute this mass was reduced to 3.4 g whilst the mass of Ti⁴⁺ increased by 22.65g. Clearly most of the Ti³⁺ has been oxidised to Ti⁴⁺. Le Roux (2001) suggested that Ti₂O₃ acts as reductant in the absence of CO and carbon, since the current experiments were conducted with CO and coke, thermodynamic calculations were done to determine whether reaction with coke, CO, or Ti₂O₃ would be more thermodynamically feasible.

Using Factsage Version 6.1, a thermodynamic software tool, the change in Gibbs free energy for Reactions 41 to 47 was determined and plotted as a function of temperature in Figure 52 and Figure 53.



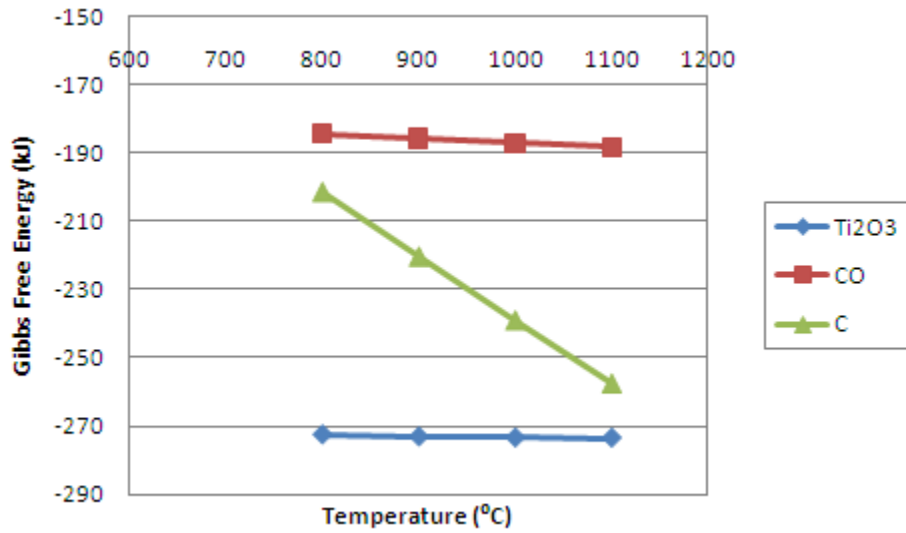


Figure 52: Change in Gibbs free energy for FeO chlorination

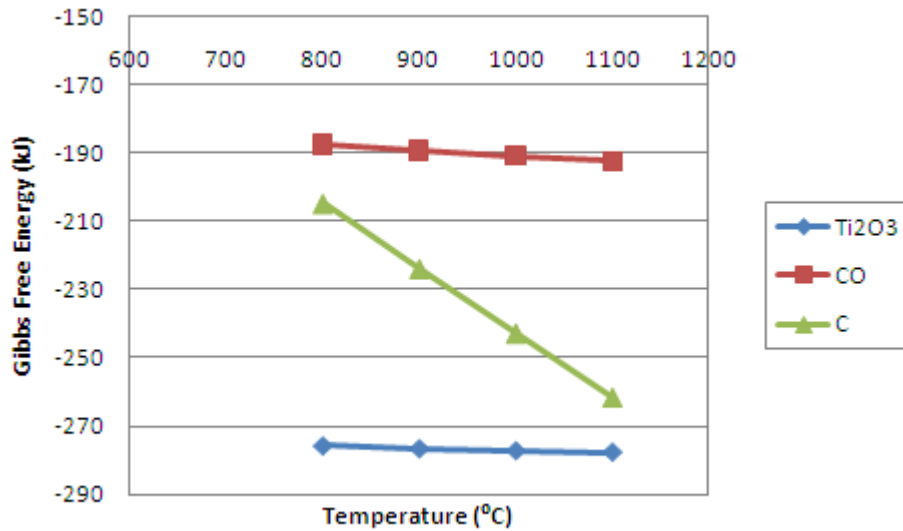


Figure 53: Change in Gibbs free energy for MnO chlorination

The change in Gibbs free energy is negative for all six reactions; however reaction with Ti₂O₃, with FeO and MnO chlorination is more negative indicating that this reaction has a greater tendency to take place. Now that it has been shown that chlorination with Ti₂O₃ is thermodynamically feasible, a mass balance was conducted over MnO, FeO and Ti₂O₃ to determine if there was sufficient Ti₂O₃ for Reactions 47 and 48 to take place. The results are presented in Table 35.

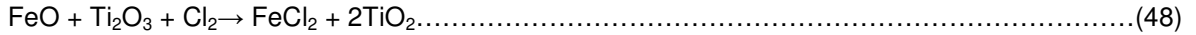
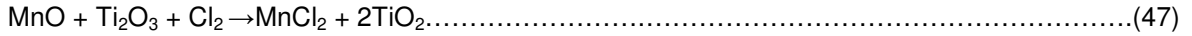


Table 35: Mass Balance for chlorination of MnO and FeO with Ti₂O₃

	Mass Chlorinated (g)	Number of Moles Reacted	Number of moles of Ti₂O₃ required for chlorination	Mass of Ti₂O₃ required for reaction (g)
FeO	13.82	0.19	0.19	27.65
MnO	2.41	0.03	0.03	4.88
Total	16.23	0.23	0.23	32.53

The theoretical mass balance (i.e. Table 35) indicates that 32.53g Ti₂O₃ is required for the chlorination of MnO and Fe whilst the actual mass balance indicates that 34g of Ti₂O₃ was oxidised to TiO₂ during the experiment. Thus the results show that there was sufficient Ti₂O₃ to act as reductant for the chlorination of MnO and FeO and the mass balance implies that 7g of Ti₂O₃ is chlorinated in the process.

The result of the 1 minute experiment has shed some light on the difference between the TiO₂ chlorination rate of Slag A and Slag B. TiO₂ chlorination in Slag A is only 20% after 30 minutes, whereas chlorination in Slag B is 41%, the difference is likely due to the Ti₂O₃ content of the slag's, Slag B has 38.80% whereas Slag A has 23.42%. The results of the 1 minute chlorination experiment imply that Ti₂O₃ not oxidised in the chlorination of FeO and MnO is then rapidly chlorinated, since Slag A has a higher FeO content compared to Slag B (i.e. 8.6 % vs 1.96 %) there is less Ti₂O₃ available for chlorination, in addition Slag B had a higher Ti₂O₃ content to start with. This explains why TiO₂ chlorination in Slag B is higher than Slag A.

Although rutile and Slag B feed have approximately the same TiO₂ (equivalent) content (i.e. 95%), overall conversion of rutile after 180 minutes is 14% lower than Slag B. This is likely due to combination of the effects of rapid chlorination of the Ti₂O₃ fraction in Slag B and the Fe content in Slag B which leaves behind a porous matrix and larger surface area for subsequent chlorination.

The mass balance over Ti⁴⁺ and Ti³⁺ was completed and is available in Appendix 4 for all the feedstocks, however since Ti₂O₃ is oxidised to Ti⁴⁺, this balance isn't particularly useful. The TiO₂ (equivalent) balance will be used for discussion purposes.

Looking at the other elements, over 90% of FeO and MnO is chlorinated within the first 30 minutes of the experiment. See Figure 54 and Figure 55.

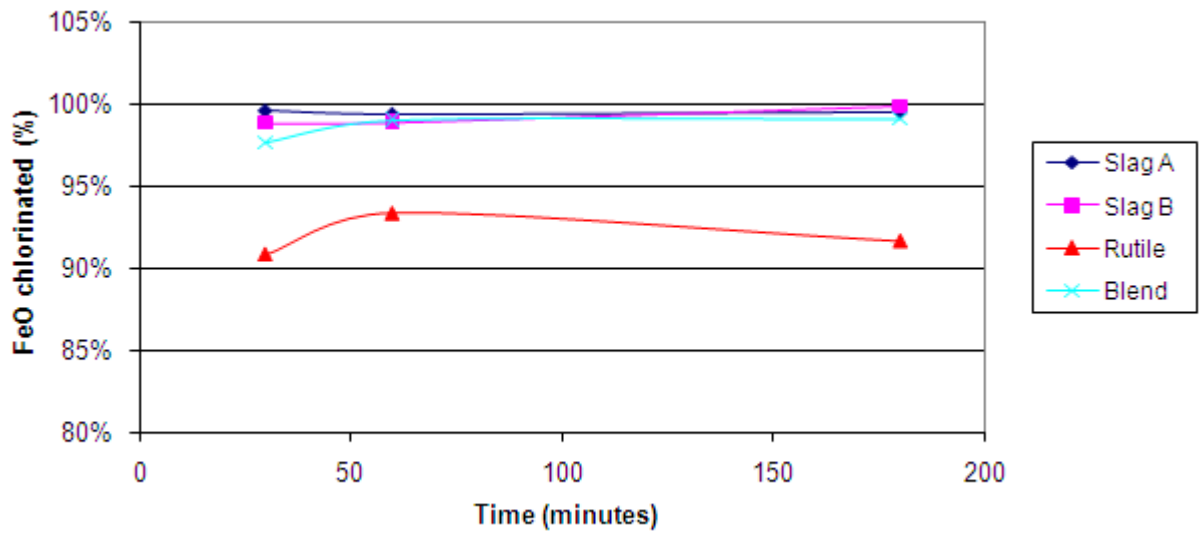


Figure 54: FeO chlorination as a function of chlorination time at 1000°C

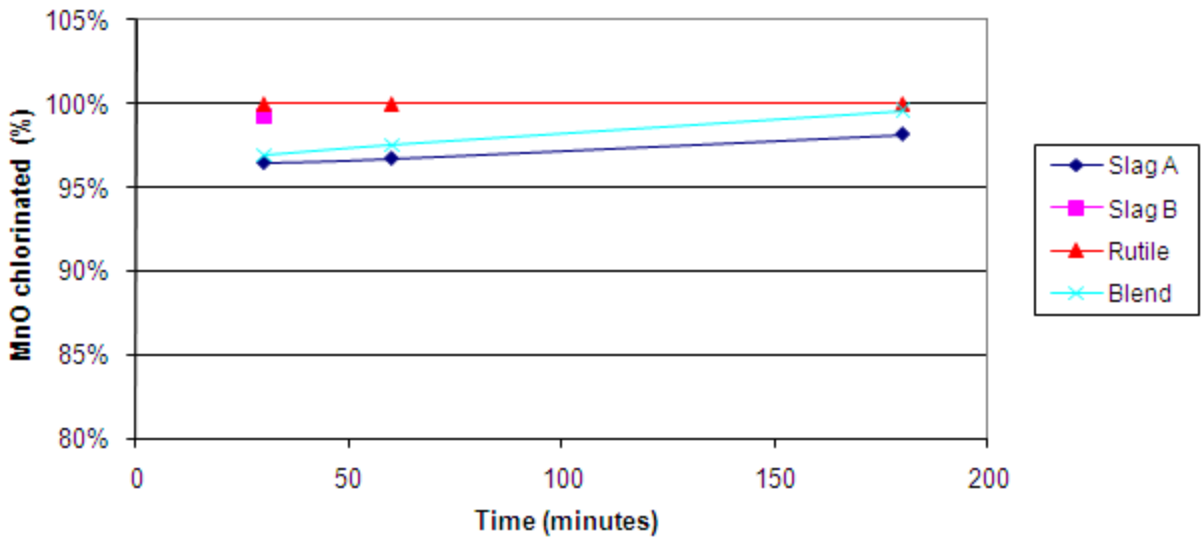


Figure 55: MnO chlorination as a function of chlorination time at 1000°C

High MgO chlorination (Figure 56) is achieved with rutile and the blend, Slag B and Slag A is slightly lower.

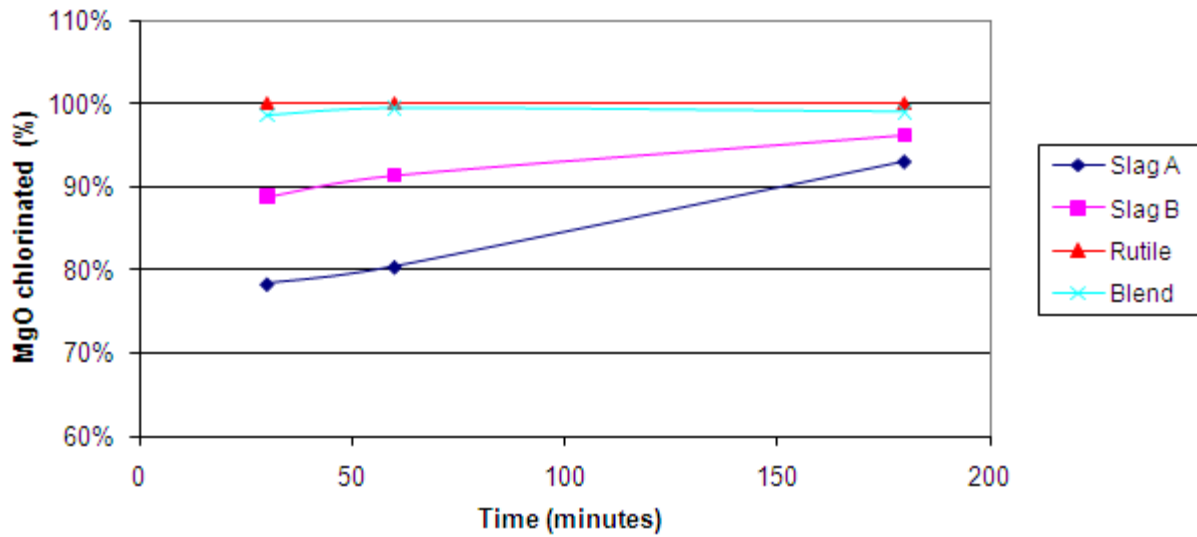


Figure 56: MgO chlorination as a function of chlorination time at 1000°C

Al₂O₃ chlorination (Figure 57) is the slowest of the elements but increases as the time proceeds except for the rutile sample which levels of at 70%.

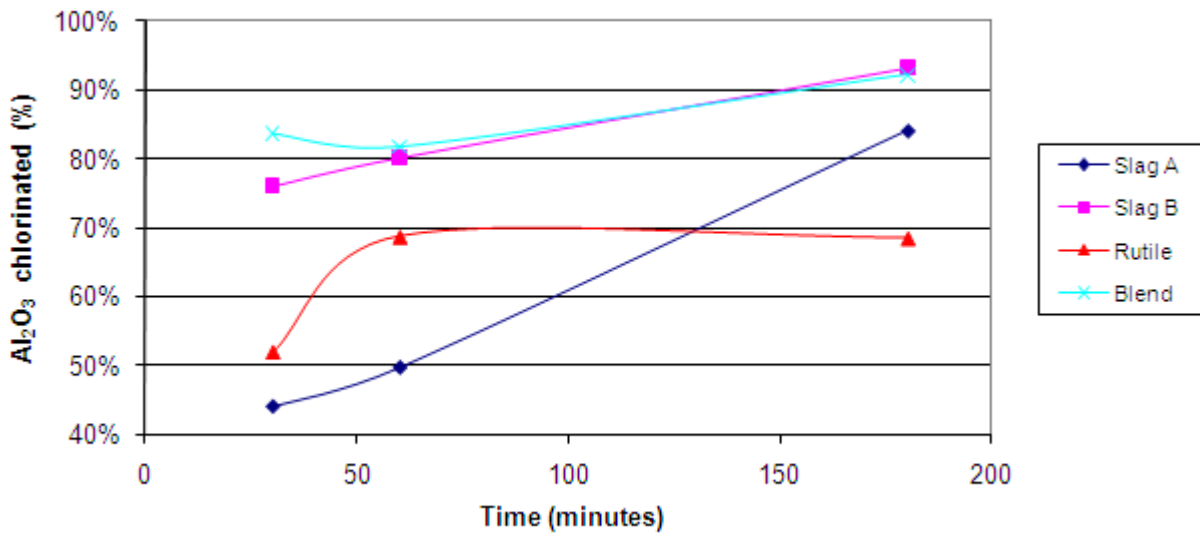


Figure 57: Al₂O₃ chlorination as a function of chlorination time at 1000°C

The chemical analysis indicates that SiO₂ percentage in the bed increases as chlorination time increases, highlighting that SiO₂ doesn't chlorinate easily.

4.2.6 Coke reaction

Petroleum coke was used as reductant for the chlorination experiments. The coke reacted (%) at 1000°C was calculated using Equation 49 and is plotted in Figure 58.

$$\text{Coke reacted} = \text{Mass of coke reacted (g)} / \text{Coke initial mass (g)} \times 100\% \dots\dots\dots(49)$$

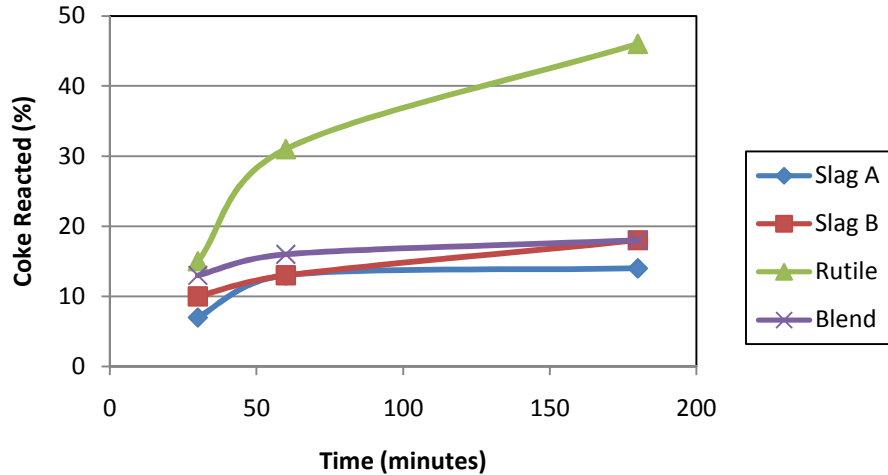


Figure 58: Amount of coke reacted at 1000°C

Den Hoed and Nell (2002) found that solid carbon is crucial to the chlorination reaction, without carbon the reaction rate is many times slower, especially that of rutile. Results from present work indicate that the coke reacted (%) is highest with rutile throughout the reaction and after 180 minutes the chlorination of rutile consumed twice as much petroleum coke than the other feedstocks.

Rutile is more oxidised than the slags, and stoichiometrically should require more coke, the coke consumption is not significantly higher than that of the slag's after the first 30 minutes (Figure 58). However considering the ratio of coke reacted to mass chlorinated, the ratio for rutile is more than double than that of the other feedstocks (Figure 59 and Figure 60).

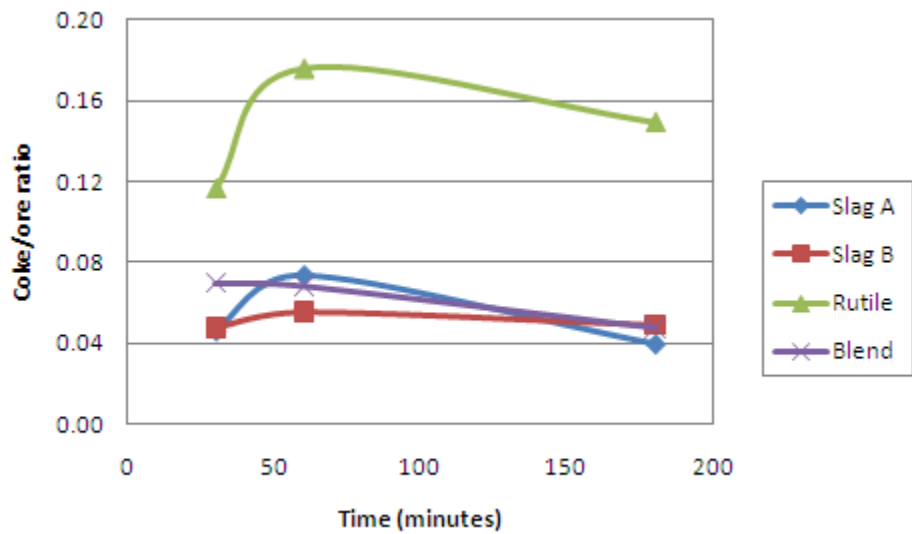


Figure 59: Coke/ore ratio vs time

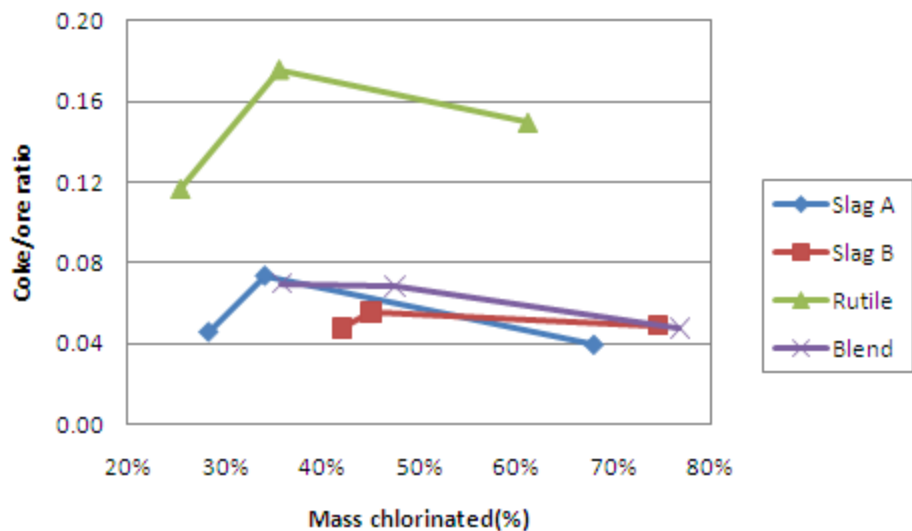


Figure 60: Coke/ore ratio vs Mass chlorinated

Results indicate that Ti_2O_3 acts as a reductant during the initial stages of chlorination in titania slags, so the amount of coke required for the chlorination reaction is reduced. Rutile doesn't have any Ti_2O_3 hence more coke is required for chlorination than with the slags. The coke/ore ratio after 30 minutes of reaction was plotted against the feedstock Ti_2O_3 content (Figure 61), and a definite decreasing coke requirement was noted for feedstocks with high Ti_2O_3 content.

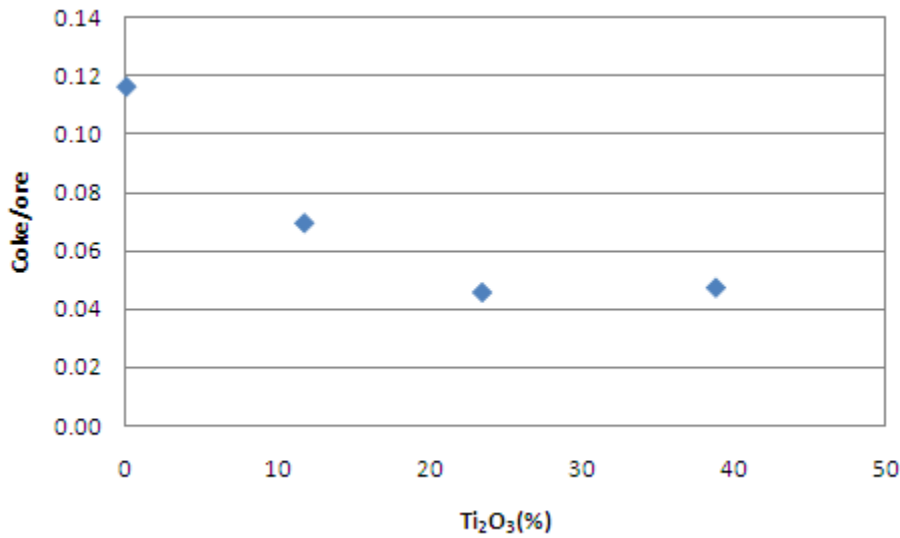


Figure 61: Coke ratio vs Ti₂O₃ content

The higher coke consumption for rutile during the first 30 minutes of the reaction has been explained but it is interesting to note that for the duration of the test, the coke consumption for slag chlorination does not increase; this is unexpected given the dependence of chlorination reaction on coke. Findings from literature (Section 2) show that the coke has to be intimately mixed with the feedstock for the chlorination rate to be improved.

Slag A had a high blowover after 180 minutes of chlorination (i.e. 52g), the high elutriation rate suggests that Slag A particles spent a significant time in the freeboard area where the chlorination reaction would have proceeded as follows:



instead of,



Reaction with CO would explain why the coke consumption did not increase during the reaction and in fact decreased after 60 minutes. As the particles become lighter and smaller, they tend to spend more time above the coke bed.

The coke consumption of the blend lies between that of Slag A and rutile but closer to the value of Slag A, leading one to believe that more slag was chlorinated than rutile thus the ratio of slag to rutile in the bed after 180 minutes of chlorination will be less than 1:1. Mineralogy was the first tool that was looked at to try and split the remaining blend bed sample into rutile and slag. There are mineralogical differences between slag

and rutile feed, however in all the partially chlorinated samples rutile was identified through SEM and XRD as the major titania phase. Given this, it is impossible to determine the ratio of slag and rutile in the remaining blend sample.

An alternative method was developed based on the physical differences between rutile and slag, SEM images illustrate that slag becomes porous as early as after 1 minute of chlorination whilst rutile remains solid even after 180 minutes. Rutile particles are also far more spherical than slag particles. Based on visual inspection of QEMSCAN PMA images (Figure 62) approximately 3500 particles of the 180 minute sample block were inspected and then classified as either slag or rutile based on porosity and particle shape. QEMSCAN image analysis indicates that the remaining bed sample of the blend contained 85wt% rutile and 15wt% slag after 180 minutes of chlorination indicating that slag chlorinated preferentially.



(a)- Rutile particles



(b)-Slag particles

Figure 62: QEMSCAN Image Grid of Slag and Rutile Particle, (a) rutile, (b) Slag A

The results of Slag B are perplexing since the blowover was not significant and one would expect the coke consumption to be closer to rutile. SEM images indicate that Slag B was porous, however its porosity was not as high as with Slag A. It could very well be that the chlorination could have taken place in the freeboard with CO as reductant; however particles density was not low enough for particles to be elutriated.

Another possible explanation for the low coke consumption originates from Nell and den Hoed's (2003) proposed chlorination mechanism. The authors suggested that $TiOCl_2$ forms on sites of the titania particle, the $TiOCl_2$ is adsorbed onto the carbon particle, where reaction with Cl_2 yields $TiCl_3$, the oxygen reacts with carbon to form CO. In the absence of carbon, CO is the oxygen scavenger. Slag particles become porous after the chlorination of Fe and Mn, with a porous particle, gas attack is not limited to the surface of the particle, and reaction of $TiOCl_2$ with CO is likely to occur since the particle is fluidised with CO gas. With the SEM and EDS point analysis, chlorine was identified along the length of particle, unlike with rutile. With

chlorination taking place inside the slag particle, the CO gas would be in better contact with the reaction site than the solid coke particles.

4.2.7 Blower

Blowover refers to the mass of material that is elutriated from the chlorinator during the experiment. This is collected and weighed at the end of the experiment. There isn't a significant difference in blowover for the various feedstocks after 60 minutes of chlorination; however Slag A and rutile show a large increase between the 60 and 180 minute experiments (See Figure 63).

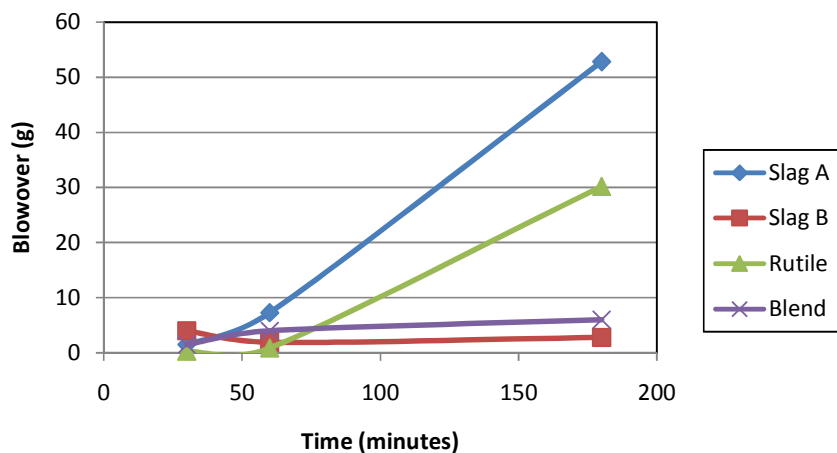


Figure 63: Blowover after chlorination at 1000°C

Figure 64 shows the average particle size of the bed sample (i.e. remaining mass) as determined by QEMSCAN and Figure 65 gives the porosity results as determined by QEMSCAN. The porosity and mean size values determined by QEMSCAN should not be taken as absolute values, but are merely used for comparative purposes. Grobler and Bosman (2009) compared particle size distribution as determined by conventional dry screening techniques to QEMSCAN PSD predictions. The results were dependent on the material under investigation, with silica; a slightly finer PSD was predicted by QEMSCAN, whereas with heavy minerals, a coarser PSD was predicted.

The results of screening and QEMSCAN compare well for the more evenly sized rutile particles (i.e. Screening: 158µm vs QEMSCAN: 160µm) whereas there is a difference of 72 µm between the two results for Slag A, with the QEMSCAN result lower than the screening result. The QEMSCAN results indicate that the average particle size of the bed sample (i.e. Figure 64) decreases with time whilst porosity (i.e. Figure 65) increases.

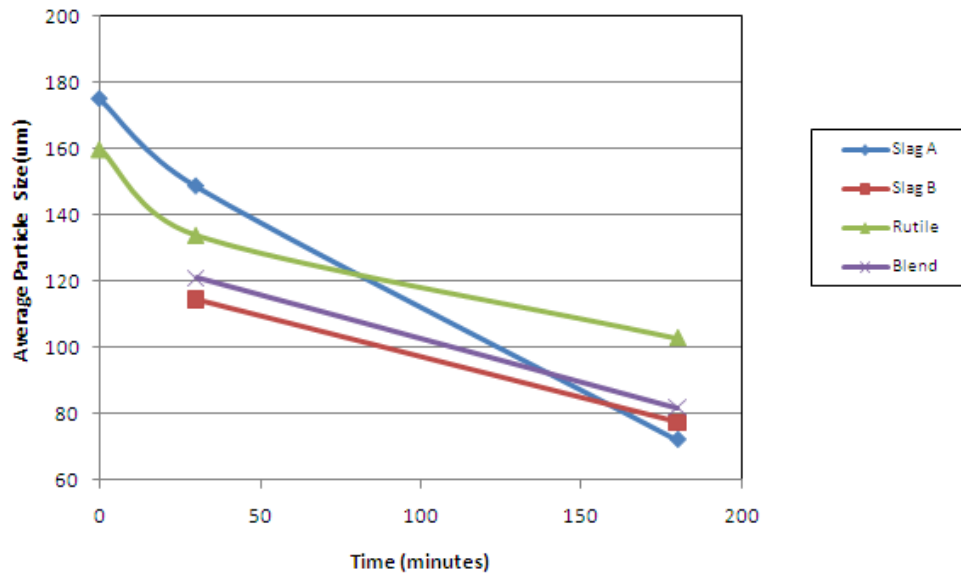


Figure 64: Average particle size as a function of chlorination time at 1000°C

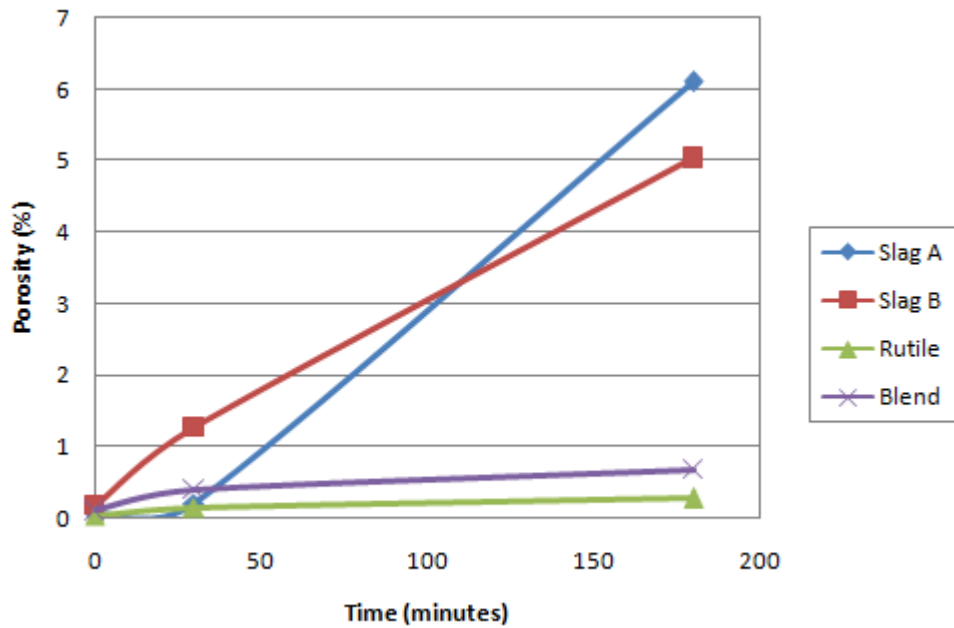


Figure 65: Porosity changes as a function of chlorination time at 1000°C

Figure 64 illustrates that the average particle size of the bed sample decreases as the chlorination time increases. The porosity measurement indicates that the slag becomes more porous whereas rutile and the

blend remains much the same. The QEMSCAN study revealed that the final bed composition of the blend consisted of 85% rutile and 15% slag, so the porosity of the blend was expected to be closer to that of rutile.

Le Roux (2001) and Zhou et al., (1996) demonstrated that FeO chlorination is rapid during the initial stages, leaving behind porous particles which lend themselves to elutriation. The porosity changes could clearly be seen in the SEM images of Slag A after 30 and 180 minutes of chlorination (Figure 66 and Figure 67) whereas the rutile remains smooth. EDS and chemical analysis confirmed that porous sample was depleted of FeO.

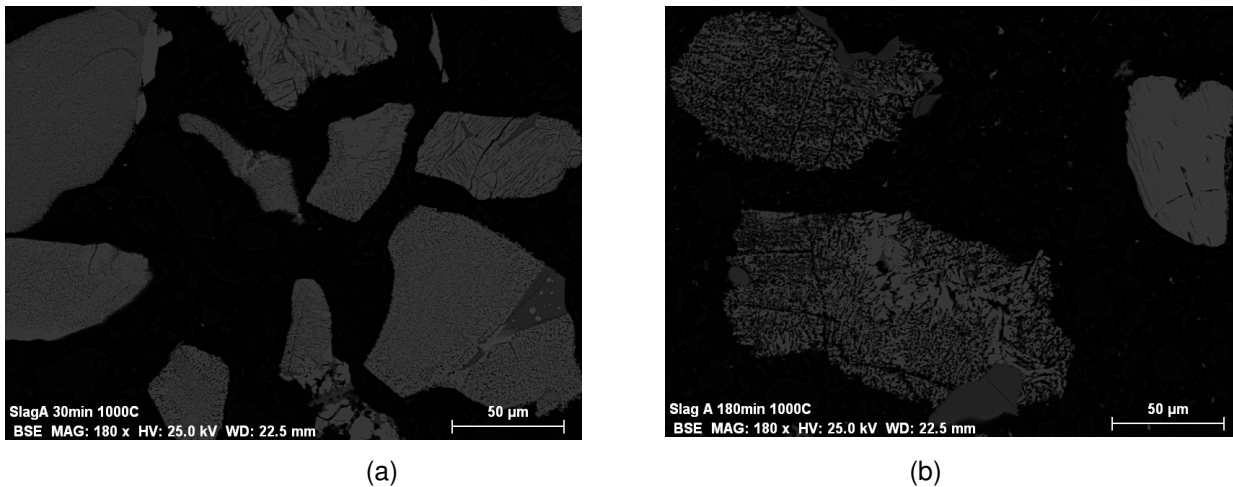


Figure 66: BSE image of Chlorinated Slag A after 30 minutes (a) and 180 minutes (b) of chlorination

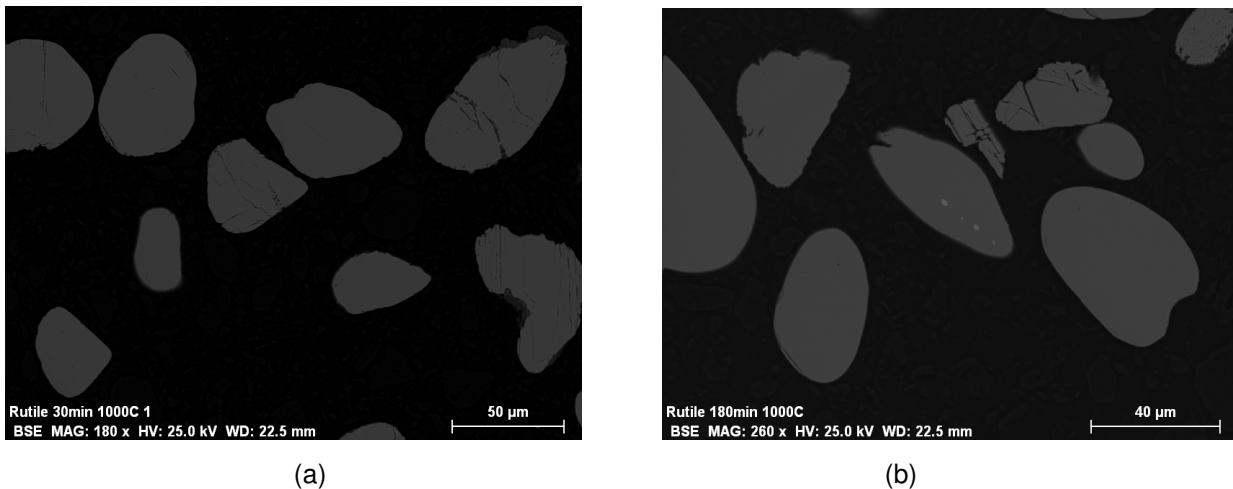


Figure 67: BSE image of Chlorinated Rutile after 30 minutes (a) and 180 (b) of chlorination

The images show that rutile chlorination does not follow the same mechanism as slag, particles become smaller but not more porous as the reaction proceeds. Slag A contains 8.6 % FeO whilst Slag B has 1.96 %

FeO; so chlorination of iron would leave behind a more porous particle for Slag A than Slag B, this explains the difference in the final blowover results although both feedstocks are a product of ilmenite smelting.

After 3 hours of chlorination, the Blend (i.e. a mixture of Slag A (50 wt %) and Rutile (50% wt %)) has a lower blowover than the individual components. A similar trend was observed in the hydrodynamic study, where the fluidisation was completed in an inert environment. The effect of particle size distribution on fluidisation behaviour has been discussed in the literature review and in the elutriation experiment results section. The sample size range of the chlorination experiments is narrower than the fluidisation experiments (-300+106 μm vs the natural size range of feedstocks). The particle size distribution and calculated d_{50} are presented in Figure 68 and Table 36. Even with the narrow size range, the rutile particles lie closer to 106 μm range whereas slag lies closer to the particle top size of 300 μm . The d_{50} of Slag A is 218 μm whilst that of rutile is 121 μm .

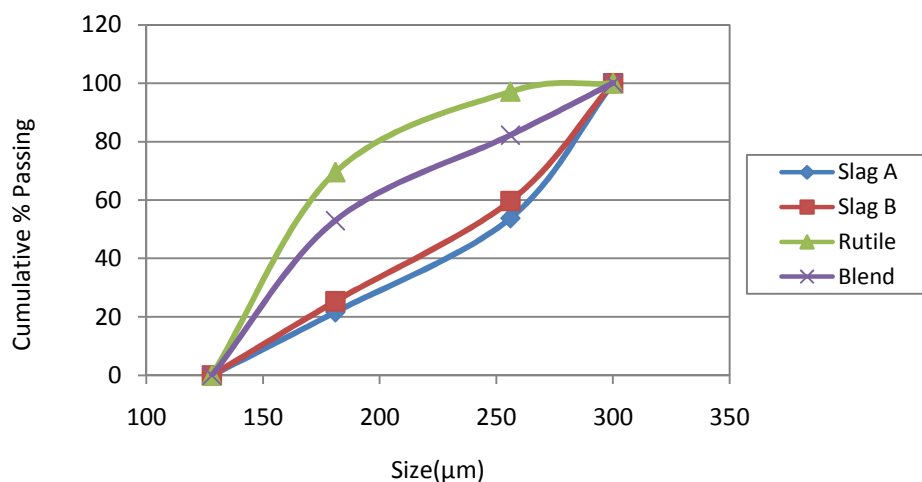


Figure 68: Particle size distribution of the sample used in chlorination experiments

Table 36: D_{50} of sample used in chlorination experiments

Feedstock	$d_{50}(\mu\text{m})$
Slag A	218
Slag B	218
Rutile	121
Blend	127

A combination of the two feedstocks spreads particles more evenly over the range of -300+106 μm and in effect the particle size distribution is wider than with the individual feedstocks. There has been evidence in literature (Sun and Grace (1990) and Beetstra et al., (2009)) that a wider particle size distribution leads to an expanded dense phase, smaller bubbles or voids, better gas solid contact and higher rates of conversion. Smaller bubbles carry less particles and entrainment is lowered.

The conclusions from reviewed literature are that the effect of smaller bubbles is twofold:

- Lower entrainment
- Higher rates of conversion

Figure 63 demonstrates that blowover of the blend is significantly lower than the individual feedstocks after 180 minutes, and Figure 69 illustrates that the mass of the blend chlorinated is higher, supporting the theory that the wider/different particle size distribution of the blend leads to a smaller bubble size and higher conversion.

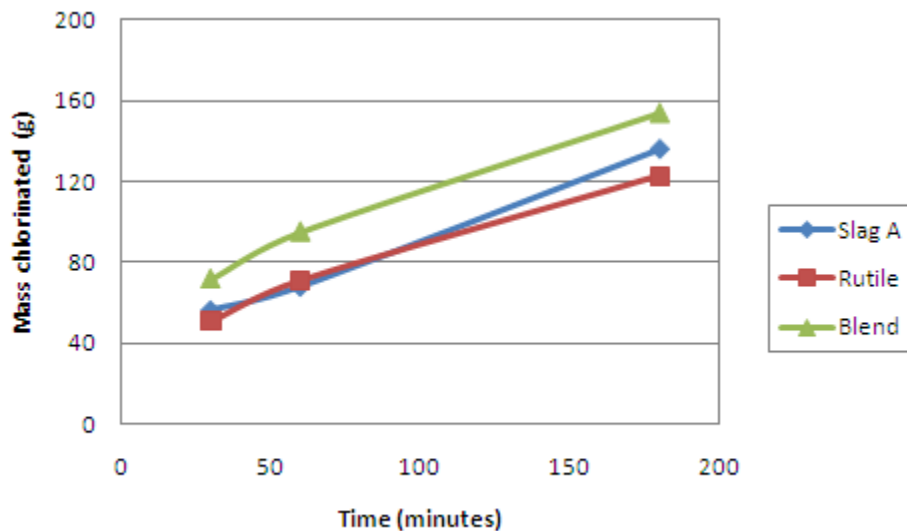


Figure 69: Mass chlorinated at 1000°C

4.2.7.1 Chlorination of the blend (50wt% Rutile, 50wt% Slag A)

4.2.7.1.1 Particle size distribution

The performance of the blend material was better than the individual feedstock's since the blowover was lower and the mass chlorinated (%) was higher. It is believed that the wider particle size distribution played a role in improving the hydrodynamic properties of the bed.

In order to test this theory that the particle size played a role in improving the result of the blend, two narrower size ranges (-150 + 106 μ m and -212 + 150 μ m) of the blend was screened and chlorinated for 3 hours at 1000 $^{\circ}$ C. The results are compared to the results of chlorination of the -300 + 106 μ m size range (See Figure 70 and Figure 71).

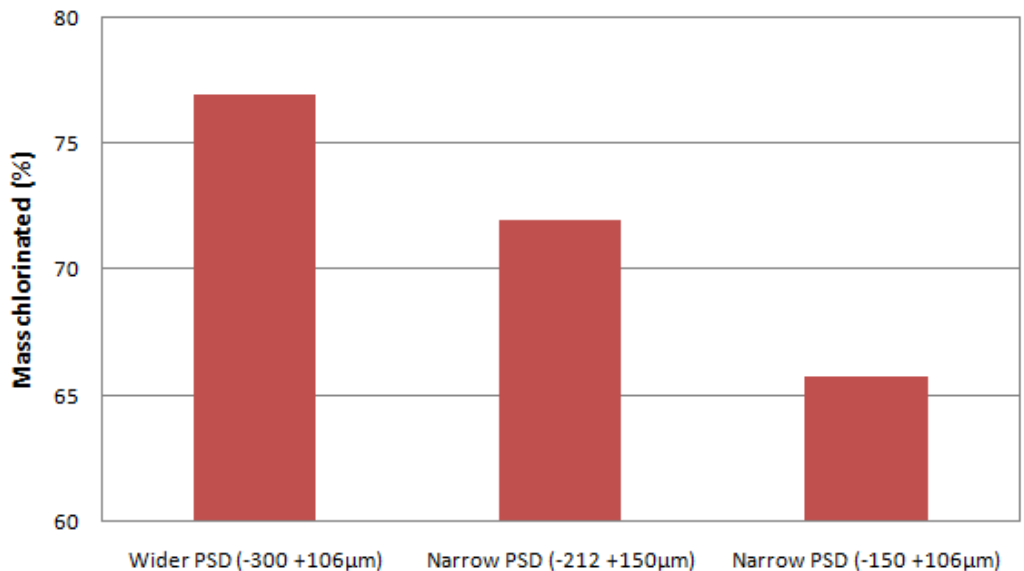


Figure 70: Effect of Particle size distribution on degree of conversion

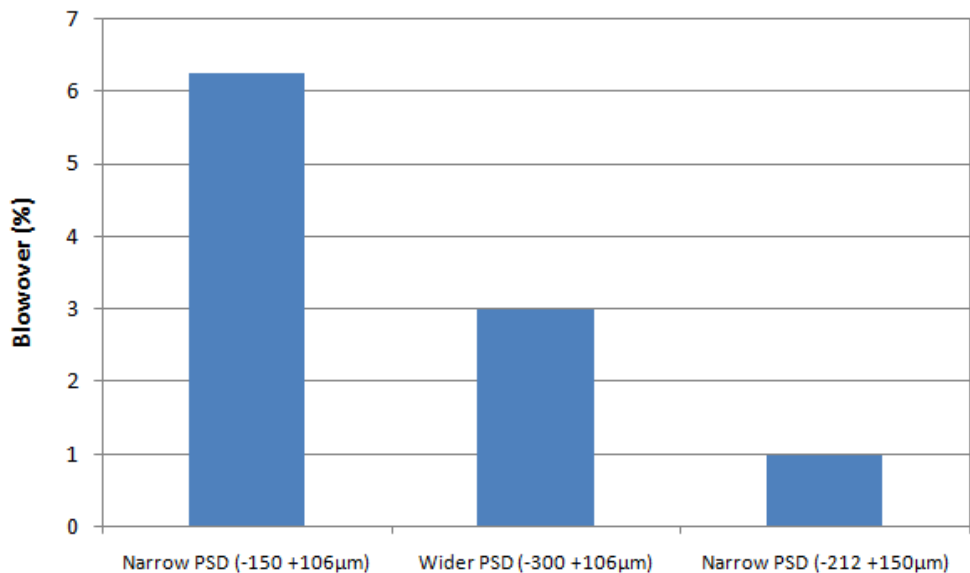


Figure 71: Effect of particle size distribution on blower

With the narrower particle size range (i.e. -150+106 μ m and -212+150 μ m), the mass chlorinated is lower than with the wider distribution (i.e. -300+106 μ m) supporting the theory that wider particle size distribution leads to higher conversion percentages. Comparing the -212 +150 μ m test to the -150+106 μ m test, interestingly a larger degree of chlorination was achieved with the -212+150 μ m range; one would have expected that the larger surface area that the smaller particles (i.e -150+106 μ m) offer would have improved chlorination rates. There is a 194 μ m difference between the top and bottom sizes of the best performing sample, a 62 μ m difference in the next best sample and a 42 μ m difference in the poorest performing sample.

The sample with the smallest particle size range had the highest blowover (i.e. 6% of the initial sample), and the blowover of the -300+106 μ m sample is higher than the -212+150 μ m sample. The results indicate that certain size ranges within the -300 + 106 μ m range will have a high blowover when chlorinated alone, however when part of a wider PSD the blowover tendency decreases, proving that the wider PSD does improve the hydrodynamic properties of the bed. The effect of particle size distribution is a complex problem since top size, bottom size and the distribution in between has an effect on the hydrodynamic properties of the bed.

4.2.7.1.2 Varying the ratio of slag to rutile in a blend

Two blends of varying rutile and slag composition were tested at 1000⁰C and 180 minutes i.e.

- Blend 1: 50wt% Slag A and 50wt% Rutile
- Blend 2: 75wt% Slag A and 25wt% Rutile

By increasing the ratio of slag to rutile in the blend mix, the mass chlorinated increased and the blowover decreased. The results (Table 37) indicate that the conversion increases as Slag A content increases but up to a point, and that point lies somewhere between 75 and 100 wt% Slag A. The addition of the rutile offers the benefit of lowering the blowover and therefore slag remains in bed for a longer time allowing it to chlorinate. The negative aspect of rutile is that it chlorinates slower than slag so the higher the rutile content in the blend, the lower the overall conversion rate. More testwork should be done to determine the optimum blend.

Table 37: Effects of varying the slag to rutile ratio in the blend

	Blend 1: 50wt% Slag A and 50wt% Rutile	Blend 2: 75wt% Slag A and 25wt% Rutile	100wt% Slag A
Feedstock Mass In (g)	200	200	200
Feedstock mass Out (g)	40.3	39.5	11.3
Particle size range	-300+106 μ m	-300+106 μ m	-300+106 μ m
Blowovers(g)	6	0.9	52.8
Mass chlorinated (g)	153.7	159.6	135.9
Mass chlorinated (%)	77.0	80.0	68.0

4.2.8 Comparison with Theoretical Models

Experimental results from the 1000°C experiments were compared to the models discussed in Chapter 2, Table 3. The slag used in the Sohn and Zhou's (1998) study contained 84.6% TiO₂, 11.1% Fe₂O₃, 1.3% Al₂O₃; the remaining 3% is a combination of SiO₂, MnO₂ and MgO. This slag composition is of a slightly poorer quality than Slag A and significantly lower than Slag B. Sohn and Zhou's (1998) slag model underestimates the fraction of TiO₂ chlorinated during the first sixty minutes; thereafter the actual results of Slag A and the model diverge then converge. The model does not provide a good fit for the Slag B data; this is likely due to the difference in slag quality used in the two studies.

Le Roux's (2001) chlorinated a South African slag of similar quality to Slag A, the model does not offer a good fit for the chlorination of Slag A or Slag B during the first 30 minutes.

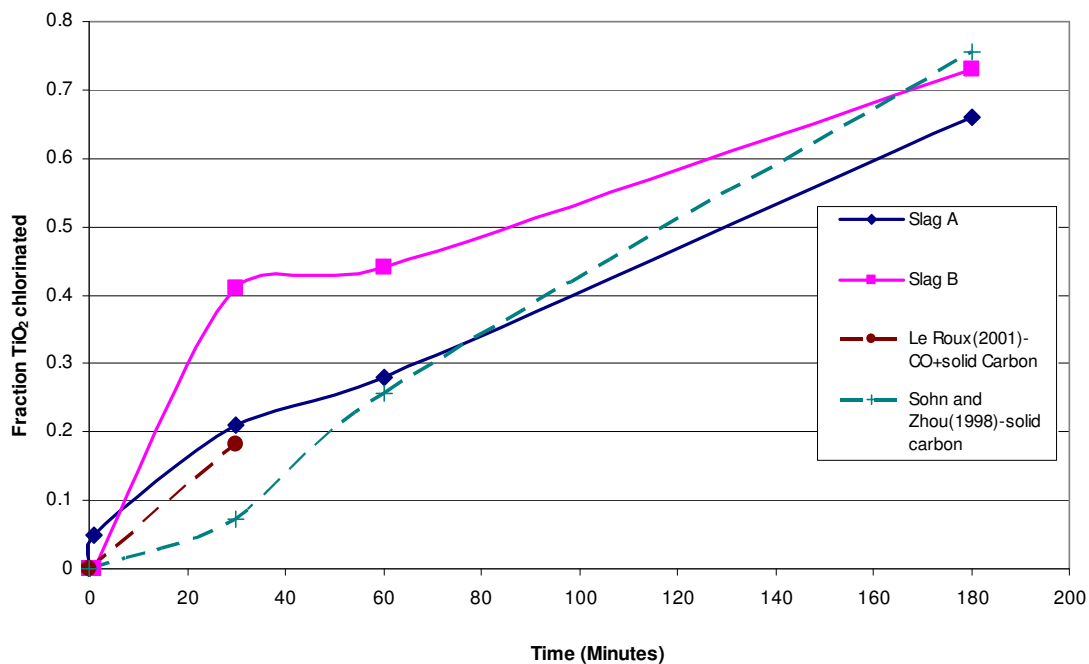


Figure 72: Comparison of experimental results for Slag with theoretical models

The three models presented in Figure 73 is for rutile chlorination in a system excluding coke, although the experimental results are for a system including coke, this is the likely reason why such a difference is noted between the actual data and the model. Sohn et al., (1998) model provided the closest fit to the data although for the first sixty minutes the model under predicts the chlorination of TiO₂.

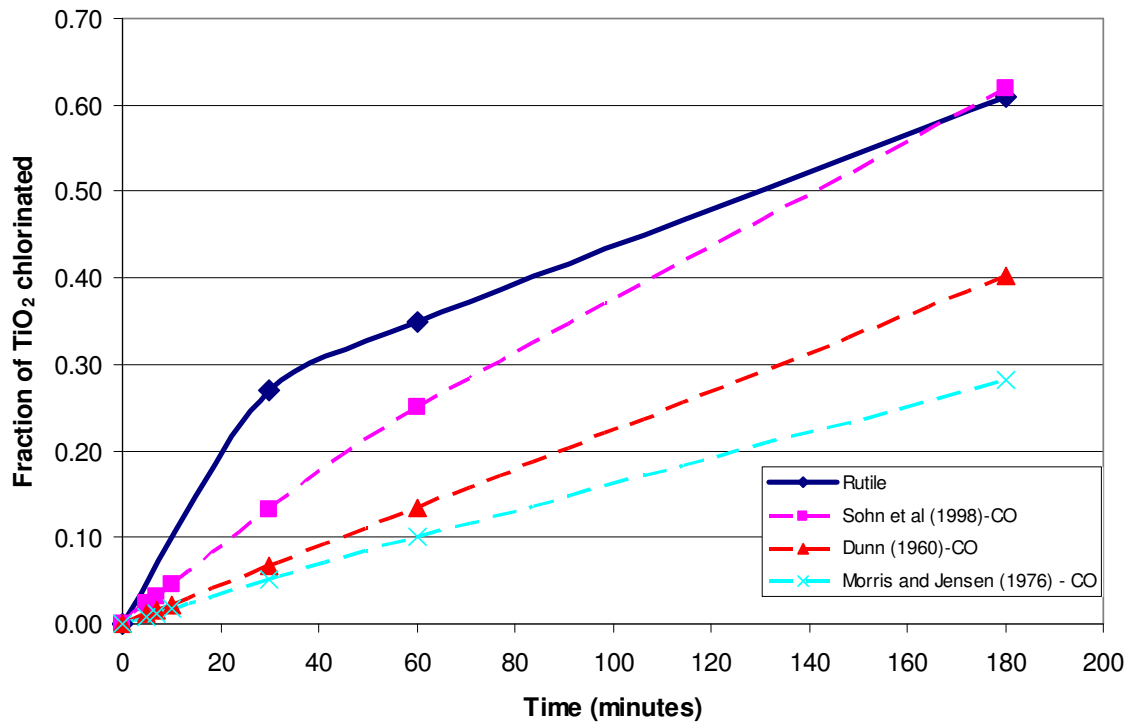


Figure 73: Comparison of experimental results of rutile with theoretical models

4.2.9 Activation Energy

The rate constant (k) is dependant on temperature and the dependence can be represented by the Arrhenius equation (i.e. Equation 52)

$$k = Ae^{-\frac{E_A}{RT}} \dots\dots\dots (52)$$

Where

- k rate constant
- E_A activation energy (kJ/mol),
- R gas constant (kJ/mol.K) and
- T temperature (K)
- A factor, independent of temperature

Since conversion rates and not chlorination rates were determined, the rate constant used for the activation energy calculation was not strictly speaking a rate constant, from hereon in the report it will be known as a conversion coefficient.

Taking the natural logarithm of Equation 52

$$\ln K = \ln A - \frac{E_A}{RT} \dots\dots\dots (53)$$

The gradient of the plot of lnk vs 1/T gives -E_A/R, see Figure 74.

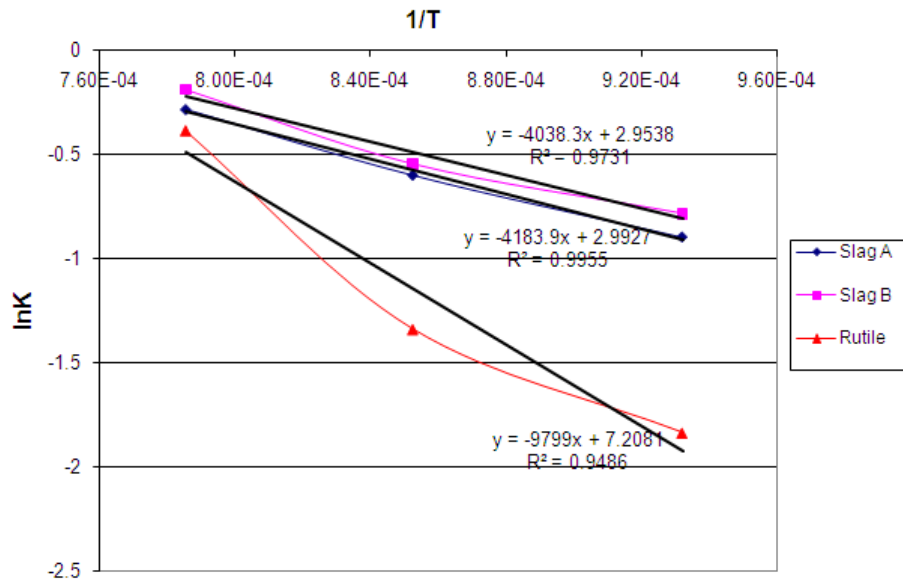


Figure 74: Activation Energy

Table 38: Calculated Activation Energy

Material	$\frac{-E_A}{R}$	Activation Energy (kJ/mol)
Slag A	-4183.9	34.8
Slag B	-4038.3	33.6
Rutile	-9799	81.4

The activation energies were compared to values in literature (See Table 39), the values for slag are close to that obtained by Sohn and Zhou (1998) and Le Roux (2001). In current experiments both coke and CO were used whilst only one of these reagents was used in the previous studies, this could account for a fraction of the differences in the values. Differences could also be due to the rate constant vs conversion coefficient issue. The high activation energy of rutile indicates that the chlorination is controlled by chemical process whilst the slag chlorination is diffusion controlled. The activation energy of a diffusion controlled reaction is typically 6 kcal/mol.

The calculated activation energy for rutile is close to Dunn's (1972) value for a CO/Cl₂ system, the addition of coke to the system lowers the activation energy. Results from literature and current experiments indicate that rutile requires more energy than the slags to start and maintain the reaction.

Table 39: Activation energy from literature

Author	Material	Activation Energy (kJ/mol)
Dunn (1960)	Rutile + CO	87.3
Morris and Jensen (1976)	Rutile + CO	158.0
Sohn et al., (1998)	Rutile + CO	175.0
Sohn and Zhou (1998)	Slag + Coke	29.0
Le Roux (2001)	Slag + CO	28.8

CHAPTER 5

5. CONCLUSION AND RECOMMENDATIONS

A hydrodynamic study and chlorination experiments were conducted on four titania feedstocks with varying physical and chemical properties i.e.

- Slag A
- Slag B
- Rutile
- Blend (i.e. a mixture of Slag A (50wt %) and Rutile (50wt %))

The hydrodynamic study was completed on a sample that was representative of the particle size distribution of the original material, whilst the chlorination experiments were performed on a narrower range of screened material (-300 + 106 μ m and -150+106 μ m). Chlorination experiments were conducted at 800, 900 and 1000°C.

The conclusions from the hydrodynamic study were:

- The round shape, particle size distribution and density of the rutile particles make it an ideal material for fluidisation. Whilst all the rutile particles are classified as Group B (i.e. easy to fluidise), a small portion of Slag A and Slag B falls in Group D. Slag B has a wide size distribution and particles are spread over three Geldart classes i.e. A, B and D.
- Slag B had the highest blowover in the elutriation experiment followed by Slag A , the blend and finally rutile
- Elutriation experiments confirmed that particles smaller than 106 μ m are likely to be elutriated from chlorinator and are therefore excluded from the chlorination process industrially and for the chlorination experiments
- The blowover of the blend was significantly lower than that of Slag A and much the same as rutile. The combination of rutile with a top size of 300 μ m and Slag A with a top size of 800 μ m significantly widens the particle size distribution of the blend, which leads to an improvement in bed hydrodynamics and results in lower blowover.

The conclusions from the chlorination study:

- Temperature has a significant effect on chlorination conversion rates, at 800°C, chlorination is significantly lower, especially that of rutile. Within the range of temperatures investigated, the chlorination of Fe and Mn oxides is not significantly affected by the temperature whilst the chlorination of TiO₂ and Al₂O₃ is highly dependent on the temperature.
- At 1000°C, the blend has the highest conversion rate, followed by Slag B, Slag A and rutile.
- The blowover mass and degree of conversion of the blend of rutile and slag was better than the individual components.
- Blend samples (i.e. 50 wt% Rutile and 50wt% Slag A) of varying particle size were chlorinated and the mix with the widest particle size distribution exhibited the highest conversion rates. Blowover also varied illustrating the effect that PSD can have on conversion rates and blowover.
- Chlorination of FeO and MnO is rapid and over 90% chlorination is achieved after the first minute of the chlorination.
- SEM images indicate that slag becomes porous with the chlorination of FeO and MnO whilst rutile remains solid throughout the reaction. Chlorine was identified through EDS analysis throughout the slag particle whereas with rutile it was only observed on the edge of the particle.
- Rutile chlorination consumed more coke than the slags. Ti₂O₃ acts as a reductant during the initial stages of chlorination so coke requirement for slag is less. The coke consumption of slag did not increase with chlorination time. Den Hoed and Nell (2003) propose that TiOCl₂ forms on titania particles and reaction with Cl₂ and reductant (either CO or carbon) yields TiCl₃ and CO or CO₂. Since slag particles becomes porous, some CO can flow through the pores and react with the oxygen whereas with rutile the particle is solid so reaction with take place on the surface of the particle with coke particles lying next to it and CO.
- Ti₂O₃ is oxidised to TiO₂ during the chlorination of FeO and MnO. Ti₂O₃ that is not used as reductant is rapidly chlorinated. Although rutile and Slag B feedstock have approximately the same TiO₂ content (i.e. 95%), overall conversion of rutile after 180 minutes is 14% lower than Slag B. This is due to combination of the effects of rapid chlorination of the Ti₂O₃ fraction and the Fe content in Slag B which leaves behind a porous matrix and larger surface area for subsequent chlorination.
- Activation energy for chlorination reaction of Slag A and Slag B is 34.76 and 33.56 kJ/mol respectively whilst rutile was 81.43 kJ/mol, these values compare well to that presented in literature.
- Entrainment reduces particle residence time in reactor and results in a decrease in process efficiency. After 3 hours of chlorination, a quarter of the initial mass of Slag A was blown out of the chlorinator so conversion rate was lowered. Feeding a blend of rutile and Slag A significantly lowered blowover and improved the conversion of metal oxides to chlorides. The results indicate that feedstocks mixtures and particle size distribution can have significant process benefits should the same trend be followed in the industrial operations.

The most interesting findings of the experiments were that the blend of rutile and slag performed better than the individual components. This is most likely due the particle size distribution of the blend which yields better hydrodynamic characteristics. The performance of blends is of significant industrial importance, it is recommended that the effects of particle size distribution are further investigated and that 3 or more component blends are also studied.

A 50/50 and a 75/25 blend of slag and rutile were investigated; by increasing the ratio of slag to rutile in the blend mix the mass chlorinated increased and the blowover decreased. The results indicate that the conversion rate increases as Slag A content increases but up to a point, and that point lies somewhere between 75 and 100 wt% Slag A. More testwork should be done to determine the optimum blend.

The -106 μ m fraction is excluded from the industrial scale chloride process, but the literature revealed that the addition of a certain amount of “fines” can improve fluidisation; it is recommended that this is tested by adding varying amount of fines (i.e. -106 μ m) and studying the blowover and chlorination behaviour.

It is clear that the particle size distribution of the feedstocks has an effect on the fluidisation behaviour but this effect is not easy to quantify, since it is dependant on a number of factors, differs from material to material, and depends on the fines weight fraction and the size of the fines. The body of scientific literature is limited on this topic and it is recommended that further work on feedstock blends and particle size distribution is undertaken.

CHAPTER 6

6. REFERENCES

Barin, I and Schuler W. (1980), Metallurgical Trans B, vol.11B, pp 199 – 207

Baeyens, J., Geldart, D and Wu, S.Y. (1992), Elutriation of fines from gas fluidised beds of Geldart A type powders – effect of adding superfines, Powder Technology 71 (1992), pp 71 – 80

Beetsra, R., Nijenhuis, J., Ellis, N and van Ommen, J.R. (2009), The influence of particle size distribution on fluidised bed hydrodynamics using high through put experimentation, AIChE Journal, vol.55, No 8, pp 2013 – 2022

Bergholm, A. (1961), Chlorination of rutile, Transactions of the Metallurgical Society of AIME, vol.221, pp 1121 – 1127

Bessinger, D. (2000), Cooling characteristics of High Titania Slag, MSc thesis, University of Pretoria

Bessinger, D., Du Plooy, H., Pistorius, P.C and Visser, C. (1997), Characteristics of some high titania slag, Heavy Minerals 1997, Johannesburg, South Institute of Mining and Metallurgy, pp 151 – 156

Bungu, N.P. (2004), Fluidised bed chlorination of oxidized titania slag, MSc, University of Pretoria

Burger, H., Bessinger, D and Moodley, S. (2009), Technical Considerations and viability of higher Titania slag feedstock for the chloride process, 7th Heavy Mineral Conference 2009, pp 187 – 194

Burger, H and Rabe, J. (2007), Exxaro Internal Report, Literature review on chlorination, pp 1 – 23

Chase, G. (2010), Study Notes 6, University of Akron,
<http://coel.ecgf.uakron.edu/~chase/Solids/SolidsNotes6%20Elutriation.pdf>, viewed 20/11/2010

Den Hoed, P and Nell, J. (2002), The carbochlorination of titaniferous oxides in a small scale fluidised bed, IFSA 2002, pp 133 – 143

Den Hoed, P and Nell, J. (2003), The behaviour of individual species in the carbochlorination of titaniferous oxides, South African Institute of Mining and Metallurgy, pp 43 – 55

Dunn, W.E. (1960), High temperature chlorination of TiO₂ Bearing Minerals, Trans AIME, vol.218, pp 6 – 12

Dunn, W.E. (1979), High Temperature Chlorination of Titanium Bearing Minerals: Part IV, Metallurgical Transactions B, pp 271 – 277

DuPont. (2007), DuPont Ti-Pure titanium dioxide- Titanium dioxide for coatings, http://www2.dupont.com/Titanium_Technologies/en_US/tech_info/literature/Coatings/CO_B_H_65969_Coatings_Brochure.pdf, viewed 20/11/2010

Engineering Toolbox. (2011), http://www.engineeringtoolbox.com/dry-air-properties-d_973.html, viewed 20/05/2011

Fisher, J.R. (1997), Developments in the TiO₂ pigments industry which will drive demand for TiO₂ mineral feedstocks, South African Institute of Mining and Metallurgy, pp 207 – 218.

Geldart, D. (1973), Types of gas fluidisation, Powder Technology 7, pp 285 – 292

George, S.E and Grace, J.R. (1978), Entrainment of particles from an aggregative fluidised bed, The American Institute for Chemical Engineers, pp 67 – 74

Grace, J. R and Sun, G. (1991), Influence of Particle Size Distribution on the performance of fluidised bed reactors, The Canadian Journal of Chemical Engineering, vol.69, pp 1126 – 1134

Grobler, J.G and Bosman, J. B. (2009), Gravity separator performance evaluation using QEMSCAN particle mineral analysis, 7th International Heavy Minerals Conference, Champagne Sports Resort, The South African Institute of Mining and Metallurgy, pp 1 – 8

Habashi, F. (1997), Handbook of Extractive Metallurgy, Wiley VCH, New York, pp 1142 – 1144

Hoffmann, A.C and Janssen, L.P.B. M and Prins, J. (1993), Particle segregation in fluidised binary mixtures, Chemical Engineering Science, vol.48, pp 1583 – 1592

Jena, P., Brocchi, E.A and Gameiro, D.H. (1998), Kinetics of the chlorination of TiO₂ by Cl₂ in the presence of graphite powder, Transactions of the Institution of Mining metallurgy, vol.107, pp 139 – 145

Kale, A and Bisaka, K. (2010), Comparative study of the chlorination kinetics of titanium feedstocks, Mintek internal report

- Kotze, H., Bessinger, D and Beukes J. (2006), Ilmenite Smelting at Ticor SA, South African Pyrometallurgy 2006, Cradle of Human Kind, South African Institute of Mining and Metallurgy, pp 203 – 214
- Kotze, H. (2007), Investigation into the effect of cooling conditions on the particle size distribution of titania slag, PhD thesis, University of Pretoria, Pretoria, viewed 2010/11/01 <http://upetd.up.ac.za/thesis/available/etd-07162008-075705/>
- Kunii, D and Levenspiel, O. (1969), Fluidization Engineering, Wiley J, New York
- Kunii, D and Levenspiel O. (1991), Fluidization Engineering, Wiley J, New York
- Le Roux, J.T. (2001), Fluidised bed chlorination of Titania slag, MSc, University of Pretoria
- Li, J., Nakazato, T and Kato, K. (2004), Effect of Cohesive powders on the elutriation of particles from a fluid bed, Chemical Engineering Science 59, pp 2777 – 2782
- McAuley, K.B., Talbot, J.P and Harris T.J.(1994), A comparison of two phase and well mixed models for fluidised bed polyethylene reactors, Chemical Engineering Science, vol.49, pp 2035 – 2045
- Minkler, W.W and Baroch E.F. (1981), The Production of Titanium, Zirconium and Hafnium in J.K Tien and J.F Elliotts (Eds), Metallurgical Treatises, Metallurgical Society of the AIME, pp 171 – 182
- Mohanty, Y. K., Roy, G.K and Biswal, K.C. (2009), Indian Journal of Chemical Journal vol.16, pp 17 – 24
- Mori, S and Wen, C.Y. (1975), Estimation of Bubble diameter in gaseous fluidised beds, AIChE Journal, vol.21, pp 109 – 115
- Morris, A. J and Jensen, F. (1976), Fluidised Bed Chlorination Rates of Australian Rutile, Metallurgical Transactions B, pp 89 – 93
- Murty, C.V.G. K., Upadhyay, R and Asokan, S. (2007), Electro smelting of ilmenite for production of TiO₂ slag – Potential of India as a Global Player, INFACON XI, pp 823 – 836
- Nell, J and den Hoed, P. (2003), Carbochlorination of rutile, titania slag and ilmenite in a bubbling fluidised bed reactor, International Mineral Processing Congress XXII, pp 1426 – 1433

Pistorius, P.C. (2001), The relationship between FeO and Ti₂O₃ in ilmenite smelter slags. Scandinavian Journal of Metallurgy. pp 120 – 125

Pistorius, P.C and Le Roux, J.T. (2002), Thermal, Chemical and Structural Changes during initial chlorination of titania slag, Canadian Metallurgical Quarterly, vol.41, pp 289 – 298

Reeves, J. W and Reeves, R.G. (1997), Misconceptions about titanium ore chlorination, Heavy Minerals 1997, Johannesburg, South African Institute of Mining and Metallurgy, pp 203 – 206

Rhee, K.I and Sohn, H.Y. (1990), The Selective Chlorination of iron from ilmenite ore by CO-Cl₂ Mixtures: Part 1: Intrinsic Kinetics, Metallurgical Transactions vol.21B, pp 321 – 329

Rowe, L.W and Opie, W. R. (1955), Production and Purification of TiCl₄, Journal of Metals, pp 1189 – 1193

Sahu, K., Alex, T., Mishra, D and Agrawal, A. (2006), An overview on the production of pigment grade titania from titania rich slag. Waste Management research 2006. pp 74 – 79

Shin, M.K., Kim, E.M., Koo, B.S., Gui, Y.H and Ki, J.Y. (2007), Entrainment Characteristics of Fine Particles in Cylindrical and Conical Inert Medium Fluidized Beds, Ind Eng. Chem 46, pp 1408 – 141

Sharma, S.D and Pugsley, T.S. (2007), Effect of particle size distribution on the performance of a catalytic fluidised bed reactor, The 12th International Fluidisation conference, pp 665 – 662

Singh, M.K and Majumder S.K. (2010), Theoretical Study on Effect of Operating Parameters on Mass Transfer in Bubbly Flow, Journal of Engineering and Applied Sciences 5, pp 163 – 170

Sobrino, C., Acosta-Iborra, A., Santana, D and De Vega, M. (2009), Bubble Characteristics in a bubbling fluidised bed with a rotating distributor, International Journal of Multiphase Flow, pp 1 – 23

Sohn, H.Y., and Zhou, L. (1998), The Kinetics of Carbochlorination of Titania slag, Canadian Journal of Chemical Engineering, 76, pp 1078 – 1082

Sohn, H.Y and Zhou, L. (1999), The chlorination kinetics of beneficiated ilmenite particles by CO+Cl₂ mixtures, Chemical Engineering Journal 72, pp 37– 42

Sohn, H.Y., Zhou, L and Cho, K. (1998), Intrinsic Kinetics and Mechanism of Rutile Chlorination by CO and Cl₂ Mixtures, Ind Eng Chem Research 37, pp 3800 – 3805

South Africa Department of Minerals and Energy (DME), (2008), An overview of South Africa's Titanium Mineral Concentrate Industry, (<http://www.dme.gov.za/pdfs/minerals/R71-2008.pdf>), viewed 11/11/2010

Stanaway K.J (1994), Overview of titanium dioxide feedstocks, Mining engineering, pp 1367 – 1370

Sun, G and Grace, J.R. (1990), The effect of particle size distribution on the performance of a catalytic fluidised bed reactor, Chemical Engineering Science, vol.45, No 8, pp 2187 – 2194

Toromanoff, I and Habashi, F. (1984), The composition of a titanium slag from Sorel, Journal of the Less common metals, 97, pp 317 – 329

Tronox Incorporated. (2007), Annual Report Pursuant to Section 13 or 15(d) of the Securities Exchange Act of 1934, [http://www.tronox.com/SiteObjects/published/20011F12491745CD824BB40E8EEA8C84/BEF77947C0EC984EB91C17C4EE76E42E/file/2007 Annual Report on 10K.pdf](http://www.tronox.com/SiteObjects/published/20011F12491745CD824BB40E8EEA8C84/BEF77947C0EC984EB91C17C4EE76E42E/file/2007%20Annual%20Report%20on%2010K.pdf), viewed 3/05/2011

Van Dyk, J.P and Pistorius, P.C. (1999), Evaluation of a process that uses phosphate additions to upgrade titania slag, Metallurgical and Materials Transactions B, vol.30 B, pp 823 – 826

Veldhuizen, J. (2000), APG/Joint venture agreement to commercialise ERMS technology, [http://www.austpacresources.com/pdfs/brokers/BNP%20Report%20\(July%2000\).pdf](http://www.austpacresources.com/pdfs/brokers/BNP%20Report%20(July%2000).pdf), viewed 3/08/2010

Wen, C.Y and Chen, L.H. (1982), Fluidised Bed Freeboard Phenomena: Entrainment and Elutriation, AIChE, vol.28, pp 117 – 128

Youn, I and Park, K.Y. (1989), Modelling of Fluidised bed chlorination of rutile, Metallurgical Transactions B, vol. 20B, pp 959 – 966

Yates, J.G and Newton, D. (1986), Fine particle effects in a fluidised bed reactor, Chemical Engineering Science, vol.41, No 4, pp 801 – 806

Zhou, L., Sohn, Y.H., Whiting, G.K and Leary, K. (1996), Microstructural Changes in Several Titaniferous materials during Chlorination reaction, I & EC Research, pp 954 – 962

Zietsman, J.H. (2004), Interactions between freeze lining and slag bath in ilmenite smelting, Ph.D. University of Pretoria

Zietsman, J.H and Pistorius, P.C. (2004), Process mechanisms in ilmenite smelting, South African Institute of Mining and Metallurgy. pp 653 – 659

Appendix 1: Particle size distribution and density of feed material

Table 40: Particle size distribution

Particle size distribution				
Size(μm)	Slag A	Rutile	Blend	Slag B
	Weight (%)			
+850	2.6%		1.6%	0.8%
-850 +600	14.6%		6.9%	10.7%
-600 +425	19.6%		10.2%	13.7%
-425 +300	20.7%		10.6%	16.8%
-300 +212	17.1%	2.0%	9.6%	15.6%
-212 +150	11.9%	19.4%	15.7%	13.3%
-150 +106	8.0%	48.8%	27.9%	9.8%
-106 + 90	2.0%	20.2%	11.1%	4.0%
-90 + 75	1.4%	8.2%	4.8%	5.0%
-75	2.1%	1.3%	1.7%	10.2%

Table 41: Density

Size(μm)	Slag A	Rutile	Slag B
+850	4.02		4.03
-850 +600			
-600 +425			
-425 +300			
-300 +212			
-212 +150	4.03	4.13	4.04
-150 +106	4.03	4.17	4.05
-106 + 90	4.06	4.21	4.04
-90 + 75	4.06	4.24	4.04
-75	4.1	4.25	4.06

Appendix 2: Geldart Graphs

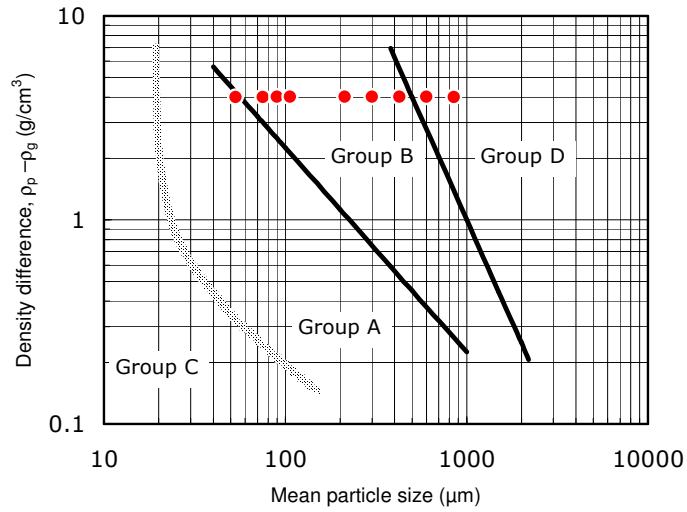


Figure 75: Geldart Classification – Slag A

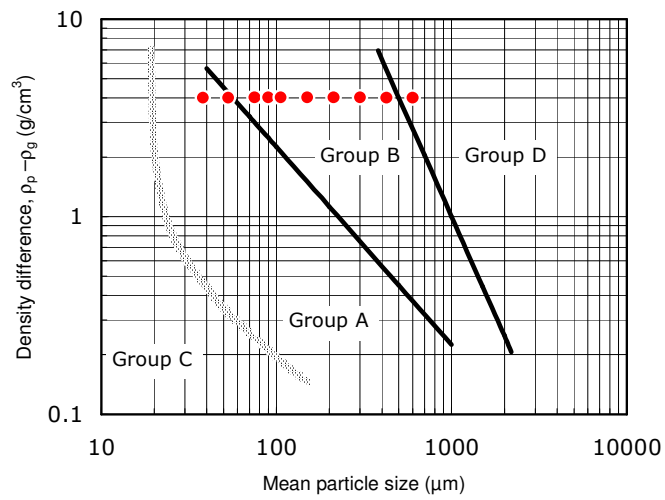


Figure 76: Geldart Classification – Slag B

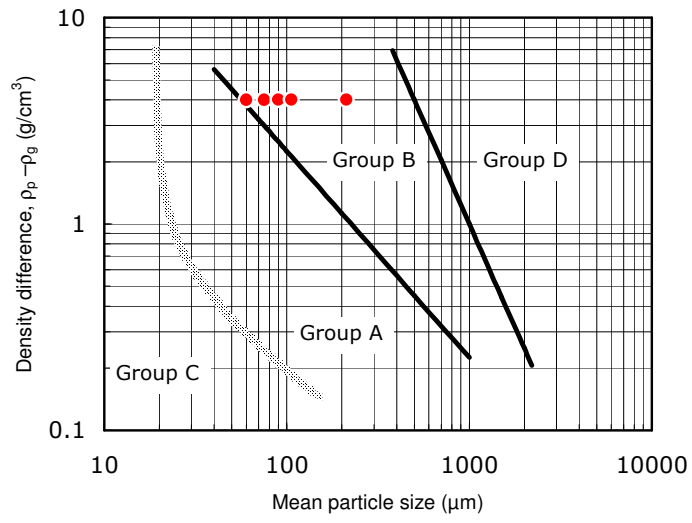


Figure 77: Geldart Classification – Rutile

Appendix 3: SEM results for Feed Material

Table 42: Normalised Point analysis of the M_3O_5 phase in Slag A

	O	Mg	Al	Si	Ti	Mn	Fe
	(wt%)						
1	32.80	0.78	0.82	0.12	54.17	1.55	9.77
2	32.00	0.95	0.89	0.21	54.66	1.39	9.91
3	32.69	0.97	0.89	0.19	54.48	1.16	9.63
4	32.28	0.88	1.01	0.00	57.31	1.60	6.92
5	32.61	0.63	0.77	0.00	57.14	1.47	7.40
6	32.59	0.85	0.93	0.00	57.35	1.58	6.69
7	32.73	0.85	0.91	0.13	57.31	1.42	6.65
Average	32.53	0.84	0.89	0.09	56.06	1.45	8.14
Standard deviation	0.27	0.11	0.07	0.08	1.41	0.14	1.43

Calculated composition (normalising O to 5): $Mg_{0.08}Al_{0.07}Ti_{2.83}Mn_{0.06}Fe_{0.32}O_5(M_{3.3}O_5)$

Table 43: Normalised Point analysis of Glassy phase Slag A

	O	Mg	Al	Si	Ti	Mn	Fe	Zr
	wt%							
1	52.07	0.00	4.31	34.67	3.88	0.00	0.00	0.00
2	50.74	0.00	4.58	36.19	2.94	0.00	0.00	0.00
3	51.60	0.00	4.19	36.56	3.19	0.00	0.00	0.00
4	50.84	0.00	4.36	34.64	4.44	0.24	0.62	0.29
5	49.52	0.00	4.68	37.15	2.48	0.00	0.60	0.41
6	49.85	0.00	3.88	30.83	7.24	0.68	0.95	0.80
7	50.17	0.47	4.07	36.79	3.29	0.00	0.54	0.00
8	50.15	0.49	4.10	37.09	3.07	0.00	0.65	0.00
Average	50.62	0.12	4.27	35.49	3.81	0.11	0.42	0.19
Standard deviation	0.82	0.21	0.25	1.99	1.41	0.23	0.34	0.28

Table 44: Normalised Point analysis of rutile phase in Slag A

	O	Ti	Mn	Fe
1	38.29	59.98	0.33	0.69
2	37.71	60.18	0.41	1.24
Average	38.00	60.08	0.37	0.97
Standard deviation	0.41	0.14	0.06	0.39

Calculated composition (normalising O to 5): $Ti_{1.1}O_2$

Table 45: Normalised Point analysis of M_3O_5 phase in Slag B

	O	Al	Si	Ti	Mn	Fe
1	33.49	1.30	0.00	61.89	1.52	1.81
2	33.44	0.99	0.00	62.67	2.90	0.00
3	33.64	1.20	0.18	62.30	1.19	1.49
4	34.34	1.31	0.00	61.98	1.08	1.29
5	33.71	1.34	0.00	61.58	1.94	1.43
6	35.30	1.00	0.00	59.79	2.43	1.48
7	33.57	1.35	0.00	61.69	1.90	1.49
Average	33.93	1.21	0.03	61.70	1.85	1.28
Standard deviation	0.68	0.16	0.07	0.92	0.66	0.59

Calculated composition (normalising O to 5): $Al_{0.09}Ti_{2.98}Mn_{0.07}Fe_{0.05}O_5(M_{3.2}O_5)$

Table 46: Normalised Point analysis of glassy phase in Slag B

	O	Na	Al	Si	S	K	Ca	Ti	Mn	Fe	Zr	Nb
	wt%											
1	51.86	0.00	5.38	20.93	1.68	0.00	4.06	1.79	14.29	0.00	0.00	0.00
2	46.82	1.08	4.54	18.30	0.00	0.00	4.10	3.98	16.66	1.13	1.81	1.58
3	53.93	1.15	3.78	23.13	0.00	1.17	3.56	2.17	11.11	0.00	0.00	0.00
4	54.84	1.79	4.13	24.61	0.00	0.78	2.64	11.20	0.00	0.00	0.00	0.00
5	48.93	2.03	5.13	31.73	0.00	0.63	2.74	2.46	5.51	0.00	0.00	0.84
6	49.54	1.94	4.89	31.83	0.00	0.68	2.48	2.26	5.69	0.00	0.00	0.69
7	46.26	1.66	5.37	21.13	0.00	0.00	5.09	4.16	13.81	0.00	0.00	2.52
8	48.14	1.63	5.41	21.81	0.00	0.00	5.03	1.96	13.59	0.00	2.44	0.00
9	48.32	1.18	5.14	21.98	0.00	0.00	4.70	1.97	12.88	0.66	2.51	0.00
10	47.91	1.87	5.56	32.88	0.00	0.63	2.55	2.34	5.17	0.00	1.09	0.00
11	49.98	2.20	5.03	29.85	0.00	0.78	2.23	6.38	3.56	0.00	0.00	0.00
12	52.42	1.34	4.07	26.47	0.00	0.00	2.63	8.79	4.28	0.00	0.00	0.00
13	50.91	1.61	4.99	32.15	0.00	0.72	2.77	1.78	5.08	0.00	0.00	0.00
Average	48.98	1.39	4.72	25.26	0.12	0.38	3.73	4.05	10.18	0.13	0.56	0.40
Standard deviation	2.66	0.57	0.57	5.16	0.47	0.42	1.04	3.03	5.28	0.35	1.00	0.80

Table 47: Normalised Point analysis of Fe in Slag B

	C	Si	Ti	Cr	Mn	Fe	Nb
	wt%						
1	2.44	4.45	1.13	1.15	2.60	87.74	0.50
2	2.66	0.00	1.53	0.00	0.86	94.95	0.00
3	2.80	0.00	0.84	0.00	0.00	96.35	0.00
4	2.71	0.00	1.28	0.00	0.00	96.01	0.00
5	3.42	0.00	2.50	0.00	0.00	94.08	0.00
Average	2.81	0.89	1.46	0.23	0.69	93.83	0.10
Standard deviation	0.37	1.99	0.63	0.52	1.13	3.52	0.22

Table 48: Normalised Average Composition of the Rutile Feed Material

	O	Al	Si	Ti	Nb	Zr
	wt%					
1	38.33	0.38	0.00	61.29	0.00	0.00
2	37.61	0.47	0.14	61.78	0.00	0.00
3	37.76	0.47	0.17	61.34	0.26	0.00
4	38.44	0.41	0.17	60.98	0.00	0.00
5	37.84	0.44	0.22	61.49	0.00	0.00
6	39.58	0.63	0.38	59.41	0.00	0.00
7	37.50	0.54	0.19	61.77	0.00	0.00
8	37.61	0.63	0.37	61.39	0.00	0.00
9	37.80	0.32	0.10	61.35	0.29	0.14
10	38.12	0.34	0.00	61.17	0.00	0.37
11	37.63	0.36	0.00	61.60	0.00	0.42
Average	38.02	0.45	0.16	61.23	0.05	0.08
Standard deviation	0.57	0.10	0.13	0.62	0.11	0.15

Calculated composition (normalising O to 2): TiO₂

Table 49: Normalised Average Composition of Zircon in rutile feed material

	O	Si	Zr
	wt%		
1	31.48	15.73	52.78
2	33.16	15.38	51.45
3	31.88	15.82	52.30
4	32.26	15.81	51.93
Average	32.20	15.69	52.12
Standard deviation	0.72	0.21	0.56

Table 50: Normalised Average Composition of Fe silicate phase

	O	Na	Mg	Al	Si	K	Ti	Fe	Ca
	wt%								
1	50.32	1.07	2.22	3.36	24.1	1.63	1.51	15.39	0.4
2	48.19	0.8	1.99	4.1	26.6	0.65	1.67	14.66	1.33
3	48.81	0.85	2.11	4.17	26.55	0.85	1.59	14.15	0.93
4	48.79	1.04	2.22	3.23	20.86	1.48	1.66	20.42	0.29
5	50.88	0.2	1.42	2.65	20.79	1.82	6.42	15.38	0.44
6	48.96	0.73	2.05	3.48	26.01	0.73	1.46	15.77	0.82
Average	49.33	0.78	2.00	3.5	24.15	1.19	2.39	15.96	0.70
Standard deviation	1.04	0.31	0.30	0.57	2.73	0.51	1.98	2.26	0.40

Appendix 4: Mass Balance

Table 51: Chlorination Results for Slag A

	Feed 0	Temperature(°C)				
		1000			900	800
		30	60	180	180 min	180 min
Slag						
In (g)		200	200	200	200	200
Out (g)		142	124.6	11.3	96.3	126
Blowovers (g)		1.5	7.3	52.8	4.7	0.5
Mass reacted (g)		56.5	68.1	135.9	99	73.5
<i>Mass chlorinated (%)</i>		28%	34%	68%	50%	37%
Petroleum coke						
In (g)		40.00	40.00	40.00	40.00	40.00
Out (g)		37.40	35.00	34.60	34.60	38.00
Mass reacted (g)		2.60	5.00	5.40	5.40	2.00
<i>% reacted</i>		7%	13%	14%	14%	5%
<i>Coke: mass reacted</i>		<i>0.05</i>	<i>0.07</i>	<i>0.04</i>	<i>0.05</i>	<i>0.03</i>
TiO₂						
% TiO₂	61.9%	96.6%	95.9%	85.8%	94.8%	95.2%
In (g)	123.84	123.84	123.84	123.84	123.84	123.84
Out (g)		137.17	119.49	9.70	91.29	119.95
Blowovers (g)		1.42	6.92	50.05	4.46	0.47
Mass Reacted (g)		-14.75	-2.57	64.09	28.09	3.41
<i>Mass Chlorinated(%)</i>		-12%	-2%	52%	23%	3%
Ti₂O₃						
% Ti₂O₃	23.4%	0.0%	0.0%	0.0%	0.0%	0.0%
In (g)	46.84	46.84	46.84	46.84	46.84	46.84
Out (g)		0.00	0.00	0.00	0.00	0.00
Blowovers (g)		0.00	0.00	0.00	0.00	0.00
Mass Reacted (g)		46.84	46.84	46.84	46.84	46.84
<i>Mass Chlorinated(%)</i>		100%	100%	100%	100%	100%

	Feed 0	Temperature				
		1000 °C		1000.00	900	800
		30	60	180	180 min	180 min
TiO₂(equivalent)						
% TiO ₂	87.5%	96.6%	95.9%	85.8%	94.8%	95.2%
In (g)	174.92	174.92	174.92	174.92	174.92	174.92
Out (g)		137.17	119.49	9.70	91.29	119.95
Blowovers (g)		1.42	6.92	50.05	4.46	0.47
Mass Reacted (g)		36.33	48.51	115.17	79.17	54.49
Mass Chlorinated(%)		21%	28%	66%	45%	31%
FeO						
% FeO	8.60%	0.05%	0.08%	0.18%	0.18%	0.12%
In (g)	17.2	17.20	17.20	17.20	17.20	17.20
Out (g)		0.07	0.10	0.02	0.17	0.15
Blowovers (g)		0.00	0.01	0.07	0.01	0.00
Mass Chlorinated (g)		17.13	17.09	17.11	17.02	17.05
Mass Chlorinated(%)		100%	99%	99%	99%	99%
Al₂O₃						
% Al ₂ O ₃	1.02%	0.80%	0.80%	1.00%	0.20%	1.10%
In (g)	2.04	2.04	2.04	2.04	2.04	2.04
Out (g)		1.14	1.00	0.11	0.19	1.39
Blowovers (g)		0.01	0.03	0.21	0.02	0.00
Mass Chlorinated(g)		0.90	1.01	1.72	1.83	0.65
Mass Chlorinated(%)		44%	50%	84%	90%	32%
SiO₂						
% SiO ₂	1.64%	2.70%	3.30%	12.10%	1.90%	2.90%
In (g)	3.28	3.28	3.28	3.28	3.28	3.28
Out (g)		3.83	4.11	1.37	1.83	3.65
Blowovers (g)		0.07	0.34	2.49	0.22	0.02
Mass Chlorinated (g)		-0.62	-1.18	-0.58	1.23	-0.40
Mass Chlorinated(%)		-19%	-36%	-18%	37%	-12%
MgO						
%MgO	0.73%	0.20%	0.20%	0.20%	0	0.30%
In (g)	1.46	1.46	1.46	1.46	1.46	1.46
Out (g)		0.28	0.25	0.02	0.00	0.38
Blowovers (g)		0.00	0.01	0.07	0.01	0.00

Mass chlorinated (g)		1.17	1.20	1.37	1.45	1.08
<i>Mass Chlorinated(%)</i>		80%	82%	94%	100%	74%
MnO						
%MnO	1.90%	0.10%	0.10%	0.10%	0	0.20%
In (g)	3.80	3.80	3.80	3.80	3.80	3.80
Out (g)		0.14	0.12	0.01	0.00	0.25
Blowovers (g)		0.00	0.01	0.06	0.01	0.00
Mass chlorinated(g)		3.66	3.67	3.73	3.79	3.55
<i>Mass Chlorinated(%)</i>		96%	96%	98%	100%	93%

Table 52: Chlorination Results for Slag B

	Feed	Temperature				
		1000 °C			900 °C	800 °C
		30 min	60 min	180 min	180 min	180 min
Slag		30	60	180		
In (g)	200	200	200	200	200	200
Out (g)		112	108	48	92	116
Blowovers (g)		4	1.9	2.8	3.7	1.8
Mass Reacted (g)		84	90.1	149.2	104.3	82.2
Mass chlorinated(%)		42%	45%	75%	52%	41%
Petroleum coke						
In (g)	40	40	40	40	40	40
Out (g)		36.00	35.00	32.70	36.10	37.50
Mass Reacted (g)		4.00	5.00	7.30	3.90	2.50
% reacted		10%	13%	18%	10%	6%
		0.048	0.055	0.049	0.037	0.030
TiO₂						
% TiO ₂	51.9%	97.5%	97.3%	95.3%	94.6%	93.8%
In (g)	132.6	103.80	103.80	103.80	103.80	103.80
Out (g)		109.20	105.08	45.74	87.03	108.81
Blowovers (g)		0.30	1.90	2.90	3.70	1.85
Mass Reacted (g)		-5.70	-3.18	55.16	13.07	-6.86
Mass Chlorinated(%)		-5%	-3%	53%	13%	-7%
Ti₂O₃						
% Ti ₂ O ₃	38.8%	0.0%	0.0%	0.0%	0.0%	0.0%
In (g)	49.2	77.60	77.60	77.60	77.60	77.60
Out (g)		0.00	0.00	0.00	0.00	0.00
Blowovers (g)		0.00	0.00	0.00	0.00	0.00
Mass Reacted (g)		77.60	77.60	77.60	77.60	77.60
Mass Chlorinated(%)		100%	100%	100%	100%	100%
TiO₂ (equivalent)						
% TiO ₂	95.0%	97.5%	97.3%	95.3%	94.6%	93.8%
In (g)	187.02	190.04	190.04	190.04	190.04	190.04

Out (g)		109.20	105.08	45.74	87.03	108.81
Blowovers (g)		0.30	1.90	2.90	3.70	1.85
Mass Reacted (g)		80.54	83.06	141.40	99.31	79.38
Mass Chlorinated(5)		42%	44%	74%	52%	42%
Fe						
% Fe	2.55%	0.05%	0.05%	0.02%	0.02%	0.08%
In (g)	5.10	5.10	5.10	5.10	5.10	5.10
Out (g)		0.06	0.05	0.01	0.02	0.09
Blowovers (g)		0.00	0.00	0.00	0.00	0.00
Mass Reacted (g)		5.04	5.05	5.09	5.08	5.01
Mass Chlorinated(%)		99%	99%	100%	100%	98%
Al₂O₃						
% Al ₂ O ₃	1.64%	0.70%	0.60%	0.46%	0.76%	1.60%
In (g)	3.12	3.28	3.28	3.28	3.28	3.28
Out (g)		0.78	0.65	0.22	0.70	1.86
Blowovers (g)		0.00	0.00	0.00	0.00	0.00
Mass Reacted (g)		2.50	2.63	3.06	2.58	1.42
Mass Chlorinated(%)		76%	80%	93%	79%	43%
SiO₂						
% SiO ₂	1.49%	1.70%	2.40%	4.50%	3.30%	2.70%
In (g)	2.12	2.98	2.98	2.98	2.98	2.98
Out (g)		1.90	2.59	2.16	3.04	3.13
Blowovers (g)		0.00	0.00	0.00	0.00	0.00
Mass Reacted (g)		1.08	0.39	0.82	-0.06	-0.15
Mass Chlorinated(%)		36%	13%	28%	-2%	-5%
MgO						
% MgO	0.25%	0.05%	0.04%	0.04%	0.05%	0.14%
In (g)	0.5	0.50	0.50	0.50	0.50	0.50
Out (g)		0.06	0.04	0.02	0.05	0.16
Blowovers (g)		0.00	0.00	0.00	0.00	0.00
Mass Reacted		0.44	0.46	0.48	0.45	0.34
Mass Chlorinated(%)		89%	91%	96%	91%	68%

MnO						
% MnO	2.80%	0.13%	0.12%	0.07%	0.13%	0.28%
In (g)	5.8	5.60	5.60	5.60	5.60	5.60
Out (g)		0.15	0.13	0.03	0.12	0.32
Blowovers (g)		0.00	0.00	0.01	0.00	0.00
Mass Reacted (g)		5.45	5.47	5.56	5.48	5.28
<i>Mass Chlorinated(%)</i>		97%	98%	99%	98%	94%

Table 53: Chlorination Results for Rutile

	Feed	Temperature				
		1000°C			900°C	800°C
		30min	60min	180min	180 min	180 min
Rutile						
In (g)		200	200	200	200	200
Out (g)		149	128	47.3	143.6	170
Blowovers (g)		0.3	0.9	30.2	9.2	1.3
Mass Reacted (g)		50.7	71.1	122.5	47.2	28.7
<i>Mass chlorinated (%)</i>		25%	36%	61%	24%	14%
Petroleum coke						
In (g)		40	40	40	40	40
Out (g)		34.1	27.5	21.7	36.2	38.8
Mass reacted		5.9	12.5	18.3	3.8	1.2
<i>% reacted</i>		15%	31%	46%	9%	3%
<i>Coke(g): feedstock reacted(g) ratio</i>		0.12	0.18	0.15	0.08	0.04
TiO₂						
% TiO₂	95.69%	94.20%	96.10%	96.30%	93.00%	95.00%
In (g)		191.38	191.38	191.38	191.38	191.38
Out (g)		140.36	123.01	45.55	133.55	161.50
Blowovers (g)		0.28	0.83	27.81	8.47	1.20
Mass reacted(g)		50.75	67.54	118.02	49.36	28.68
<i>Mass Chlorinated (%)</i>		27%	35%	62%	26%	15%
FeO						
% FeO	0.49%	0.06%	0.05%	0.09%	0.13%	0.10%
In (g)		0.98	0.98	0.98	0.98	0.98
Out (g)		0.09	0.06	0.04	0.19	0.17
Blowovers (g)		0.00	0.00	0.04	0.01	0.00
Mass Reacted (g)		0.89	0.91	0.90	0.78	0.81
<i>Mass Chlorinated (%)</i>		91%	93%	92%	80%	82%
Al₂O₃						
% Al₂O₃	0.31%	0.20%	0.15%	0.26%	0.20%	0.30%
In (g)		0.62	0.62	0.62	0.62	0.62
Out (g)		0.30	0.19	0.12	0.29	0.51
Blowovers (g)		0.00	0.00	0.07	0.02	0.00
Mass Reacted (g)		0.32	0.43	0.42	0.31	0.11

<i>Mass Chlorinated(%)</i>		52%	69%	68%	50%	17%
SiO₂						
% SiO₂	1.44%	2.80%	2.50%	2.10%	4.50%	3.50%
In (g)		2.88	5.60	5.00	4.20	9.00
Out (g)		4.17	3.20	0.99	6.46	5.95
Blowovers (g)		0.02	0.06	1.87	0.57	0.08
Mass Reacted (g)		-1.31	2.34	2.14	-2.83	2.97
<i>Mass Chlorinated(%)</i>		-45%	43%	43%	-54%	34%
V₂O₅						
% V₂O₅	0.49%	0.42%	0.42%	0.44%	0.14%	0.03%
In (g)		0.98	0.98	0.98	0.98	0.98
Out (g)		0.63	0.54	0.21	0.20	0.05
Blowovers (g)		0.00	0.00	0.11	0.03	0.00
Mass Reacted(g)		0.35	0.44	0.66	0.74	0.92
<i>Mass Chlorinated(%)</i>		36%	45%	67%	76%	94%

Table 54: Chlorination Results for Blend

		Temperature		
		1000 °C		
	Feed	30	60	180
Blend				
In (g)	200	200	200	200
Out (g)		126.8	101	40.3
Blowovers (g)		1.5	4	6
Mass Reacted (g)		71.7	95.0	153.7
<i>Mass chlorinated (%)</i>		36%	48%	77%
Petroleum coke				
In (g)	40	40	40	40
Out (g)		35	33.5	32.7
Mass Reacted (g)		5.0	6.5	7.3
<i>% reacted</i>		13%	16%	18%
<i>Coke(g): feedstock reacted(g) ratio</i>		<i>0.070</i>	<i>0.068</i>	<i>0.047</i>
TiO₂				
% TiO₂	80.45%	95.60%	95.10%	90.20%
In (g)	160.89	160.89	160.89	160.89
Out (g)		121.22	96.05	36.35
Blowovers (g)		0.00	0.00	0.00
Mass Reacted (g)		39.67	64.84	124.54
<i>Mass Chlorinated(%)</i>		25%	40%	77%
Ti₂O₃				
% Ti₂O₃	10.00%	10.08%	10.08%	10.08%
In (g)	19.99	19.99	19.99	19.99
Out (g)		0.00	0.00	0.00
Blowovers (g)		0.00	0.00	0.00
Mass Reacted (g)		19.99	19.99	19.99
<i>Mass Chlorinated(%)</i>		100%	100%	100%
TiO₂(equivalent)				
% TiO₂	91.55%	95.60%	95.10%	90.20%
In (g)	183.1	183.1	183.1	183.1
Out (g)		121.22	96.05	36.35
Blowovers (g)		0.00	0.00	0.00

Mass Reacted (g)		61.88	87.05	146.75
Mass Chlorinated(%)		34%	48%	80%
FeO				
% FeO	4.52%	0.17%	0.09%	0.21%
In (g)	9.03	9.03	9.03	9.03
Out (g)		0.21	0.09	0.08
Blowovers (g)		0.00	0.00	0.00
Mass Reacted (g)		8.82	8.94	8.95
Mass Chlorinated(%)		98%	99%	99%
Al₂O₃				
% Al ₂ O ₃	0.78%	0.20%	0.28%	0.30%
In (g)	1.55	1.55	1.55	1.55
Out (g)		0.25	0.28	0.12
Blowovers (g)		0.00	0.00	0.00
Mass Reacted (g)		1.30	1.27	1.43
Mass Chlorinated(%)		84%	82%	92%
SiO₂				
% SiO ₂	1.36%	3.20%	2.70%	7.90%
In (g)	2.72	2.72	2.72	2.72
Out (g)		4.06	2.73	3.18
Blowovers (g)		0.00	0.00	0.00
Mass Reacted (g)		-1.34	-0.01	-0.46
Mass Chlorinated(%)		-49%	0%	-17%
MgO				
% MgO	0.36%	0.08%	0.00%	0.00%
In (g)	0.71	0.71	0.71	0.71
Out (g)		0.10	0.00	0.00
Blowovers (g)		0.00	0.00	0.00
Mass Reacted (g)		0.61	0.71	0.71
Mass Chlorinated(%)		99%	99%	99%
MnO				
% MnO	1.03%	0.05%	0.05%	0.02%
In (g)	2.05	2.05	2.05	2.05
Out (g)		0.06	0.05	0.01
Blowovers (g)		0.00	0.00	0.00
Mass Reacted (g)		1.99	2.00	2.04
Mass Chlorinated(%)		97%	98%	100%

Appendix 5: SEM Results for chlorinated bed samples

Table 55: Normalised Point analysis of Slag A - Sample 3

	O	Mg	Al	Si	Cl	Ca	Ti	Mn	Nb	Phase
	(wt%)									
1	38.66	0.00	0.00	0.00	0.00	0.00	57.93	0.00	3.42	Rutile - Ti _{1.03} O ₂
2	38.22	0.00	0.24	0.13	0.00	0.00	60.13	0.00	1.28	Rutile - Ti _{1.07} O ₂
3	37.84	0.00	0.36	0.00	0.00	0.00	60.36	0.00	1.44	Rutile - Ti _{1.09} O ₂
4	38.08	0.00	0.16	0.00	0.00	0.00	61.01	0.00	0.75	Rutile - Ti _{1.08} O ₂
5	38.13	0.00	0.00	0.00	0.00	0.00	61.27	0.00	0.59	Rutile - Ti _{1.08} O ₂
6	38.32	0.00	0.32	0.00	0.00	0.00	59.99	0.00	1.37	Rutile - Ti _{1.06} O ₂
7	38.58	0.00	0.34	0.00	0.00	0.00	59.72	0.00	1.36	Rutile - Ti _{1.06} O ₂
8	38.57	0.00	0.13	0.00	0.00	0.00	60.80	0.00	0.49	Rutile - Ti _{1.06} O ₂
9	39.19	0.00	0.16	0.00	0.00	0.00	60.11	0.00	0.54	Rutile - Ti _{1.04} O ₂
10	39.37	0.00	0.20	0.11	0.00	0.00	59.94	0.00	0.38	Rutile - Ti _{1.03} O ₂
11	38.67	0.00	0.14	0.00	0.00	0.00	60.67	0.00	0.52	Rutile - Ti _{1.05} O ₂
12	38.88	0.00	0.20	0.00	0.00	0.00	59.94	0.00	0.98	Rutile - Ti _{1.04} O ₂
13	56.71	0.90	3.85	33.59	0.24	1.69	3.03	0.00	0.00	Glassy phase
14	56.39	0.00	2.95	35.00	0.00	1.88	3.77	0.00	0.00	Glassy phase
15	57.93	0.00	3.20	31.62	0.00	4.32	2.93	0.00	0.00	Glassy phase
17	54.30	2.28	4.39	34.33	0.67	0.69	3.35	0.00	0.00	Glassy phase

Table 56: Normalised Point analysis of Slag B - Sample 4

	O	Na	Al	Si	Cl	Ca	Ti	Phase
	(wt%)							
1	55.36	1.08	2.02	38.27	0.00	0.55	2.72	Glassy Phase
2	54.90	1.31	1.93	37.66	0.00	0.94	3.27	Glassy Phase
3	39.18	0.00	0.00	0.00	0.00	0.00	60.82	Rutile - Ti _{1.04} O ₂
4	39.57	0.00	0.00	0.00	0.43	0.00	59.99	Rutile - Ti _{1.01} O ₂
5	38.46	0.00	0.00	0.00	0.00	0.00	61.54	Rutile - Ti _{1.06} O ₂
6	38.20	0.00	0.21	0.00	0.00	0.00	61.59	Rutile - Ti _{1.07} O ₂
7	57.47	0.94	5.64	25.52	1.32	4.87	4.24	Glassy Phase
8	58.04	0.94	4.93	27.92	0.58	3.74	3.85	Glassy Phase
9	53.89	1.19	1.36	42.31	0.00	0.00	1.25	Glassy Phase
10	52.47	1.43	1.50	43.22	0.00	0.00	1.38	Glassy Phase
11	72.02	0.00	2.88	0.11	0.00	0.00	24.98	Glassy Phase
12	53.90	1.38	1.43	35.41	0.00	0.00	7.88	Glassy Phase
13	39.22	0.00	0.00	0.00	0.00	0.00	60.78	Rutile - Ti _{1.04} O ₂
14	38.41	0.00	0.00	0.00	0.00	0.00	61.59	Rutile - Ti _{1.07} O ₂
15	39.02	0.00	0.00	0.00	0.00	0.00	60.98	Rutile - Ti _{1.04} O ₂
16	40.12	0.00	0.00	0.00	0.76	0.24	58.88	Rutile - Ti _{1.0} O ₂
17	38.16	0.00	0.00	0.00	0.00	0.00	61.84	Rutile - Ti _{1.08} O ₂
19	37.91	0.00	0.34	0.00	0.00	0.00	61.76	Rutile - Ti _{1.08} O ₂
20	41.00	0.00	0.17	0.12	0.00	0.00	58.71	Rutile - Ti _{1.00} O ₂

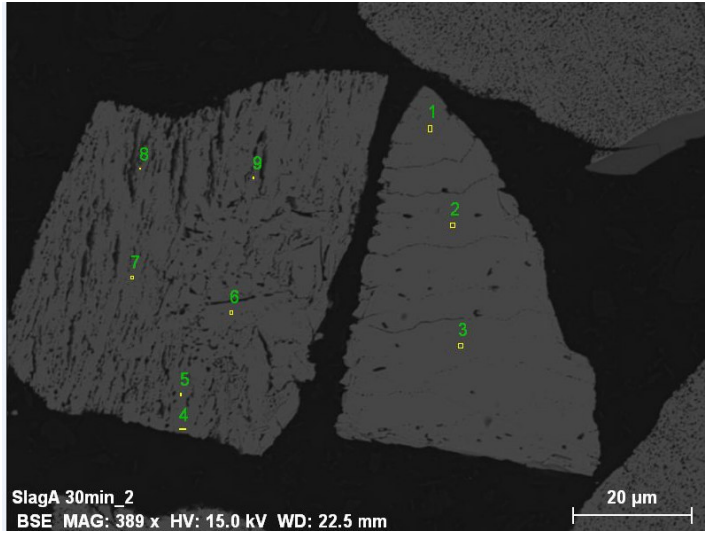


Figure 78: BSE image of Slag A after 30 minutes of chlorination at 1000°C - Sample 8

Table 57: Normalised Point analysis of Slag A - Sample 8

	O	Al	Cl	Ti	Phase
	(wt%)				
1	38.20	0.17	0.00	61.21	Rutile-Ti _{1.07} O ₂
2	37.62	0.15	0.00	61.69	Rutile -Ti _{1.08} O ₂
3	37.90	0.17	0.00	61.42	Rutile - Ti _{1.08} O ₂
4	37.84	0.17	0.00	61.99	Rutile - Ti _{1.09} O ₂
5	38.50	0.19	0.00	61.30	Rutile -Ti _{1.06} O ₂
6	39.30	0.15	0.18	60.37	Rutile -Ti _{1.03} O ₂
7	39.28	0.27	0.21	60.24	Rutile -Ti _{1.03} O ₂
8	38.36	0.43	0.00	61.21	Rutile-Ti _{1.07} O ₂
9	38.74	0.25	0.00	61.00	Rutile -Ti _{1.05} O ₂

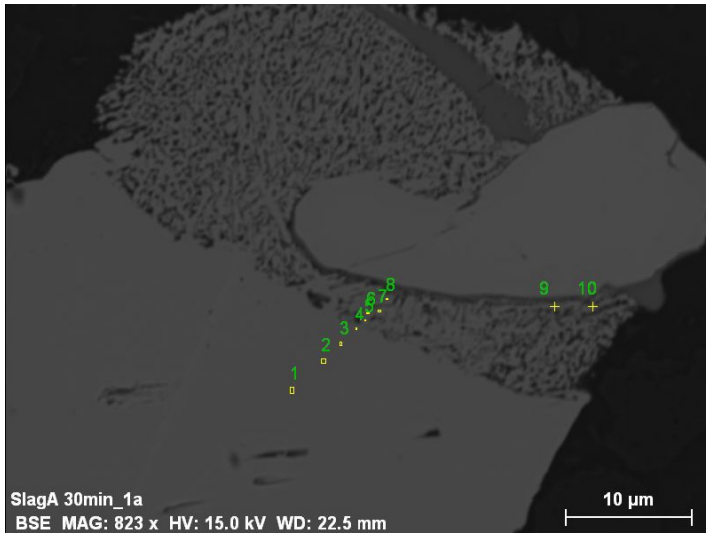


Figure 79: BSE image of Slag A after 30 minutes of chlorination at 1000°C – Sample 9

Table 58: Normalised Point analysis of Slag A - Sample 9

	O	Al	Si	Cl	Ti	Zr	Phase
	Wt%						
1	38.45	0.28	0.00	0.00	61.27	0.00	Rutile -Ti _{1.07} O ₂
2	38.77	0.35	0.00	0.00	60.88	0.00	Rutile -Ti _{1.05} O ₂
3	38.36	0.33	0.00	0.00	61.31	0.00	Rutile -Ti _{1.07} O ₂
4	39.41	0.17	0.00	0.00	60.42	0.00	Rutile -Ti _{1.02} O ₂
5	38.70	0.00	0.00	0.24	61.06	0.00	Rutile -Ti _{1.05} O ₂
6	39.64	0.00	0.00	0.46	59.90	0.00	Rutile -Ti _{1.01} O ₂
7	41.36	0.00	0.00	0.98	57.66	0.00	Rutile -Ti _{0.93} O ₂
8	41.59	0.17	0.00	0.2	58.04	0.00	Rutile -Ti _{0.93} O ₂
9	41.09	0.00	0.44	0.00	58.30	0.17	Rutile -Ti _{0.95} O ₂
10	40.30	0.13	0.14	0.44	58.98	0.00	Rutile -Ti _{0.98} O ₂

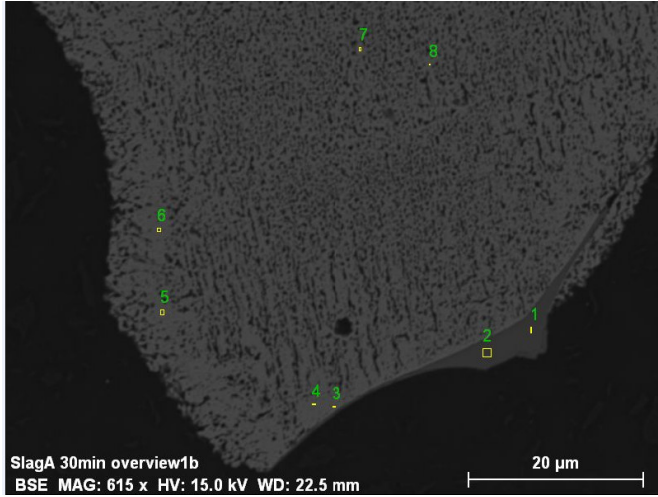


Figure 80: BSE image of Slag A after 30 minutes of chlorination at 1000°C – Sample 10

Table 59: Normalised Point analysis of Slag A – Sample 10

	O	Mg	Al	Si	Cl	Ca	Ti	Mn	Fe	Phase
	(wt%)									
1	52.59	0.68	4.37	35.14	0.00	3.03	2.42	0.42	0.63	Glassy
2	51.07	0.56	4.04	37.34	0.00	2.43	2.24	0.50	0.62	Glassy
3	39.32	0.00	0.23	0.51	0.27	0.00	59.67	0.00	0.00	Rutile - $Ti_{1.01}O_2$
4	38.01	0.00	0.22	0.00	0.00	0.00	61.78	0.00	0.00	Rutile - $Ti_{1.08}O_2$
5	38.08	0.00	0.30	0.00	0.00	0.00	61.63	0.00	0.00	Rutile - $Ti_{1.08}O_2$
6	38.44	0.00	0.28	0.00	0.18	0.00	61.10	0.00	0.00	Rutile - $Ti_{1.06}O_2$
7	38.84	0.00	0.17	0.00	0.00	0.00	60.99	0.00	0.00	Rutile - $Ti_{1.05}O_2$
8	38.52	0.00	0.20	0.00	0.19	0.00	61.08	0.00	0.00	Rutile - $Ti_{1.06}O_2$

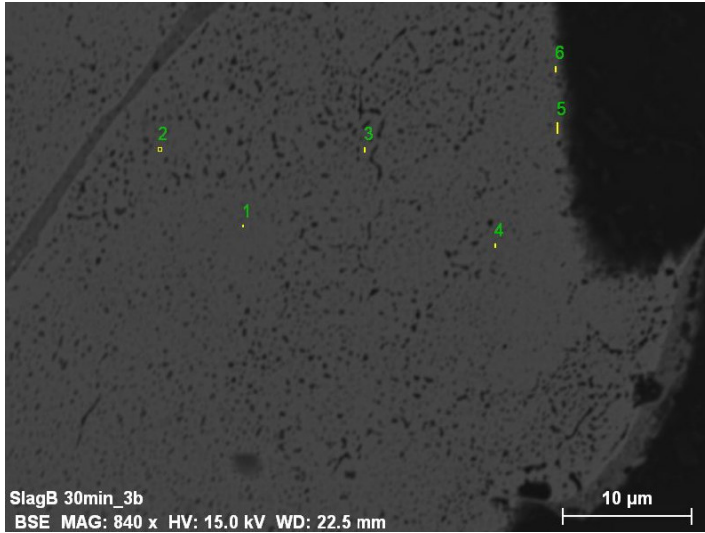


Figure 81: BSE image of Slag B after 30 minutes of chlorination at 1000°C- Sample 11

Table 60: Normalised Point analysis of Slag B - Sample 11

	O	Al	Cl	Ti	Phase
	wt%				
1	39.74	0.46	0.00	59.80	Rutile - $Ti_{1.00}O_2$
2	38.84	0.62	0.21	60.33	Rutile - $Ti_{1.04}O_2$
3	38.65	0.32	0.00	61.03	Rutile - $Ti_{1.06}O_2$
4	39.07	0.22	0.55	60.16	Rutile - $Ti_{1.03}O_2$
5	39.48	0.68	0.23	59.60	Rutile - $Ti_{1.01}O_2$
6	38.34	0.52	0.19	60.94	Rutile - $Ti_{1.06}O_2$

Appendix 6: XRD Results

Table 61: XRD Results for the Feed samples

	Approximate formula	Slag A	Slag B	Rutile
M_3O_5	$(Fe,Ti,Mn)Ti_2O_5$	95	88	
Rutile	TiO_2	4	4	87
Anatase	TiO_2			9
Quartz	SiO_2			1
Zircon	$ZrSiO_4$			1
Metallic iron	Fe	<1		
Dolomite				2
Ilmenite	$FeTiO_3$		8	

Table 62: XRD Results for Slag A chlorination

Mineral	Approximate Formulae	800°C for 180 min	900°C for 180 min	1000°C for 30 min	1000°C for 60 min	1000°C for 180 min
Rutile	TiO_2	100	100	100	97	-
Quartz	SiO_2	-	-	-	3	-

Table 63: XRD Results for Slag B chlorination

Mineral	Approximate Formulae	800°C for 180 min	900°C for 180 min	1000°C for 30 min	1000°C for 60 min	1000°C for 180 min
Rutile	TiO_2	97	100	99	100	99
Anatase	TiO_2	2	-	-	-	-
Quartz	SiO_2	-	-	1	-	-
Zircon	$ZrSiO_4$	<1	-	-	-	1

Table 64: XRD Results for Rutile chlorination

Mineral	Approximate Formulae	800°C for 180 min	900°C for 180 min	1000°C for 30 min	1000°C for 60 min	1000°C for 180 min
Rutile	TiO ₂	89	91	93	95	92
Anatase	TiO ₂	8	5	3	1	-
Quartz	SiO ₂	1	1	1	1	1
Zircon	ZrSiO ₄	2	3	3	3	6

Table 65: XRD Results for the blend chlorination

Mineral	Approximate Formulae	1000°C for 30 min	1000°C for 60 min	1000°C for 180 min
Rutile	TiO ₂	97	95	94
Quartz	SiO ₂	2	3	3
Zircon	ZrSiO ₄	1	2	3

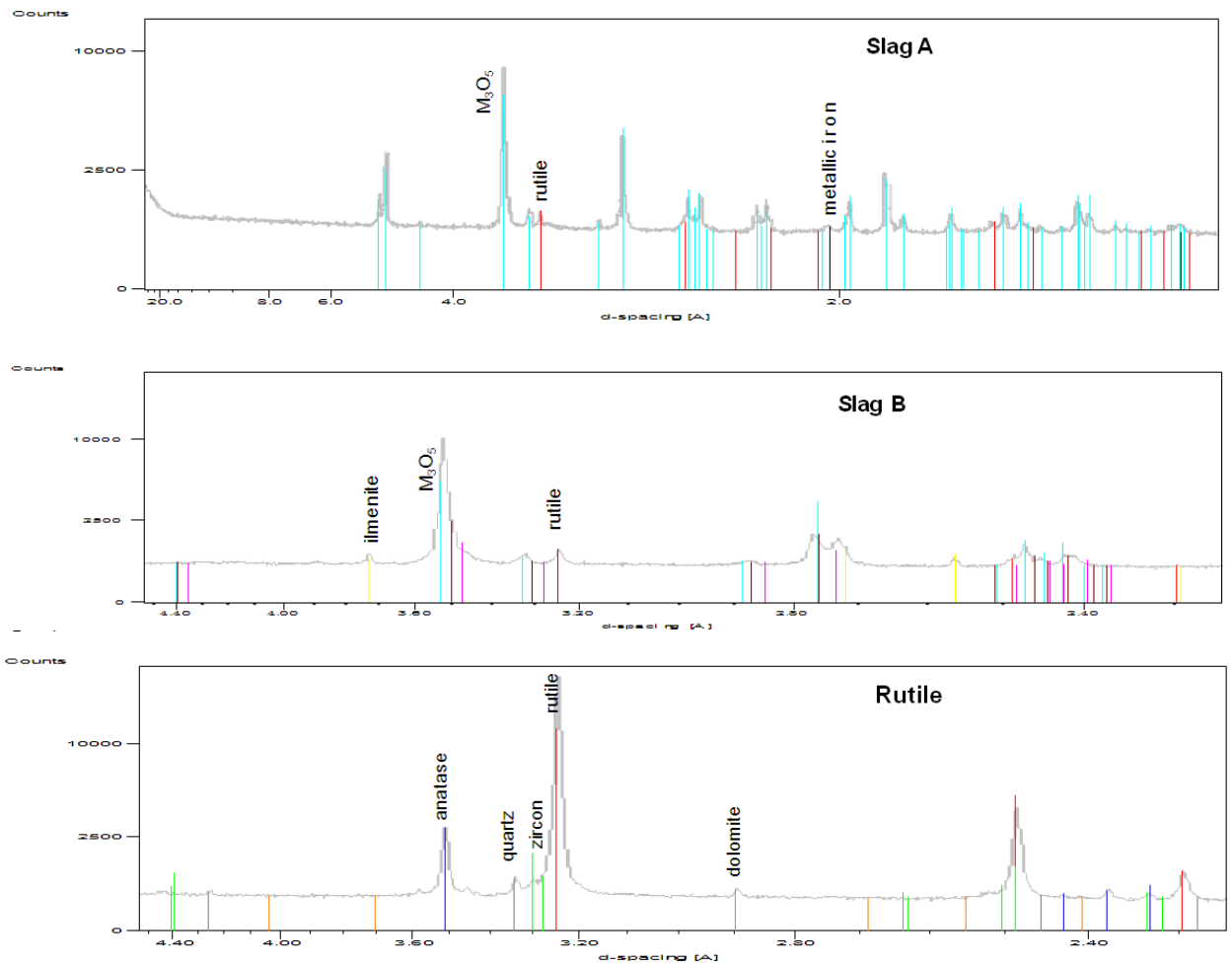


Figure 82: Diffractograms for feed materials

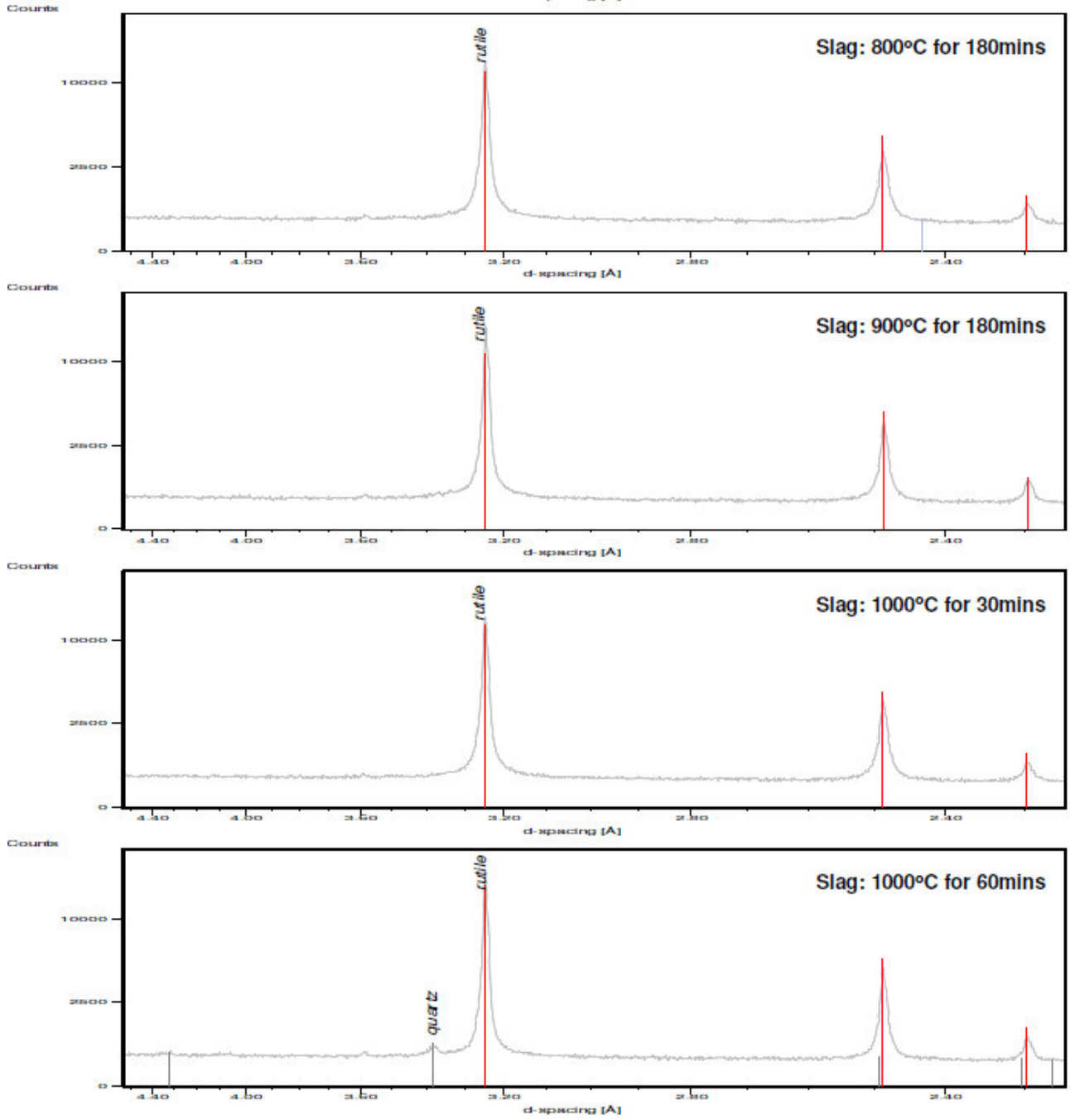


Figure 83: Diffractograms for Slag A

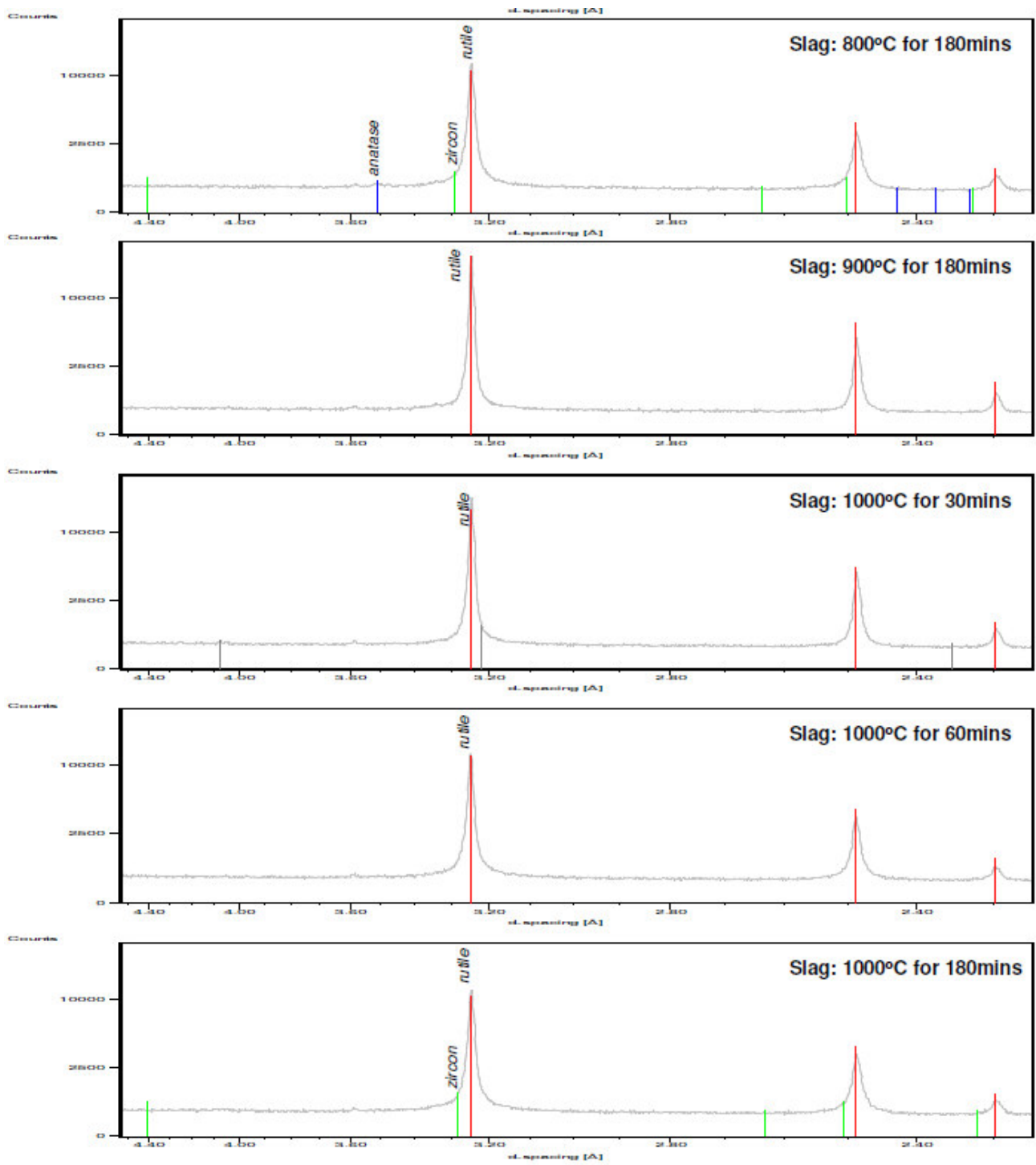


Figure 84: Diffractograms for Slag B

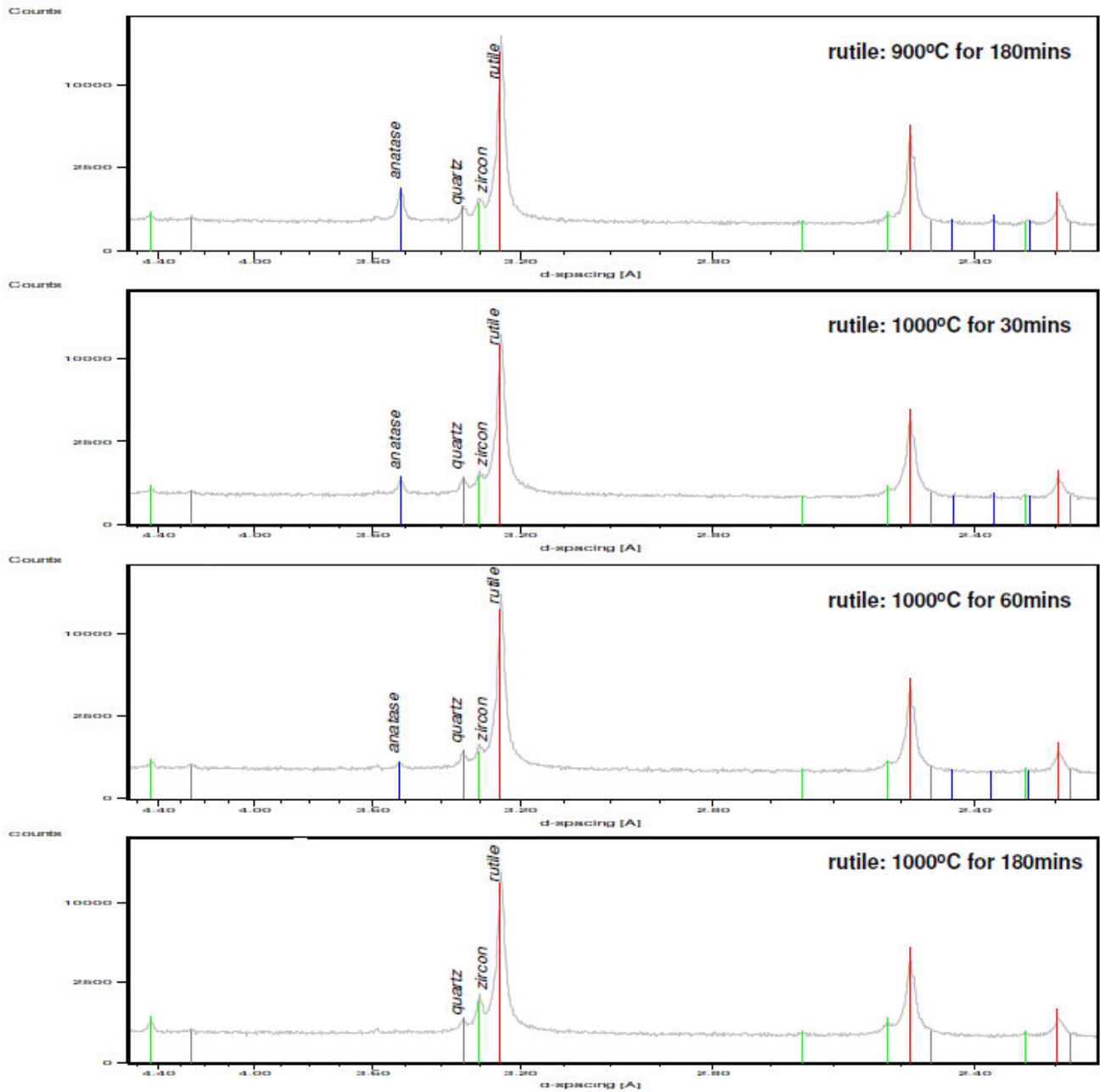


Figure 85: Diffractograms for Rutile

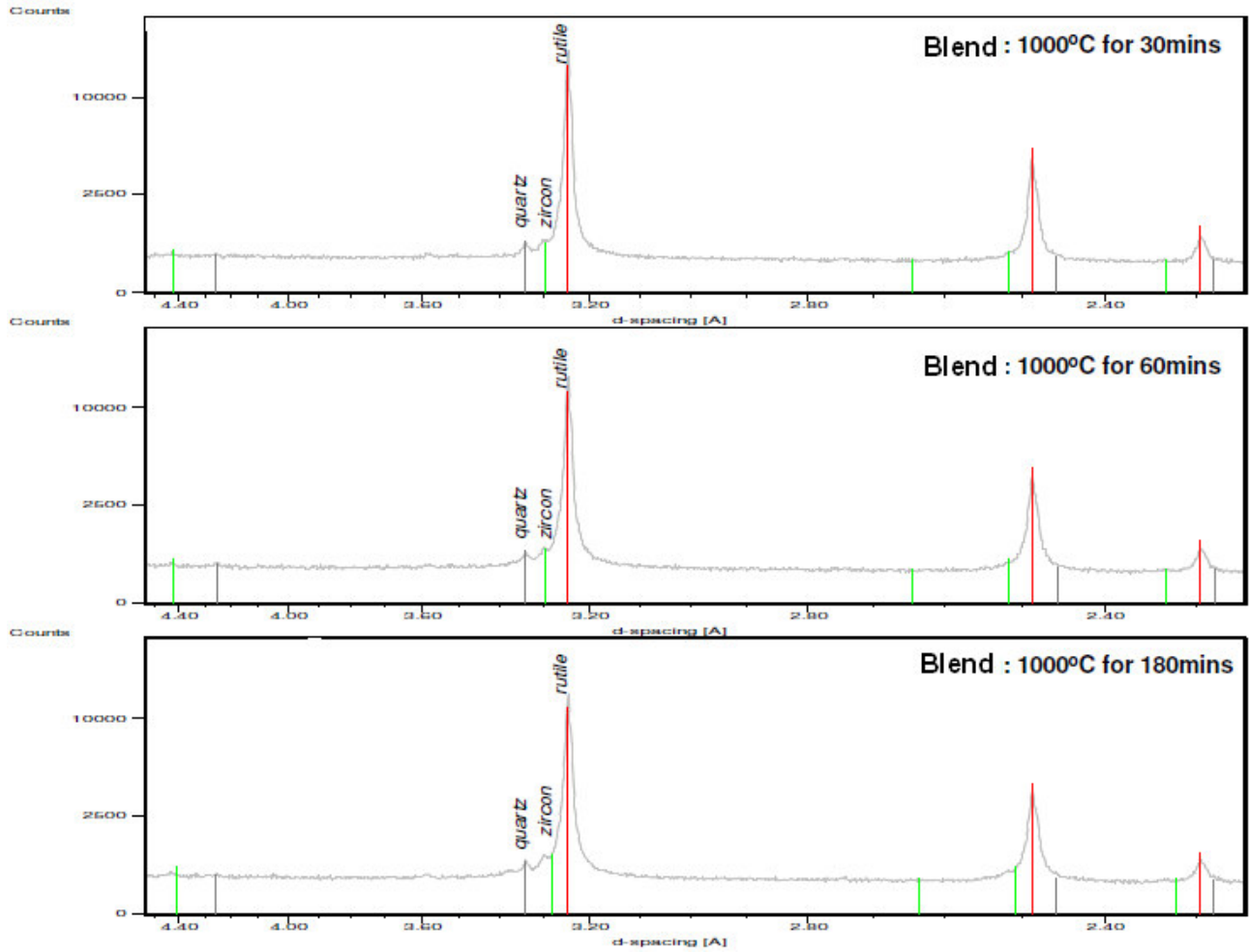


Figure 86: Diffractograms for Blend

